



CORRELATION OF MOLECULAR MOTIFS AND NON-CLASSICAL-HYDROGEN-BONDING INTERACTIONS IN CRYSTAL OF 2,7-DIMETHOXY-3-(1- NAPHTHOYL)NAPHTHALENE

Akiko Okamoto^{[a]*}, Takehiro Tsumuki^[a], Kosuke Sasagawa^[a], Siqingaowa^[a] and
Noriyuki Yonezawa^[a]

Keywords: Non-classical hydrogen-bonding interaction, molecular motif, dimeric molecular aggregates, two-dimensionally spread layer

The crystal structure is reported for 2,7-dimethoxy-3-(1-naphthoyl)naphthalene (**I**), C₂₃H₁₇O₃, one of β -aroylated naphthalene compounds. In crystal, two naphthalene ring moieties of respective molecules are non-coplanarly located to each other, and two molecules are nested inside one another through a pair of C–H $\cdots\pi$ hydrogen-bonding interactions (C–H \cdots Cg = 2.73 Å) forming a dimeric molecular aggregate. Each dimeric molecular aggregate is linked with four adjacent dimers by regular-squarely directed four (sp³)C–H \cdots OCH₃ hydrogen bonds between the methoxy groups (C–H \cdots O = 2.50 Å) forming two-dimensionally spread plane. The planes are stacked into piles of layers along *ac* diagonal. On the other hand, the β -aroylated naphthalene homologues, 3-benzoylated naphthalene derivative **I** and 3-(2-naphthoylated) one **II**, are proved to take unidimensional molecular accumulation. Though each dimeric molecular aggregate has four identical interactions between adjacent dimeric molecular aggregates in crystal of homologue **I**, the rectangular, *i.e.*, non-regular-square aligned situation of four interactions makes the linkage of each aggregate with only two adjacent dimers resulting in ribbon structure. In crystal of homologue **II**, molecules are stacked without formation of dimeric aggregates in columnar structure. On the basis of the results of systematic comparison of molecular packing structure and effective noncovalent-bonding interactions among title compound **I** and the β -aroylated naphthalene homologues **I** and **II**, the presence of large difference in strength of intermolecular interactions, *i.e.*, predominant or apparently sole functioning of either C–H \cdots O hydrogen bond or C–H $\cdots\pi$ hydrogen-bonding interaction induces only unidimensional molecular accumulation, *e.g.*, ribbon-like alignment composed of dimeric molecular aggregates or columnar assembling of molecules. ¹H NMR spectra suggest that conformational interconversion behaviour of title compound **I** through rotation around two kinds of C–C bonds in solution is disturbed rather largely compared to two homologous compounds **I** and **II**. Spatial organization characteristics of single molecular and molecular packing structures of β -aroylated naphthalene homologues in crystal are comparatively analyzed along with those in solution for the sake of elucidation of relationship among spatial organization, noncovalent bonding intermolecular interaction in crystal, and steric factors in solution.

*Corresponding Authors

Fax: +81-42-388-7291

E-Mail: aokamoto@cc.tuat.ac.jp

[a] Department of Organic and Polymer Materials Chemistry,
Tokyo University of Agriculture and Technology, 2-24-16
Naka-machi, Koganei, Tokyo 184-8588, Japan

eighty compounds having 1,8-diaroylated naphthalene skeleton or the homologous/analogous structure have been reported by the authors' group *via* the Cambridge Structure Database (CSD).^{5,6}

Introduction

Studies on molecular interactions in organic crystals¹ increase importance for many aspects of crystal engineering and materials design, for example, as a reply to the growing demands for fine-tuning of strength and effectiveness of the noncovalent-bonding interactions of crystal.^{2,3} Recently, selective and exclusive electrophilic aromatic arylation at α -/ α,α' -(1-/1,8-) positions of naphthalene derivative has been found by the authors' group, which gives tandem aroylated products of 1-aroylated 2,7-dialkoxynaphthalene compounds as intermediating compounds and 1,8-diaroylated products as prolonged reacted ones.⁴ Fortunately, the 1-aroylated and the 1,8-diaroylated naphthalene compounds are generally susceptible to affording qualified single crystals suitable for X-ray crystal analysis. The single molecular structure and the structural features of the molecular packing for roughly

Molecular structures of 1,8-diaroylated 2,7-dialkoxynaphthalene compounds in crystals have common features that two aroyl groups are non-coplanarly situated to the 2,7-dialkoxynaphthalene core and oriented in an opposite direction along with a few exceptional compounds bearing unidirectional-aligned aroyl groups.⁶ In the molecular packing of 1,8-diaroylated 2,7-dialkoxynaphthalene compounds, four kinds of noncovalent-bonding interactions, (sp²)C–H \cdots O=C hydrogen bond, (sp³)C–H \cdots O hydrogen bond, C–H $\cdots\pi$ hydrogen-bonding interaction, and $\pi\cdots\pi$ stacking are observed in decreasing order of frequency.⁷ These observed crystal structural features indicate that the molecules of the 1,8-diaroylated naphthalene compounds are aggregated by significant contribution of non-classical hydrogen bonding interactions, which are generally recognized as weak molecular interactions in the crystal. To clarify such a curious situation, the authors have attempted to reveal correlation among single molecular structure, molecular packing structure, and effective non-classical hydrogen bonding

interactions by systematic comparison of crystal structures among designed 1,8-diaroylated naphthalene homologues.⁸

Recently, crystal structures of β -aroylated naphthalene homologues, 3-benzoyl-2,7-dimethoxynaphthalene (**I**)⁹ and 2,7-dimethoxy-3-(2-naphthoyl)naphthalene (**II**)¹⁰ have been determined by the authors' group (Fig. 1). The determination of the crystal structures of two compounds has highly motivated for the authors to complete the probe substance triad for analysis of the effective non-classical hydrogen bonding interactions in crystal by complementation of crystal structural information of the analogous molecule bearing 1-naphthoyl group. Herein, the X-ray crystal structure of the 2,7-dimethoxynaphthalene compound bearing α -naphthoyl group at the 3-position (**1**) is reported (Fig. 2) and the difference in both single molecular crystal structure and crystal packing structure is discussed by comparing with those of the 3-benzoylated and 3- β -naphthoylated homologues (**I** and **II**) to clarify the influence and the role of intermolecular noncovalent-bonding interactions in the molecular packing.

Furthermore, the molecular spatial organizations of these compounds in solution are discussed with the aid of NMR spectral method. By this protocol, extraction of the steric factors functioning in determination of the molecular spatial organization is attempted on the basis of comparison of structure in distinct situations with the presence of significant intermolecular noncovalent-bonding interactions in crystal and without nearly absence of intermolecular interactions in solution.

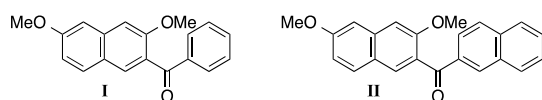


Figure 1. β -aroylated naphthalene homologues **I** and **II**.

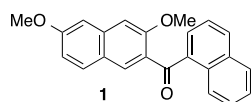


Figure 2. Title compound (**1**).

Experimental

All reagents were of commercial quality and were used as received. Solvents were dried and purified using standard techniques.¹¹ 2,7-Dimethoxynaphthalene¹² and phosphorus pentoxide–methanesulfonic acid mixture¹³ were prepared according to literatures. Synthetic methods and spectral data for β -aroylated naphthalene homologues **I** and **II** have been reported in literatures.^{9,10}

Measurements

¹H NMR spectra were recorded on a JEOL JNM-AL300 spectrometer (300 MHz) or a JEOL ECX400 spectrometer (400 MHz). Chemical shifts are expressed in ppm relative to internal standard of Me₄Si (δ 0.00). ¹³C NMR spectra were recorded on a JEOL ECX400 spectrometer (100 MHz).

Chemical shifts are expressed in ppm relative to internal standard of CDCl₃ (δ 77.0). IR spectra were recorded on a JASCO FT/IR-4100 spectrometer (KBr tablet). High-resolution FAB mass spectra were recorded on a JEOL MStation (MS700) ion trap mass spectrometer in positive ion mode.

X-ray crystallography

For the crystal structure determination, the single-crystal of title compound **1** was used for data collection on a four-circle Rigaku RAXIS RAPID diffractometer (equipped with a two-dimensional area IP detector). The graphite-monochromated Cu K α radiation (λ = 1.54187 Å) was used for data collection. The lattice parameters were determined by the least-squares methods on the basis of all reflections with $F^2 > 2\theta(F^2)$.

Refinement

Crystal data, data collection and structure refinement details are summarized in Table 1. All H atoms could be located in difference Fourier maps, but were subsequently refined in optimized positions as riding atoms, with C–H = 0.95 (aromatic) and 0.98 (methyl) and with $U_{\text{iso}}(\text{H}) = 1.2 U_{\text{eq}}(\text{C})$. For data collection: *PROCESS-AUTO* (Rigaku, 1998); cell refinement: *PROCESS-AUTO* (Rigaku, 1998); data reduction: *CrystalStructure* (Rigaku, 2007); program(s) used to solve structure: *SIR2004* (Burla *et al.*, 2007)¹⁴; program(s) used to refine structure: *SHELXL97* (Sheldrick, 2008); molecular graphics: *ORTEP III* (Burnett & Johnson, 1996).¹⁵ The hydrogen bond geometries of title compound **1** are listed in Table 2.

Table 1. Crystallographic data and structure refinement parameters.

<i>Crystal data</i>	
Chemical formula	C ₂₃ H ₁₈ O ₃
M _r	342.37
Crystal system, space group	Monoclinic, <i>P</i> 2 ₁ / <i>c</i>
Temperature (K)	193
<i>a</i> , <i>b</i> , <i>c</i> (Å)	8.8585 (2), 22.1886 (5), 9.10165(19)
β (°)	104.139 (1)
<i>V</i> (Å ³)	1734.80 (7)
<i>Z</i>	4
Radiation type	CuK α
μ (mm ⁻¹)	0.69
Crystal size (mm)	0.60 × 0.30 × 0.10
<i>Data collection</i>	
Diffractometer	Rigaku R-AXIS RAPID
Absorption correction	Numerical NUMABS
<i>T</i> _{min} , <i>T</i> _{max}	0.682, 0.934
No. of measured, independent and observed [$I > 2\sigma(I)$] reflections	30270, 3173, 2587
<i>R</i> _{int}	0.054
($\sin \theta/\lambda$) _{max} (Å ⁻¹)	0.602
<i>Refinement</i>	
$R[F^2 > 2\sigma(F^2)]$, $wR(F^2)$, <i>S</i>	0.041, 0.113, 1.09
No. of reflections	3173
No. of parameters	238
H-atom treatment	H-atom parameters constrained
$\Delta\rho_{\text{max}}$, $\Delta\rho_{\text{min}}$ (e Å ⁻³)	0.17, -0.15

Computer programs: *PROCESS-AUTO* (Rigaku, 1998), *PROCESS-AUTO* (Rigaku, 1998, *CrystalStructure* (Rigaku, 2007), *SIR2004* (Burla *et al.*, 2007), *SHELXL97* (Sheldrick, 2008), *ORTEPIII* (Burnett & Johnson, 1996).

Table 2. Hydrogen bond geometry (\AA , $^\circ$).

$D-H\cdots A$	$D\cdots A$
$C22-H22C\cdots O3^i$	3.437(2)
$C6-H6\cdots Cg^{ii}$	3.6749(14)

Symmetry codes: (i) $-1+x, 1/2-y, 1/2+z$; (ii) $1-x, -y, 1-z$. Cg is the centroid of the C16–C21 ring.

Synthesis of 2,7-dimethoxy-3-(1-naphthoyl)naphthalene (1)

The title compound (**1**) was prepared by treatment of a mixture of 2,7-dimethoxynaphthalene (376 mg, 2.0 mmol) and 1-naphthoic acid (379 mg, 2.2 mmol) with phosphorus pentoxide–methanesulfonic acid mixture (P_2O_5 : MsOH = 1: 10 w/w; 4.4 mL). After the reaction mixture was stirred at 333 K for 6 h, the mixture was poured into ice-cooled water and extracted with $CHCl_3$ (15 mL \times 3). The combined extracts were washed with 2 M aqueous NaOH (20 mL \times 3) followed by washing with brine (20 mL \times 3). The organic layer thus obtained was dried over anhydrous $MgSO_4$. The solvent was removed under reduced pressure to give a cake (688 mg, quant.). The crude product was purified by flush silica gel chromatography (toluene; yield 64%). Colourless platelet single crystals suitable for X-ray diffraction were obtained by repeated crystallization from $CHCl_3$.

1H NMR δ (400 MHz, $CDCl_3$): 3.73 (3H, s), 3.94 (3H, s), 7.03 (1H, dd, $J = 2.0, 9.2$ Hz), 7.09 (1H, d, $J = 2.0$ Hz), 7.11 (1H, s), 7.43 (1H, t, $J = 8.0$ Hz), 7.53–7.59 (2H, m), 7.62 (1H, d, $J = 8.0$ Hz), 7.67 (1H, d, $J = 9.2$ Hz), 7.91–7.94 (2H, m), 7.99 (1H, d, $J = 8.0$ Hz), 8.60 (1H, d, $J = 8.0$ Hz) ppm. ^{13}C NMR δ (100 MHz, $CDCl_3$): 55.34 (OMe), 55.61 (OMe), 104.86, 105.74, 117.10, 123.05, 124.31, 125.92, 126.26, 127.59, 128.30, 128.97, 129.77, 130.40, 130.88, 131.95, 132.16, 133.74, 137.10, 137.73, 156.47 (OAr), 159.67 (OAr), 197.45 (C=O) ppm; IR (KBr): 1660 (C=O), 1628 (Ar), 1503 (Ar), 1250 (C–O–C), 1221 (C–O–C) cm^{-1} . HRMS (FAB; *m*-nitrobenzyl alcohol [*m*-NBA]) m/z : $[M+H]^+$ calcd. for $C_{23}H_{19}O_3$, 343.1334, found, 343.1244. m.p. = 454.8–456.3 K.

Results and Discussion

The single molecular structure of title compound **1** is illustrated in Fig. 3.¹⁶ The interplanar angle between the two naphthalene rings (C1–C10 and C12–C21) is 88.15 (4°). The dihedral angle between the bridging carbonyl plane [C3–(C11=O1)–C12] and the naphthalene ring of the 2,7-dimethoxynaphthalene core (C1–C10) is larger than that between the bridging carbonyl plane and the naphthalene ring of the 1-naphthoyl group (C12–C21) [65.13 (7°) versus 35.32 (7°)]; C4–C3–C11–O1 torsion angle = -61.43 (19°) versus O1–C11–C12–C21 torsion angle = -33.4 (2°).

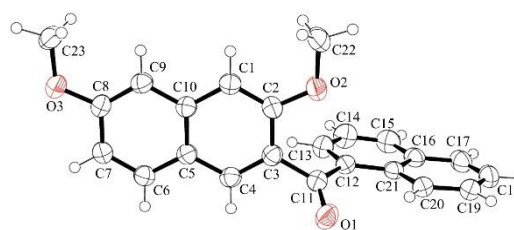
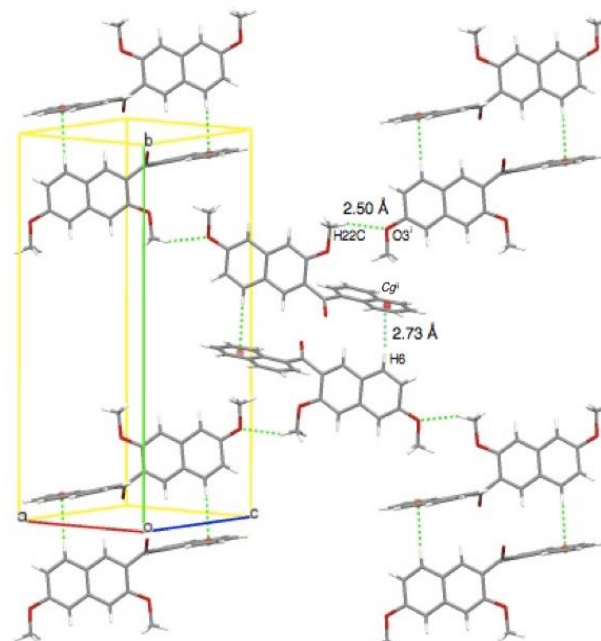


Figure 3. The molecular structure of **1**, with atom numbering. Displacement ellipsoids are drawn at the 50% probability level.

In crystal, dimeric molecular aggregates, each of which is composed of two molecules of title compound **1** nesting inside one another, are two-dimensionally arranged to form a layer (Fig. 4). The layers are piled along ac diagonal (Fig. 5). A pair of intermolecular (sp^2)C–H $\cdots\pi$ hydrogen-bonding interactions between the naphthalene rings of 2,7-dimethoxynaphthalene core and 1-naphthoyl moiety of the counterpart molecule induce the dimeric molecular aggregate ($C6-H6\cdots Cg = 2.73$ \AA ; Cg is the centroid of the C16–C21 ring; symmetry codes: $1-x, -y, 1-z$; Fig. 4 and Table 2). In addition, four (sp^3)C–H \cdots OCH $_3$ hydrogen bonds between the methoxy groups link each dimeric molecular aggregate with the four adjacent dimeric molecular aggregates making two-dimensionally accumulated spread structure ($C22-H22C\cdots O3 = 2.50$ \AA ; symmetry codes: $-1+x, 1/2-y, 1/2+z$; Fig. 4, Table 2).

Figure 4. A layer composed of dimeric molecular aggregates in



title compound (**1**), showing (sp^3)C–H \cdots OCH $_3$ hydrogen bonds and a pair of intermolecular C–H $\cdots\pi$ hydrogen-bonding interactions. Cg is the centroid of the C16–C21 ring [see Table 2 for details; symmetry codes: (i) $-1+x, 1/2-y, 1/2+z$; (ii) $1-x, -y, 1-z$].

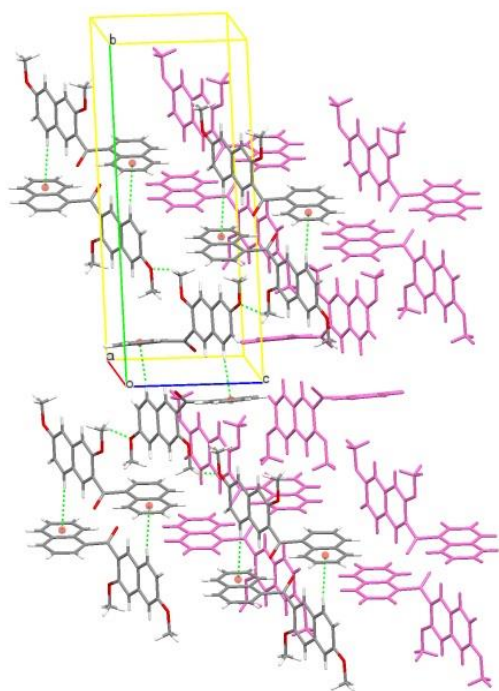


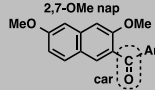
Figure 5. A partial view of the crystal packing of title compound **1**.

There are a lot of reports about dimeric molecular aggregates induced by classical hydrogen bonding interactions such as electronegative-atom-bound hydrogen...electronegative atom bonds.¹⁷ On the other hand, electronegative atom-bound hydrogen... π interactions-induced dimeric molecular aggregates have been reported fewer than the former type of dimeric molecular aggregate.¹⁸ Furthermore, dimeric molecular aggregates induced by van der Waals interactions or C-H... π hydrogen-bonding interactions have been rarely reported. In the crystal of title compound **1**, dimeric molecular aggregates are formed by C-H... π hydrogen bonding interaction. This is one of the most rare cases for such molecular dimeric formation in crystal. It also means that the more effective types of interactions are probably prevented because of substantially immanent intramolecular and intradimeric hindrance of arene moieties.

The crystal structures of two homologous compounds for title compound **1**, *i.e.*, 3-benzoyl-2,7-dimethoxynaphthalene (**I**)⁹ and 2,7-dimethoxy-3-(2-naphthoyl)naphthalene (**II**),¹⁰ which have benzoyl group and 2-naphthoyl group at 3-position of the 2,7-dimethoxynaphthalene core respectively in place of 1-naphthoyl group, have been reported recently. Arene ring of aroyl group in these homologous molecules is non-coplanarly located to the 2,7-dimethoxynaphthalene core in the similar fashion for title compound **1**. Table 3 summarizes selected interplanar/dihedral angles of homologues **I**, **II**, and title compound **1**. Interplanar angle between arene rings of aroyl group and 2,7-dimethoxynaphthalene moiety is in the order of homologue **I** [68.32(5)°] < homologue **II** [78.02(3)°] < title compound **1** [88.15(4)°]. The interplanar angle of title compound **1** is rather close to the corresponding interplanar angles in α - and α,α' -positions aroylated naphthalene homologues, *i.e.*, 79.07(4)° and 88.19(4)° for 2,7-dimethoxy-1-(1-naphthoyl)naphthalene, which contains two independent molecules in the crystallographic unit-cell,¹⁹ and 89.84° and

85.06° for 2,7-dimethoxy-1,8-bis(1-naphthoyl)-naphthalene.^{8d} Dihedral angle between the bridged C-(C=O)-C carbonyl plane and the 2,7-dimethoxynaphthalene ring core is in the order of homologue **I** (54.32°) < title compound **1** [65.13(7)°] < homologue **II** (70.56°). Besides, dihedral angle between bridged C-(C=O)-C carbonyl plane and aromatic ring of aroyl group is in the order of homologue **II** (11.53°) < homologue **I** (21.45°) < title compound **1** [35.32°(7)].

Table 3. Selected interplanar/dihedral angles in compound **1** and homologues **I** and **II** (°).

	Compound	Homologue	Homologue
	1	I	II
2,7-OMe nap and Ar	88.15(4)	68.32(5)	78.02(3)
car...2,7-OMe nap	65.13	54.32	70.56
car...Ar	35.32	21.45	11.53

In the case of title compound **1**, both the 2,7-dimethoxynaphthalene ring core and the aromatic ring of the aroyl group largely deviate from the bridged C-(C=O)-C carbonyl plane, and the deviations are larger than homologue **I**. For homologue **II**, the dihedral angle of the naphthalene core versus the bridging carbonyl plane is the largest and that of aroyl group against the bridging carbonyl plane is the smallest among three compounds. These relative values of interplanar/dihedral angles manifest that title compound **1** has the largest internal steric hindrance among three β -aroylated naphthalene compounds.

As described above, title compound **1** affords plane shape alignment as second order accumulation of dimeric aggregates. Contrarily, in crystal of homologue **I**, dimeric molecular aggregates are aligned forming ribbon-like structure. The dimeric molecular aggregate is induced by a pair of intermolecular (sp³)C-H...O=C hydrogen bonds between the core naphthalene ring and the carbonyl group (C4-H4...O1 = 2.58 Å; symmetry codes: -x+2, -y, -z+1), and is connected with two adjacent dimeric molecular aggregates situated on the opposite side through intermolecular (sp³)C-H...OCH₃ hydrogen bonds between the methoxy groups (C18-H18B...O3 = 2.42 Å; symmetry codes: x-1, y, z-1), forming ribbon-like structure along *ac* diagonal (Fig. 6, top).

Table 4. Noncovalent-bonding interactions of title compound **1**, and homologues **I** and **II**.

	Compound	Homologue	Homologue
	1	I	II
<i>C-H...O hydrogen bonds</i>			
(sp ³)C-H...OCH ₃	2.50 ⁱ	2.42 ⁱⁱⁱ	-
(sp ²)C-H...O=C	-	2.58 ^{iv} (pair)	-
<i>C-H...π hydrogen bonding interactions</i>			
(sp ³)C-H... π	-	-	2.80 ^v
(sp ²)C-H... π	2.73 ⁱⁱⁱ (pair)	-	-

The C-H...O interactions are elucidated on the basis of shorter distance of two atoms less than the sum of the van der Waals radii.

C–H... π hydrogen bonding interactions are shown in Table when the distance between the H atom and the centroid of the ring is shorter than 3 Å. Symmetry codes: (i) $-1+x, 1/2-y, 1/2+z$; (ii) $1-x, -y, 1-z$; (iii) $x-1, y, z-1$; (iv) $-x+2, -y, -z+1$; (v) $x, y-1, z$.

In the case of homologue **II**, the molecules are directly stacked into columnar alignment along *b* axis (Fig. 6, bottom). The columnar structure is stabilized by intermolecular (sp³)C–H... π hydrogen-bonding interactions between the methoxy group and the naphthalene ring of the 2-naphthoyl group of the adjacent molecule (C22–H22A...Cg = 2.80 Å; symmetry codes: $x, y-1, z$). The noncovalent-bonding interactions for dimer formation and their alignment in crystals of three homologous compounds discussed above are summarized in Table 4.

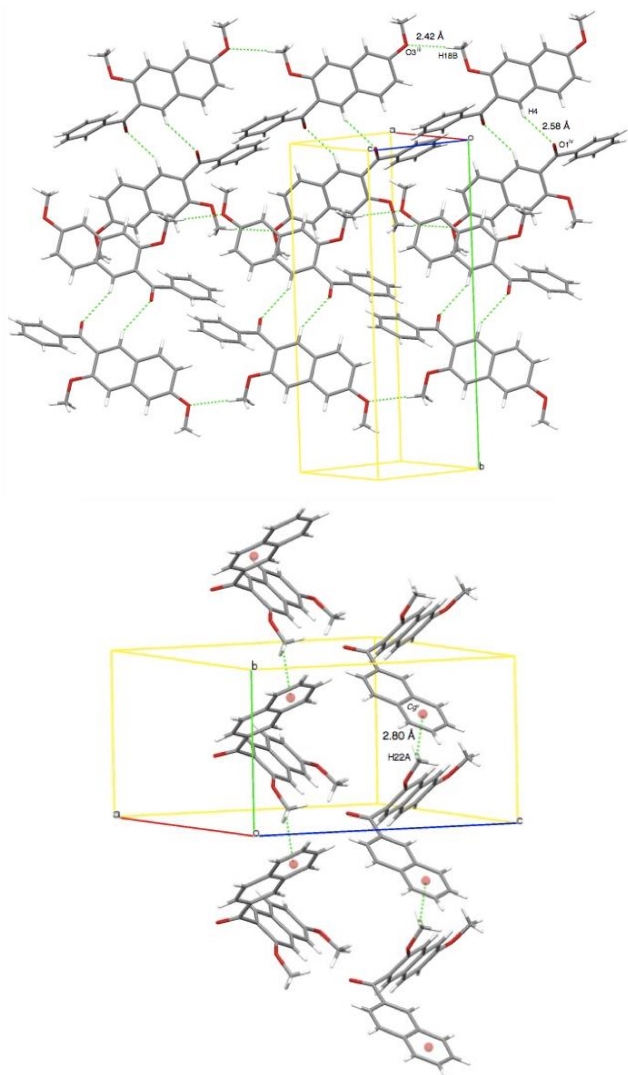


Figure 6. Crystal packing of homologues **I** and **II**: Ribbons composed of dimeric molecular aggregates in homologue **I** [top; see Table 4 for details; symmetry codes: (iii) $x-1, y, z-1$ (for C18–H18B...O3 hydrogen bonds); (iv) $-x+2, -y, -z+1$ (for C4–H4...O1 hydrogen bonds)] and column structures induced by C–H... π hydrogen-bonding interactions in homologue **II** [bottom; see Table 3 for details; symmetry codes: (v) $x, y-1, z$ (for C22–H22A...Cg interactions)].

Title compound **1** has deep similarities with both of homologues **I** and **II** in terms of fashion and kind of noncovalent-bonding interactions. Title compound **1** forms a dimeric molecular aggregate as well as homologue **I**.

However, higher-order arrangement of dimeric aggregate of title compound **1** and homologue **I** differs distinctively, *i.e.*, title compound **1** forms plane of dimeric aggregates, whereas homologue **I** makes ribbon-like structure of dimers. In both of title compound **1** and homologue **I**, the dimeric molecular aggregates are linked by C–H...O (etheral oxygen) hydrogen bonding interactions (C–H...OCH₃) between methoxy groups. In crystalline molecular packing of homologue **I**, a dimeric aggregate forms a couple of counter directed (sp³)C–H...OCH₃ hydrogen bondings with one adjacent dimeric aggregate. The linkages are also formed with another adjacent dimeric aggregate. Accordingly, ribbon structure of homologue **I** through the connection of dimeric aggregates by two couples of (sp³)C–H...OCH₃ hydrogen bondings is obtained.

The difference in higher-ordered structure between title compound **1** and homologue **I** presumably arises from the spatial organization of respective dimeric molecular aggregates. The dimeric molecular aggregate of title compound **1** is induced by a pair of C–H... π hydrogen-bonding interactions in place of a pair of C–H...O(carbonyl oxygen) hydrogen-bonding ones (C–H...O=C) for homologue **I**. Accordingly, in dimeric molecular aggregate of title compound **1**, naphthalene rings of α -naphthoyl moieties are situated to be faced perpendicularly toward edges of core naphthalene ring of the counter monomer resulting in achieve compact and round shaped aggregate arrangement. On the other hand, for dimeric molecular aggregate of homologue **I** is formed by the non-classical hydrogen bonding interaction between carbonyl oxygen and aromatic hydrogen of the naphthalene core of the counter molecules by rather loose contact, which allows each naphthalene ring of dimeric molecular aggregate to position outer site of aggregate resulting in construction of opened dimeric shape. In the compact shape of the dimeric molecular aggregate of title compound **1**, the 2- or 7-positioned methoxy groups should take the intramolecular position to minimize the steric hindrance in the allowed dimer plane, resulting in alignment of four orientations pointing to the corners of nearly regular-square. Contrarily, the methoxy groups in the dimeric aggregate of homologue **I** take the position on the parallel lines in the rectangular-square shape leading the connection of their edges to form ribbon-like structure.

For crystal of homologue **II**, C–H... π hydrogen-bonding interactions lead to columnar structure. On the basis of above observation, both of C–H...O(etheral) hydrogen bond and C–H... π hydrogen-bonding interaction are considered as requisites to form two-dimensional molecular network composed of dimeric molecular aggregates. When different interactions of comparative strength present, the predominant interaction might determine the orientation of the relative position of two molecules. If the head-to-tail orientating interaction is predominant, a type of columnar stacking is formed. Otherwise, the head-to-head orientating interaction overcomes, the formation of dimeric aggregate of molecules are precedent. Then, the interaction between dimeric aggregates should determine the most stable alignment under the restriction of inherent steric restriction of the molecule. Accordingly, the spatial organization of the vectors of the effective interactions, *i.e.*, three-dimensional direction, fixes plane- or ribbon-shaped higher ordered accumulation composed of dimeric molecular aggregates. Consequently, either C–H... π hydrogen-bonding interaction

or C–H \cdots O(ethereal) hydrogen bond as the predominant interaction probably leads one-dimensional molecular arrangements such as columnar structure. As described above, title compound **1** plausibly has largest internal steric repulsion among three β -aroylated homologous compounds. The internal steric repulsion seems to interfere formation of superior intradimer and interdimer interactions for dimer to align on the parallel direction such as C–H \cdots O(ethereal) hydrogen bonds that effectively function between dimeric aggregates of homologue **I**. Consequently, cooperation of two couples of intermolecular interactions with counter orientation and same strength functioning between dimeric molecular aggregates most effectively forms two-dimensionally spread arrangement when the interactions are oriented in the perpendicular directions. To the contrary, lack of either of interactions strongly leads unidirectional connection of molecules such as columnar or ribbon structure instead two-dimensional arrangement hardly forms.

In a natural sequence of the structural study on title compound **1** and the homologues **I** and **II**, the molecular spatial organization of these compounds in solution have been investigated referring the results of X-ray crystal analysis. Fig. 7 exhibits ^1H NMR spectra of the methoxy (δ 3.6–4.0 ppm) and aromatic (δ 6.0–9.0 ppm) regions for title compound **1** and the homologous compounds **I** and **II**. The signals assigned to the 2- and 7-methoxy groups of the 2,7-dimethoxynaphthalene core in homologues **I** and **II** are observed at almost the same chemical shifts, respectively. In the case of title compound **1**, the signals assigned as the proton of the 2-methoxy group are shifted to higher magnetic field than other two homologues. Ahead of comparison of chemical shift in the aromatic protons for homologues **I** and **II**, regional equivalency of the related protons sliding the three homologues are organized. In addition to the apparent equivalency for each proton on 2,7-dimethoxynaphthalene core such as those of 1- and 4-positions on three homologous compounds (**e** and **a**), the protons of 1(3)- and 4-positions in 2-naphthoyl group [**f'** (**f**) and **g**] of homologue **II** are fixed to correspond to protons of 2(6)- and 3(5)-positions of the benzoyl group (**f** and **g**) in homologue **I**, respectively. From the standpoint of proton equivalency or proton correspondence among these homologous molecules, the corresponding signals of these common protons in homologue **II** are found essentially shifted to lower magnetic field than homologue **I**.

In the case of title compound **1**, the protons on 1- and 4-positions of the 2,7-dimethoxy-naphthalene moiety (**e** and **a**) and 2- and 3-positions of the 1-naphthoyl group (**f** and **g**) are common with two homologues. For one common proton (**a**) in the 2,7-dimethoxynaphthalene core, the signal is shifted slightly to lower magnetic field than homologues **I** and **II**, whereas the signal of the other common proton (**e**) is almost same with the two homologues. The signal of the 3-position of the 1-naphthoyl group (**g**) is intermediately situated between two homologues. On the other hand, the signal of the proton of the 2-position of the 1-naphthoyl group (**f**) of title compound **1** is shifted more largely to lower magnetic field than other two homologues. For natural extension of consideration of chemical shifts of the corresponding protons in benzoyl, α -naphthoyl, and β -naphthoyl groups, as the β -aroyl groups in homologue **I**, title compound **1**, and homologue **II**, the normalized or roughly assessed virtual chemical shifts are compared with the experimentally observed chemical shifts for these protons.

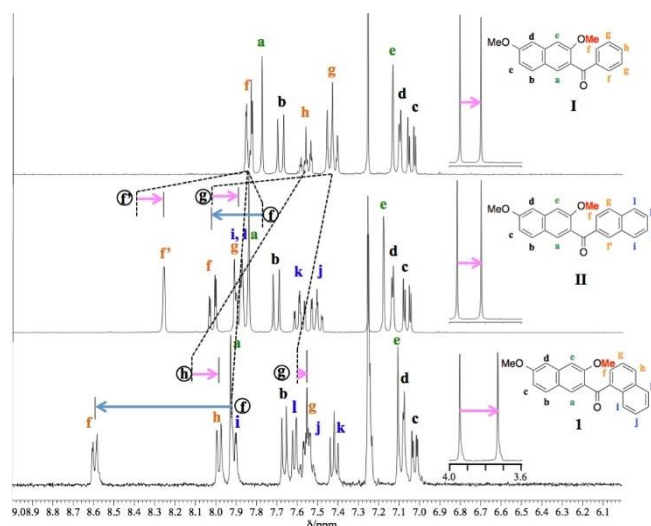
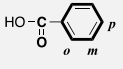
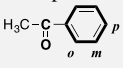
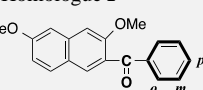


Figure 7. ^1H NMR spectra in CDCl_3 at r.t. (300 MHz): Homologue **I** (top), homologue **II** (middle), and compound **1** (bottom). Dotted-lines on the charts with circled alphabetical denotations display the positions of estimated signals for protons corresponding to the same alphabetical denotations. The estimated chemical shifts are listed in Table 7, which are determined according to the method described in the note of Tables 7, 6, and 5.

First, comparison of chemical shifts of protons in phenyl groups of homologue **I** with those of analogous arenecarbonyl compounds has been undertaken. Table 5 shows the chemical shifts of protons of benzoyl groups in ^1H NMR spectra of homologue **I**, acetophenone, and benzoic acid. Table 5 also displays difference in chemical shift among *o*-, *m*-, and *p*-positioned protons on individual benzoyl groups. The chemical shifts for *o*-, *m*-, and *p*-protons in three compounds are observed in the range of 7.84–8.12 ppm (0.28), 7.41–7.45 ppm (0.04), and 7.56–7.62 ppm (0.06), respectively. The values in the parentheses are the ranges of the chemical shift distribution for the protons of the corresponding positions. Furthermore, the difference in chemical shifts between two protons of the same molecules are found in the ranges of -0.41 to -0.67 (0.26) for *m*- against *o*-, +0.13 to +0.17 (0.04) for *p*- against *m*-, and -0.28 to -0.50 (0.22) for *p*- against *o*-positions, respectively. The deviations in chemical shift among three aromatic protons of homologue **I** (designated as **f**, **g**, and **h**) show good accordance with those observed among the corresponding protons of benzoic acid and acetophenone. These data suggest that the ^1H NMR spectra of benzoyl groups of homologue **I**, acetophenone, and benzoic acid show essentially same spectral patterns, meaning that spatial organization of benzoyl group of homologue **I** has rather conventional structural-hindrance situation as such a type of aromatic ketone and carboxylic acid molecules without specified steric effect.

On the analogy of above consideration, the virtual chemical shifts of protons of α - and β -naphthoyl groups (**f**, **g**, and **f'**) have been estimated in order to compare the observed values with for elucidation of unusual deviation of the chemical shifts of these compounds.

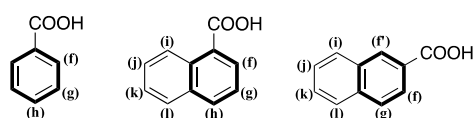
Table 5. Chemical shifts and their differences of the protons on benzoyl groups of benzoic acid, acetophenone and homologue I

	Posi- tions	Chem. shifts	$\Delta\delta(m-o)^{b)}$ $\Delta\delta(p-m)^{b)}$	$\Delta\delta(p-o)^{b)}$
Benzoic acid ^{a)}	<i>o</i> -	8.12	-0.67	
	<i>m</i> -	7.45		-0.50
	<i>p</i> -	7.62	+0.17	
Acetophenone ^{a)}	<i>o</i> -	7.89	-0.48	
	<i>m</i> -	7.41		-0.33
	<i>p</i> -	7.56	+0.15	
Homologue I	<i>o</i> -	7.84	-0.41	
	<i>m</i> -	7.43		-0.28
	<i>p</i> -	7.56	+0.13	
		/ppm	/ppm	/ppm

^{a)} Chemical shifts of benzoic acid and acetophenone are referred to the Spectral Data Base (SDBS) provided by National Institute of Advanced Industrial Science and technology (AIST), in CDCl₃.

^{b)} $\Delta\delta$'s are calculated by subtraction of the reference chemical shift of the signals for individual protons from those of designated protons.

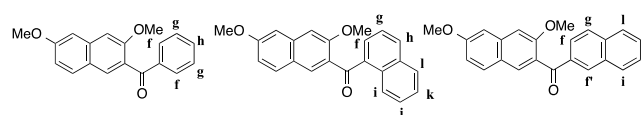
Deviation values from the estimated value in chemical shifts among these protons are calculated referring to those of the corresponding arenecarboxylic acid (Fig. 8 and Table 6). The observed values and the deviation are displayed in Table 7 (Fig. 9). That is, employing the deviation values for the corresponding arenecarboxylic acids from benzoic acid shown in Table 6, the chemical shifts for protons of homologue II and title compound I are estimated on the basis of the chemical shifts of homologue I and tabulated in Table 7. The estimation was performed as follows: the virtual chemical shifts of protons of 2,7-dimethoxy-3-(1-naphthoyl)naphthalene (title compound I) and homologue II were calculated by adding/drawing the corresponding deviation values determined for α - and β -naphthoic acids against benzoic acid and listed in Table 6 [α -naphthoic acid: +0.08 (f), +0.17 (g), +0.56 (h); β -naphthoic acid: -0.07 (f), +0.59 (g), +0.55 (f')] to/from the observed chemical shifts for homologue I, 3-benzoyl-2,7-dimethoxynaphthalene.

**Figure 8.** Designation of protons on benzoic acid, α -naphthoic acid and β -naphthoic acid**Table 6.** Chemical shifts of the protons on aroyl group of benzoic acid, α -naphthoic acid and β -naphthoic acid with deviation of the shifts from the corresponding protons of benzoic acid

Acid	Chemical shift/ppm							
	f	g	h	f'	i	j	k	l
Benzoic ^{a)}	8.12	7.45	7.62	8.12	-	-	-	-
α -naphthoic	8.20	7.62	8.18	-	8.93	7.68	7.61	8.04
[deviation] ^{b)}	+0.08	+0.17	+0.56					
β -naphthoic ^{a)}	8.05	8.04	-	8.67	8.15	7.64	7.68	8.03
[deviation] ^{b)}	-0.07	+0.59	-	+0.55				

^{a)} Chemical shifts of benzoic acid and acetophenone are referred to the Spectral Data Base (SDBS) provided by National Institute of Advanced Industrial Science and technology (AIST), in DMSO-*d*₆. ^{b)} Deviation value is calculated by subtraction of the chemical shift of signals for individual protons on benzoic acid from the chemical shift of the corresponding protons on α - or β -naphthoic acids.

In Fig. 7, the several virtual chemical shifts are inserted for the selected aromatic protons of title compound I and homologue II as a vertical dot-line with circled f, g, f', and h designations, which are estimated on the basis of the chemical shifts for protons of homologue I and relationship among chemical shifts for protons of α -naphthoic acid and β -naphthoic acid versus those of benzoic acid as the reference compound with homologue I (Table 6 and Table 7). The comparison between the observed chemical shifts and the estimated ones obtained according to above mentioned manipulation shows that there are characteristic magnetic field shifts of observed chemical shift values for protons on the carbons adjacent to and near the carbonyl-substituted carbon.

**Figure 9.** Designation of protons on title compound I and homologues I/II

Especially, the observed chemical shift of the 2-positioned proton of the 1-naphthoyl group of title compound I (f, δ 8.60 ppm) shows the largest deviation compared to the estimated value (δ 7.92 ppm). And about 3-positioned proton on the 1-naphthoyl group of title compound I (g), the observed value (δ 7.56 ppm) and the estimated one (δ 7.60 ppm) are almost same. On the other hand, the observed chemical shift of the 3-positioned proton of 2-naphthoyl group (f, δ 8.02 ppm) in homologue II deviates from the estimated one (δ 7.77 ppm) on a same direction toward lower magnetic field as well as proton (f) in title compound I, however the deviation magnitude is medium. At the same time, the observed chemical shift of 1-positioned proton of 2-naphthoyl group (f', δ 8.26 ppm) in homologue II has found to deviate on the opposite direction with a moderate magnitude compared to the estimated value (δ 8.39 ppm) toward higher magnetic field. Totally, deviation on observed chemical shift of the 1- and 3-positioned protons (f and f') from the estimated values for homologue II is almost equalized, whereas the deviation between observed chemical shift and estimated one for proton (f) in title compound I is emphasized apparently. In title compound I, the deviation of observed chemical shift from estimated one for 2-positioned proton (f) is apparently emphasized against small deviation for 3-positioned proton (g).

This observation displays that the deshielding effect against homologue **II** is almost equalized on 1- and 3-positioned protons (**f** and **f'**), whereas the deshielding effect is applied with distinctive disproportionation on 2- and 3-positioned protons (**f** and **g**) for title compound **1**

Table 7. Observed and estimated chemical shifts of the selected protons of title compound **1** and homologues **I/II** with deviation between observed and estimated values.

	Chemical shift/ppm			
	f	g	h	f'
Benzoylated naphthalene I	7.84	7.43	7.56	7.84
α -naphthoylated 1 (observed)	8.60	7.56	7.99	
(estimated)	7.92	7.60	8.12	
[deviation] ^{a)}	[+0.68	-0.04	-0.13]	
β -naphthoylated II (observed)	8.02	7.90	-	8.26
(estimated)	7.77	8.03	-	8.39
[deviation] ^{a)}	[+0.25	-0.12	-	-0.13]

^{a)} Deviation for the protons from the corresponding protons of homologue **I**. "(Estimated) chemical shift values" are calculated by addition/subtraction of the deviation values between α/β -naphthoic acid and benzoic acid tabulated in Table to/from the observed chemical shift of the signal for individual protons on title compound **1** (α -naphthoylated compound **1**) or homologue **II** (β -naphthoylated homologue **II**). "[Deviation] values" are calculated by subtraction of the estimated chemical shift of the signal for individual protons from those of the corresponding observed chemical shifts.

The unbalanced deviation magnitudes of chemical shifts of signals along with opposition of direction observed in title compound **1** indicate that these protons are distinctively influenced by different magnetic field effect. The large lower magnetic field deviation of the proton (**f**) of carbonyl adjacent position on 1-naphthoyl group in title compound **1** is considered due to the efficient deshielding effect of the opposing induced magnetic field. On the other hand, the good coincidence between the observed and the estimated chemical shifts for 3-positioned proton (**g**) on 1-naphthoyl group of title compound **1** means that the proton receives almost no effect or compensated effects originated from congestedly accumulated aromatic ring moieties. From the viewpoint of function of induced magnetic field arising from circuit current on the aromatic ring, the proton (**f**) receiving opposing magnetic field more strongly is interpreted to situate in near spatial position against the effective aromatic rings for longer time. This supposed spatial alignment should mean the congested and hindered spatial organization of arene rings to each other resulting in almost perpendicular position of two naphthalene rings. These restrictions lead the conformation more fixed with contact relation of arene rings with only a small space for conformational perturbation. In addition, the highly crowded spatial situation of α -naphthoyl connection might support fixation of α -naphthyl-carbonyl- β -naphthyl bonding in title compound **1**. Contrarily, the two naphthalene rings in homologue **I** have enough room to take various conformations around ketonic carbonyl bonding. It plausibly affords almost equal average distances between individual aromatic protons and the adjacent naphthalene ring, which leads moderate deviation to lower in chemical shift for homologue **I**.

Furthermore, orientation of methoxy group at 2-position of the 2,7-dimethoxynaphthalene moiety is also fixed loosely by steric hindrance of 1-naphthoyl group in title

compound **1**. In consequence of this, the signal ascribed to the methoxy group at the 2-position of the 2,7-dimethoxynaphthalene is shifted to higher magnetic field by the local magnetic field induced from circulating ring current of 2,7-dimethoxynaphthalene core, which opposes the external magnetic field. On the other hand, homologues **I** and **II** rather smoothly undergo interconversion among rotational isomers with the rather lower barrier. Under these circumstances, the induced magnetic field effect that functions distinctly in title compound **1** is in turn largely depressed in homologues **I** and **II**. Furthermore, signals of title compound **1** are observed influenced by clearly different magnetic field effects. These results strongly indicate that conformational flexibility of title molecule **1** is lower than the two homologous molecules. Consequently, degree of fixation of conformation is decreased in an order of title compound **1**, homologue **II**, and homologue **I** (Figure 10). These interpretations are supported by rather good agreement with estimation of internal steric hindrance elucidated on the basis of X-ray crystal structure analyses.

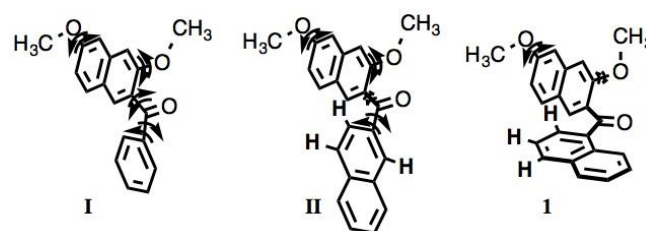


Figure 10. Plausible spatial organization in solution: homologue **I** (left), homologue **II** (middle), and compound **1** (right).

Conclusion

Crystal structure of 3-(1-naphthoyl)-2,7-dimethoxynaphthalene has been determined. In the crystal packing, the molecules are arranged in a layer composed of the dimeric molecular aggregates. Systematic comparison of single molecular structure and molecular packing with noncovalent-bonding interactions for three homologous β -aroylated naphthalene compounds has revealed correlation of single molecular and molecular packing structure motif in crystal and effective non-classical hydrogen-bonding interactions. Both C-H...O=C hydrogen bond and C-H... π hydrogen bonding interactions of comparable magnitude and suitable spatial orientation are required to form two-dimensional molecular packing motif. To perform planar alignment of molecules, formation of dimeric aggregate of C2 symmetry having two couples of functional groups, methoxy groups, in the regular-squarely oriented directions is significant. In title compound **1**, two methoxy groups of 2,7-dimethoxynaphthalene core as donating role groups in (sp³)C-H...O(etheral) hydrogen bonding interaction and the other two methoxy groups as acceptors are situated perpendicularly in regular-square directions enabling functioning of four identical interactions along four directions toward the four corners of regular-square plane.

Lack of either of the presence of the predominant effectiveness of non-symmetric interaction induces one-dimensional molecular packing motif such as ribbon or columnar structure.

To stabilize the molecular packing in the crystal on condition that the single molecular structure is of conformationally fixed spatial organization of aromatic rings accumulation without coplanarity, the title molecules are arranged to enable cooperative contribution of larger number of moderately effective non-classical hydrogen bonding interactions in crystal being performed. In addition, intramolecular steric hindrance should oblige title compound **1** to take conformationally fixed single molecular spatial organization. As a result, cumulatively noncovalent-bonding interactions, especially two or more kinds of non-classical hydrogen bonding interactions, are only allowed to function on perpendicular directions not on the same a parallel direction, resulting in stabilization by dimer aggregation and formation of layers composed of the regular-squarely arranged dimeric molecular aggregates for title compound **1**.

In ^1H NMR study, signals of title compound **1** influenced by distinctively different magnetic field effect are observed. These results strongly indicate that conformational flexibility of title molecule **1** is lower than the two homologous molecules. The result indicates that origin of deshielding effect is essentially identical, however the degree against individual protons is different between title compound **1** and homologue **II**. In the case of homologue **II**, induced magnetic field arising from circuit current on 2,7-dimethoxynaphthalene ring core is distributed into two protons (**f** and **f'**) at 1- and 3- positions of the 2-naphthoyl group with comparative magnitude but on opposite directions when observed chemical shifts are compared to the estimated ones.

On the other hand, the induced magnetic field influences apparently into only 2-positioned proton (**f**) of 1-naphthoyl group in title compound **1**. This implicitly leads us to the conclusion that the naphthalene ring of 2-naphthoyl group in homologue **II** is considered loosely fixed to the 2,7-dimethoxynaphthalene ring and swaying, whereas that of 1-naphthoyl group in title compound **1** plausibly is almost fixed in some perpendicular fashion against the 2,7-dimethoxynaphthalene ring. Naturally, the 2-positioned methoxy group of the 2,7-dimethoxynaphthalene ring in title compound **1** might be influenced strongly by induced magnetic field arising from circuit current on the fixed 1-naphthoyl group. The concluded relative degree of fixation of conformation derived from ^1H NMR analyses show good agreement with elucidated characteristics of crystal structures.

Spatial organizations of these compounds in crystal and in solution are commonly interpreted from the point of intermolecular steric hindrance of individual compounds that determines the molecular conformational flexibility and potential for formation of effective non-classical hydrogen bonding interactions.

Acknowledgements

The authors express their gratitude to Professor Keiichi Noguchi, Instrumentation Analysis Center, Tokyo University of Agriculture & Technology, for technical advice.

References

- (a) Desiraju, G. R., *Chem. Commun.*, **1997**, 1475–1482. (b) Desiraju, G. R., Steiner, T., *The Weak Hydrogen Bond in Structural Chemistry and Biology*, **1999**, Oxford University Press. (c) Kupcewicz, B., Malecka, M., *Cryst. Growth Des.*, **2015**, *15*(8), 3893–3904. (d) Tsuzuki, S., Hayamizu, K., Seki, S., *J. Phys. Chem. B*, **2010**, *114* (49), 16329–16336. (e) Tsuzuki, S., Orita, H., Honda, K., Mikami, M., *J. Phys. Chem. B*, **2010**, *114*(49), 16329–16336. (f) Tsuzuki, S., Sato, N., *J. Phys. Chem. B*, **2013**, *117*(22), 6849–6855. (g) Hisaki, I., Sasaki, T., Tohnai, N., Miyata, M., *Chem. Eur. J.*, **2012**, *18*(33), 10066–10073. (h) Miyata, M., Tohnai, N., Hisaki, I., *Acc. Chem. Res.*, **2007**, *40*, 694–702.
- (a) Meyer, F., Dubois, P., *CrystEngComm*, **2013**, *15*, 3058–3071. (b) Wilcken, R., Zimmermann, M. O., Lange, A., Joerger, A. C., Boeckler, F. M., *J. Med. Chem.*, **2013**, *56*, 1363–1388.
- (a) Riley, K. E., Murray, J. S., Fanfrlík, J., Rezáč, J., Solá, R. J., Concha, M. C., Ramos, F. M., Politzer, P., *J. Mol. Model.*, **2013**, *19*, 4651–4659. (b) Metrangolo, P., Neukirch, H., Pilati, T., Resnati, G., *Acc. Chem. Res.* **2005**, *38*, 386–395.
- (a) Okamoto, A., Yonezawa, N., *Chem. Lett.*, **2009**, *38*, 914–915. (b) Okamoto, A., Mitsui, R., Yonezawa, N., *Chem. Lett.*, **2011**, *40*, 1283–1284.
- (a) Mohri, S., Ohisa, S., Isozaki, K., Yonezawa, N., Okamoto, A., *Acta Cryst.*, **2015**, *C71*, 344–350. (b) Mohri, S., Ohisa, S., Tsumuki, T., Yonezawa, N., Okamoto, A., *Acta Cryst.*, **2014**, *E70*, 278–280. (c) Yoshiwaka, S., Sasagawa, K., Noguchi, K., Yonezawa, N., Okamoto, A., *Acta Cryst.*, **2014**, *C70*, 1096–1100. (d) Narushima, S., Mohri, S., Yonezawa, N., Okamoto, A., *Acta Cryst.*, **2014**, *E70*, 170–173.
- (a) Hijikata, D., Takada, T., Nagasawa, A., Okamoto, A., Yonezawa, N., *Acta Cryst.*, **2010**, *E66*, o2902–o2903. (b) Mitsui, R., Nagasawa, A., Noguchi, K., Okamoto, A., Yonezawa, N., *Acta Cryst.*, **2010**, *E66*, o1790. (c) Sasagawa, K., Takeuchi, R., Kusakabe, T., Yonezawa, N., Okamoto, A., *Acta Cryst.*, **2013**, *E69*, o444–o445.
- Okamoto, A., Yonezawa, N., *J. Synth. Org. Chem. Jpn.*, **2015**, *73*(4), 339–360.
- (a) Yoshiwaka, S., Hijikata, D., Yonezawa, N., Okamoto, A., *Eur. Chem. Bull.*, **2015**, *4*(4), 202–206. (b) Yoshiwaka, S., Ohisa, S., Yonezawa, N., Okamoto, A., *Eur. Chem. Bull.*, **2014**, *3*(12), 1142–1147. (c) Okamoto, A., Yoshiwaka, S., Mohri, S., Hijikata, D., Yonezawa, N., *Eur. Chem. Bull.*, **2014**, *3*(8), 829–834. (d) Okamoto, A., Tsumuki, T., Yonezawa, N., *Eur. Chem. Bull.*, **2015**, *4*(11), 522–530.
- Kato, Y., Takeuchi, R., Muto, T., Okamoto, A., Yonezawa, N., *Acta Cryst.*, **2011**, *E67*, o668.
- Tsumuki, T., Murohashi, S., Nagasawa, A., Okamoto, A., Yonezawa, N., *Acta Cryst.*, **2012**, *E68*, o2653.
- Armarego, W. L. F., Chai, C. L. L., *Purification of Laboratory Chemicals, Seventh edition*, **2013**, Elsevier Inc., Oxford.
- Kuwano, R., Morioka, R., Kashiwabara, M., Kameyama, N., *Angew. Chem. Int. Ed.*, **2012**, *51*, 4136–4139.
- Eaton, P., Carlson, G. R., Lee, J. T., *J. Org. Chem.*, **1973**, *38*, 4071–4073.
- Burla, M. C., Caliandro, R., Camalli, M., Carrozzini, B., Cascarano, G. L., De Caro, L., Giacovazzo, C., Polidori, G., Siliqi, D., Spagna, R., *J. Appl. Cryst.*, **2007**, *40*, 609–613.
- Burnett, M. N., Johnson, C. K., *ORTEP III*. Report ORNL-6895, **1996**. Oak Ridge National Laboratory, Tennessee, USA.
- CCDC-1439406 contains the supplementary crystallographic data for this paper. These data can be obtained free of charge from The Cambridge Crystallographic Data Centre via www.ccdc.cam.ac.uk/data_request/cif.

- ¹⁷(a) Zakaria, C. M., Ferguson, G., Lough, A. J., Glidewell, C., *Acta Cryst.*, **2001**, C57, 914–917. (b) Yasodha, V., Govindarajan, S., Low, J. N., Glidewell, C., *Acta Cryst.*, **2007**, C63, m207–m215. (c) Fukunaga, T., Kashino, S., Ishida, H., *Acta Cryst.*, **2004**, C60, o718–o722. (d) Ravikumar, K., Sridhar, B., *Acta Cryst.*, **2009**, C65, o502–o505.
- ¹⁸(a) Nagaraj, B., Narasimhamurthy, T., Yathirajan, H. S., Nagaraja, P., Narasegowda, R. S., Rathore, R. S., *Acta Cryst.*, **2005**, C61, o177–o180. (b) Castillo, J. C., Abonía, R., Cobo, J., Glidewell, C., *Acta Cryst.*, **2009**, C65, o303–o310.
- ¹⁹Tsumuki, T., Isogai, A., Kawano, H., Yonezawa, N., Okamoto, A., *Acta Cryst.*, **2013**, E69, o663.

Received: 05.06.2016.

Accepted: 29.07.2016.



COPPER-NICKEL TARTARATES COMPOSITES: A REUSABLE AND GREEN CATALYSTS FOR THE SYNTHESIS OF QUINOLINES AND DIHYDROPYRIMIDINES DERIVATIVES

S. S. Pawar^[a], C. S. Patil^[b], V. B. Tadke^[a], S. M. Vhankate^[a], S. A. Dhanmane^[a] and R. P. Pawar^{[b]*}

Keywords: Cu-Ni-Tartarate, composites, catalysts, quinolines, Biginelli reaction, dihydropyrimidines.

A series of Cu-Ni tartarate composites at various compositions is prepared and used as green catalyst for the synthesis of quinoline and dihydropyrimidine derivatives. Time required for the completion of reaction using such new catalyst is comparatively less and affording high percentage yield of products.

* Corresponding Authors
E-Mail: rppawar@yahoo.com

- [a] Department of Chemistry, Fergusson College, Pune, Maharashtra, India
[b] Department of Chemistry, Deogiri College, Aurangabad, Maharashtra, India

precursor of 8-hydroxy quinoline which is a versatile chelating agent and precursor to pesticides. Oxidation of quinoline affords quinolinic acid, a precursor to herbicide sold under the name "Assert". These compounds were synthesized by different methods reported using various catalysts.⁷⁻¹⁷

INTRODUCTION

A wide range of organic reactions take place only in presence of suitable catalyst under suitable conditions. Different organic reactions have been reported using various heterogeneous catalysts such as synthesis of spirochromenes and spiroacridines,¹ and 3,4-dihydropyrimidinones² using ammonium chloride. A novel method is reported for the synthesized 3,4,5-trisubstituted furan-2(5H)-ones by the three component reaction between aldehyde, amine and diethyl acetylene dicarboxylate using β -cyclodextrin supramolecule and $\text{SnCl}_2 \cdot 2\text{H}_2\text{O}$ as catalyst respectively.³⁻⁴

Several natural products possessing interesting biological activities containing the dihydropyrimidine-5-carboxylate core have recently been isolated. An electron donating group at *para* position of the aromatic aldehydes readily gives dihydropyrimidines (DHPMS) as compare to electron withdrawing groups.

Biginelli reaction was invented for the synthesis of pyrimido[4,5-d]pyrimidine via one-pot condensation of 1,3 diketone, urea and aldehydes. Recently, the modification of Biginelli reaction is reported using catalyst KHSO_4 ⁵ and other basic catalysts.⁶

Quinoline derivatives also called 1-azanaphthalene or benzo[b] pyridine received increasing attention due to their wide biological and pharmacological activities. These derivatives belongs to important heterocyclic compounds that constitute core structure of many naturally occurring substance that have interesting biological & pharmaceutical properties like anti-malarial, anti-inflammatory, anti-microbial, anti-cancer, anti-HIV, etc. It is used as a principal

Previously, we have synthesized and characterized mixed metal oxalate and tartarate complexes.¹⁸⁻¹⁹ Present investigation focuses on the synthesis of quinoline and dihydropyrimidine derivatives using different composition of copper nickel tartarates $[\text{Cu}_x\text{Ni}_{1-x} (\text{C}_4\text{H}_4\text{O}_6)] \cdot \text{H}_2\text{O}$ as catalysts.

Experimental

All chemicals used were of analytical grade and used without further purifications. Copper-Nickel tartarates with different composition ($x = 0.2$ to 1.0) were prepared and characterized by the methods and techniques reported earlier.¹⁸⁻¹⁹

Synthesis of quinolines

In a 50 mL round bottom flask, to a mixture of substituted anilines (1 mol) and ethylacetoacetate (1 mol) 5 mol % catalyst in ethanol (15 mL) was added. The reaction mixture was refluxed at 120°C for appropriate time. After completion of reaction (confirmed by TLC), the reaction mixture was diluted with cold water. The separated solid product was filtered on suction pump, washed several times with cold water. The crude product was recrystallized from ethanol solvent. The product formation was confirmed on the basis of melting point and spectral data analysis. Using the same procedure other derivatives has been also prepared and confirmed by spectral analysis.

Synthesis of dihydropyrimidines

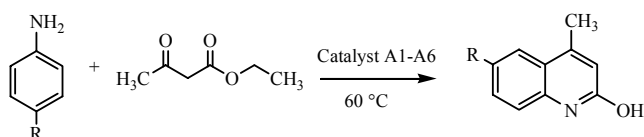
In a typical procedure, to a mixture of 1.10 mL of benzaldehyde (1 mol), 1.30 mL of ethylacetoacetate (1 mol),

0.9 g of urea (1 mol) and catalytic amount of Cu-Ni tartarate composites (six different weight proportions) was refluxed for 4 to 4.30 h. It was cooled to room temperature and poured onto ice cold water. The separated solid product was filtered and recrystallized using ethanol solvent. Above experimental procedure of dihydropyrimidines synthesis is repeated for the synthesis of other derivatives confirmed on the basis of melting points and spectral analysis.

Results and discussion

In continuation of our earlier work, various quinolines have been synthesized by the cyclocondensation of aromatic amines with different 1,3 diketone using Cu-Ni-Tartarate composites as a catalyst (Scheme 1).

The reaction time and the yield of product of the reaction of substituted aniline with ethyl acetoacetate are given in table 1.

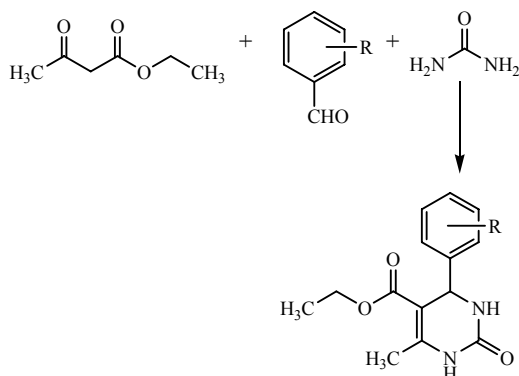


Scheme 1. Synthesis of quinolines.

Table 1. Synthesis of substituted quinolines.

S. No.	R	Time (Min)	Yield (%)
1	H	20	90
2	Cl	10	89
3	Br	15	90
4	NO ₂	25	91
5	OMe	15	87
6	Me	18	82

Synthesis of Biginelli dihydropyrimidines and their derivatives has been carried out by the condensation of 1,3 diketone, urea and aldehydes using Cu-Ni-Tartarate composites as a catalyst (Scheme-2).



Scheme 2. Synthesis of Biginelli dihydropyrimidines.

The reaction time and the yield of products of the reaction of different aromatic aldehydes with ethyl acetoacetate are given in Table 2.

Table 2. Synthesis of Biginelli dihydropyrimidines.

S. No.	Ar	Time, h	Yield	m. p., °C
1	C ₆ H ₅	1.30	92 %	205-207
2	4-OHC ₆ H ₄	1.35	94 %	221-222
3	4-OCH ₃ C ₆ H ₄	1	92 %	198-200
4	4-OH-3-OCH ₃ C ₆ H ₃	1.45	91 %	257-259
5	3,4-(OCH ₃) ₂ C ₆ H ₃	1.15	88 %	172-173
6	4-NO ₂ C ₆ H ₄	1	87 %	209-211
7	4-ClC ₆ H ₄	1.2	92 %	211-213
8	4-BrC ₆ H ₄	1.5	92 %	212-214
9	3-NO ₂ C ₆ H ₄	1.2	90 %	208-201
10	2-ClC ₆ H ₄	1.2	94 %	213-215
11	2-Furyl	1.2	89 %	208-210

It is observed that Cu-Ni tartarates composites behave as suitable catalyst in the synthesis of quinoline and dihydropyrimidine derivatives. During synthesis of quinolines and dihydropyrimidines, the time required for completion of reaction using new catalyst is comparatively less. Percentage yield of products are slightly higher in presence of new catalyst for the synthesis of quinolines and dihydropyrimidines. These composites have active centre present in the structure and behave like Lewis acid, hence show a powerful catalytic activity toward synthesis of quinoline and dihydropyrimidine derivatives. Moreover, the catalyst is reusable, thus used several time in reactions without losing their efficiency.

It is further noted that new catalyst having higher percentage of Cu/Ni-tartarate is remarkably more active for the synthesis of quinolines (Table 3 and Table 4). The catalytic activity of A1 Cu/Ni-tartarate can be explained on the basis of more active centers and more surface area present as compare to other catalysts. Activity of new catalysts also depends on temperature. As the reaction temperature changes from room temperature up to 60 °C, the time required for completion of reaction is reduced and yield of product quinolines also increases to certain extent.

Similarly, new catalyst having more percent of Ni/Cu-tartarate is remarkably more active for the synthesis of dihydropyrimidines (Table 5 and Table 6). The catalytic activity of A4 Ni/Cu-tartarate may be explained on the basis of more active centers and more surface area present as compare to other catalyst. Activity of new catalysts also depends on temperature. As the reaction temperature changes from room temperature upto 80 °C, it is observed that the time required for completion of reaction is less and also yield of product dihydropyrimidines increases to certain extent. This temperature effect is due to the fact that, at higher temperature available kinetic energy is more than that of room temperature. It is observed that electron donating group at *para* position readily gives DHPMS as compare to electron withdrawing groups at respective positions of aromatic aldehydes.

Table 3. Time required for completion and yield of Quinoline using new catalysts.

Catalyst	Time of	% Yield
InCl ₃ (Control)	125	75
A1 - Cu(0.8)Ni(0.2) (C ₄ H ₄ O ₆).x H ₂ O	30	81
A2 - Cu(0.6)Ni(0.4) (C ₄ H ₄ O ₆).x H ₂ O	28	86
A3 - Cu(0.4)Ni(0.6) (C ₄ H ₄ O ₆).x H ₂ O	25	91
A4 - Cu(0.2)Ni(0.6) (C ₄ H ₄ O ₆).x H ₂ O	40	78
A5 - Cu(C ₄ H ₄ O ₆).x H ₂ O	45	80
A6 - Cu(0.1) (C ₄ H ₄ O ₆). x H ₂ O	47	77

Table 4. Effect of reaction temperature on the yield of quinoline using catalyst A3.

S. No.	Reaction	Time for	% Yield
1	23 °C	25 min	26
2	75 °C	25 min	71
3	100 °C	25 min	82
4	120 °C	25 min	91

Table 5. Time required for completion and yield of dihydropyrimidines using new catalysts.

Catalyst	Time of	%
Conc. HCl (Control)	4 to 4.30	70
A1 - Cu(0.8)Ni(0.2)(C ₄ H ₄ O ₆).x H ₂ O	3.00 to 3.30	72
A2 - Cu(0.6)Ni(0.4) (C ₄ H ₄ O ₆).x H ₂ O	3.15 to 3.30	69
A3 - Cu(0.4)Ni(0.6) (C ₄ H ₄ O ₆).x H ₂ O	2.30 to 2.45	73
A4 - Cu(0.2)Ni(0.6) (C ₄ H ₄ O ₆).x H ₂ O	1.30 to 2.00	84
A5 - Cu(C ₄ H ₄ O ₆).x H ₂ O	1.30 to 2.00	65
A6 - Cu(0.1) (C ₄ H ₄ O ₆). x H ₂ O	1.30 to 2.00	75

Table 6. Effect of reaction-temperature during synthesis of Dihydropyrimidine derivative using catalyst A4.

S. No.	Reaction	Time of completion	% Yield
1	23 °C	50 min	56
2	45 °C	40 min	68
3	60 °C	30 min	79
4	80 °C	30 min	87

Characterization of quinoline and dihydropyrimidine derivatives

4-Methyl-2-hydroxyquinolines (Entry 1, Table 1): ¹H NMR (400 MHz, DMSO-d₆): δ ppm 2.41 (s, 3H, C₄-CH₃), 6.21 (s, 1H, C₃-H), 7.35-8.18 (m, 4H, Ar-H), 11.68 (s, 1H, NH). IR (KBr) cm⁻¹ 1334, 1512, 2478, 3403.

4-Methyl-6-bromo-2-hydroxyquinolines (Entry 3, Table 1): ¹H NMR (400 MHz, DMSO-d₆): δ ppm 2.43 (s, 3H, C₄-CH₃), 6.22 (s, 1H, C₃-H), 7.35-8.26 (m, 3H, Ar-H), 11.65 (s, 1H, NH). IR (KBr) cm⁻¹ 1338, 1510, 2485, 3408.

4,6-Dimethyl-2-hydroxyquinolines (Entry 6, Table 1): ¹H NMR (400 MHz, DMSO-d₆): δ ppm 2.42 (s, 3H, C₄-CH₃), 2.44 (s, 3H, C₆-CH₃), 6.23 (s, 1H, C₃-H), 7.36-8.21 (m, 3H, Ar-H), 11.65 (s, 1H, NH). IR (KBr) cm⁻¹ 1338, 1510, 2485, 2864, 3415.

5-Ethoxycarbonyl-6-methyl-4-(4-hydroxyphenyl)-3, 4-dihydropyrimidine-2(1H)-one (Entry 2, Table 2): m.p. 221-222 °C; ¹H NMR (400 MHz, CDCl₃): δ ppm 1.6 (t, 3H), 1.9 (s, 3H), 4.65 (q, 2H), 5.05 (s, 1H), 5.8 (s, 2H), 5.5 (s, 1H), 6.6 (d, 2H), 7.05 (d, 2H); ¹³C NMR (100 MHz, CDCl₃): δ ppm 23.123, 24.011, 29.726, 50.001, 62.584, 117.356, 121.814, 127.645, 136.015, 145.143, 153.468, 169.542; IR (KBr) cm⁻¹ 3383, 3236, 2920, 1627, 1516, 1447.

5-Ethoxycarbonyl-6-methyl-4-(4-methoxyphenyl)-3, 4-dihydropyrimidine-2(1H)-one (Entry 3, Table 7): m.p. 198-200 °C; ¹H NMR (400 MHz, CDCl₃): δ ppm 1.15 (t, 3H), 2.29 (s, 3H), 3.72 (s, 3H), 4.05 (q, 2H), 5.28 (s, 1H), 6.20 (brs, 1H, NH), 6.84 (d, 2H), 7.21 (d, 2H), 8.75 (brs, 1H, NH); ¹³C NMR (100 MHz, CDCl₃): δ ppm 14.404, 16.742, 55.47, 60.18, 67.301, 101.723, 114.154, 128.039, 136.494, 146.399, 154.021, 159.421, 165.365; IR (KBr) cm⁻¹ 3276, 3112, 2979, 2826, 1614, 1512, 1720, 1653, 1463, 1082, 842.

Conclusion

A new approach for the synthesis of quinolines and dihydropyrimidines has been developed using new Cu-Ni tartarate composites catalysts.

References

- Dabiri M., Bahramnejad M., Baghbanzadeh M., *Tetrahedron*. **2009**, *65* (45), 9443-9447.
- Shaabani A., Bazgir A., Teimouri F., *Tetrahedron Lett.* **2003**, *44*(4), 857-859.
- Murthy S. N., Madhav B., Kumar A. V., Rao K. R., Nageswar Y. V. D., *Tetrahedron*. **2009**, *65*(27), 5251-5256.
- Nagarapu L., Kumar U. N., Upendra P., Bantu R., *Synth. Comm.* **2012**, *42*(14), 2139-2148.
- Shi F., Jia R., Zhang X., et al., *Synthesis*. **2007**, *18*, 2782-2790.
- Sharma P., Rane N., Gurrani V. K., *Bioorg. Med. Chem. Lett.* **2004**, *14*, 4185-4190.
- Kidwai, Mazaahir B., Vikas M., Neeraj K. B., Divya., *Indian J. Chem.*, **2009**, *48B* (5), 746-748.
- Mehdi A., Mohammad M., Sharareh B., Long-Guan Z., Mehdi R.N., *Tetrahedron Lett.*, **2010**, *51*, 27-29.
- Manas C., Ajanta M., Sulakshana K., Ratna M., Kenichiro N., Athina G. and Pitta E., *ARKIVOC*. **2010**, *11*, 265-290.
- Tian L., Xian X. Y., Jiang H. Y., Chao J., Yu S. W., Hui J. Z., Zi F. M., Wei D. Y., *Chinese Chemical Letters*, **2011**, 253-255.
- Revanasiddappa B. C., Subrahmanyam E. V. S., Satyanarayana D., John Thomas, *Int. J. Chem. Techn Res.*, **2009**, *1* (4), 1100-1104.
- Swenson R. E., Sowin T. J., Zhang H. Q., *J. Org. Chem.* **2002**, *67*, 9182-9185.
- Cho C. K., Hooh B., Shim S.C., *J. Heterocycl. Chem.* **1999**, *36*, 1175-1178.
- Makioka Y., Shindo T., Taniguchi Y., Takaki K., Fujiwara Y., *Synthesis*. **1995**, 801-806.
- Sangu K., Fuchibe K., Akiyama T., *Org. Lett.* **2004**, *6*, 353-355.
- Crousse B., Begue J. P., Bonnet-Delpon D., *Tetrahedron Lett.* **1998**, *39*, 5765-5768.
- Crousse B., Begue J. P., Bonnet-Delpon D., *J. Org. Chem.* **2000**, *65*, 5009-5013.

¹⁸Pawar S. S., Patil C. S., Tadke V. B., Vhankate S. M., Dhanmane S. A., Pathade G. R. and Pawar R. P., *Int J Pharm Sci Res.* **2014**, 5(4), 1557-65.

¹⁹Vhankate S. M., Pawar S. S., Dhanmane S. A., Dhavale N. S., Fulzele K., Patil C. S., Pawar R. P. and Tadke V. B., *SRTMU's Res. J. Sci.* **2013**, 2(1), 88 – 100.

Received: 30.04.2016.
Accepted: 31.07.2016.



FUNGAL STRAIN OF *ASPERGILLUS ORYZAE* IMMOBILIZED ON SILICA GEL FOR Au(III) SORPTION

Dnyaneshwar K. Kulal^[a], Amol V. Pansare^[a], Amol A. Shedje^[a] and Vishwanath R. Patil^{[a]*}

Keywords: Pharmaceutical formulated product, *Aspergillus oryzae*, immobilization, atomic absorption spectroscopy, solid phase extraction.

Biomasses have significant impact on the development of new solid phase extraction methods for metal analysis. Adsorbent, prepared by incorporating dried biomass (*Aspergillus oryzae*) immobilized on activated silica, was presently developed for Au(III) enrichment. The main factors affecting the adsorption-desorption process like pH, sample volume, eluent and eluent flow rate were optimized. Under the optimum conditions, good recovery was obtained at about 99.4 ± 0.1 %, performed by Flame Atomic Absorption Spectrometry. At optimized pH 2.0, Au(III) was quantitatively sorbed and recovered with 1:1 mixture of 0.2 M HCl mixed with 0.2 M thiourea. The enrichment factor was found as 125, and the limit of detection is $0.88 \mu\text{g L}^{-1}$ whereas limit of quantification is $2.93 \mu\text{g L}^{-1}$. The proposed method was successfully applied in the analysis of tap water, pharmaceutical formulated product and synthetically prepared dummy sample. Equilibrium data also were fitted by linear regression methods through Langmuir, Freundlich, Temkin, Dubinin and Radushkevich (D-R) and Harkin –Jura isotherm models.

*Corresponding Authors

E-Mail: vishwanathpatil03@gmail.com

[a] Department of Chemistry, University of Mumbai, Santacruz (E), Mumbai – 400 098, India

Introduction

It is well known that Au (III) has received an increasing amount of attention in research due to its wide applications in industries, utilization in Chemistry, biology, medicine, corrosion resistant as well as economic activity and occurrence on the Earth at very low natural content.¹⁻² The concentration of Au(III) in environmental samples is extremely low, e.g. 0.5 ng g^{-1} for 10 g samples (rocks, sediments, soils) and 0.05 ng mL^{-1} for 1 L water samples reported by Medve in 2004.³ Hence determination of Au (III) in environmental and biological samples is difficult. Therefore, it is a challenge for researchers to develop an effective method for analysis of trace level of Au (III).^{4,5}

Commonly used techniques for elemental Au (III) analysis is Flame Atomic Absorption Spectrometry (FAAS) and Inductively Coupled Plasma Atomic Emission Spectrometry (ICP-AES), however, they suffer from spectral and chemical interferences. Separation and pre-concentration is an essential step for the accurate measurement and analysis of the various metal species.^{6,7} To enhance the accuracy and sensitivity in the determination of Au (III), an enrichment step is necessary.⁸ Nowadays, solid phase extraction (SPE) has gained importance as a separation and pre-concentration method as it is a clean, simple, flexible technique with availability of a large number of sorbents.^{9,10} For the determination of Au(III), many solid phase extraction methods have been developed e.g., polyethylenimine (PEI) ion-exchange polymer which is coated with alumina in the presence of NaNO_3 ,¹¹ rubeanic acid (dithiooxamide) chelate on silica gel,¹² cysteine modified silica gel (SiG-cys),¹³

multiwalled carbon nanotubes (MWNTs),¹⁴ octadecyl silica membrane disks modified by pentathia-15-crown-5,¹⁵ and low density polyhydroxy polyurethane foam (LPPF)¹⁶ as a solid support material. Due to availability, less environmental contamination and cost, biosorbents have gained an advantage in solid phase extraction,^{17,18}

Biosorption involves the use of immobilized biomass for heavy metal removal.¹⁹ Sorbents such as *Fomitopsis carnea*,²⁰ *L-cysteine*,²¹ *tricarbohydrazide modified attapulgite*,²² oat and wheat biomasses,²³ and *sargassum natans*²⁴ have been reported for Au(III) sorption-desorption. Heavy metal decontamination using live cells often causes restriction, as a continuous supply of nutrient is required and there is also the possibility of toxicity to the microorganism. This can be overcome by the use of dead microbial biomass, which involve the use of ion exchange as a mechanism for transport through the cell wall and does not require the significant condition for the maintenance of a viable biomass.

Fungal biomass is advantageous due to low cost and easy availability from fermentation and pharmaceutical industries.²⁵ Dead cells of different varieties of *Aspergillus oryzae* species have been utilized for heavy metal removal. The treatment of biomass with activated silica shows significant changes in the cell wall.²⁶ Alkali treatment of *Tolypocladium* and *Penicillium oxalicum* species improves deacetylation of chitin and causes an increase in the binding sites, thereby enhancing the sorption capacity significantly.²⁷

In the present work, a newly developed sorbent, based on *Aspergillus oryzae* immobilized on activated silica (AOAS) has been investigated for enrichment of Au (III). Sorbet was successfully applied for Au (III) enrichment from the Ayurvedic formulated product, dummy sample and tap water prior to its FAAS determination.

Experimental

The determination of Au (III) was carried out using a flame atomic absorption spectrophotometer *AA*Analyst 200 (Perkin Elmer, USA) equipped with an air-acetylene burner with deuterium arc background correction. The Au(III) hollow cathode lamp was operated at 10 mA current. The absorbance was measured at 217 nm with a spectral band width of 0.5 nm. The pH values were measured with Elico LI-127 digital pH meter (Elico India Ltd., India) supplied with a combined glass electrode. Double distilled water was obtained from LAB-SIL quartz double distiller (LAB-SIL Instruments Pvt. Ltd., India). A glass column (150 mm x 10 mm, J-sil, India make) was used for column studies. The fungal biomass was separated from liquid media using research centrifuge Model R-24 (REMI, India). Fourier transforms infrared spectrometer, model Spectrum one FTIR spectrometer (Perkin Elmer, USA) was used for characterization of sorbent. Scanning electron microscopy (SEM) [QUANTA-200, FEI Ltd., Netherlands] was used for surface morphological study.

Reagents and solutions

The stock standard solution containing 1000 mg L⁻¹ solution of Au (III) was prepared by dissolving appropriate amount of (HAuCl₄.H₂O) from Sisco Research Laboratories in slightly acidic double distilled water. The solution was standardized volumetrically,²⁸ and working standard solutions were prepared by appropriate dilution. Silica gel 60-120 mesh which was activated with conc. HCl²⁹ was used as solid support for sorbent preparation. For culture, all media were used from Himedia laboratories Pvt. Ltd. All other chemicals used were of Analytical Reagent grade.

Preparation of *Aspergillus oryzae* immobilized activated silica

A laboratory strain of lyophilized *Aspergillus oryzae* obtained from National Collection of Industrial Microorganism (NCIM), Pune, India was used for sterilization. Sterilization of liquid medium and glass wares was done by autoclaving at 121°C for about 20 min. A fungus cultivated in solid media composed of sabouraud dextrose broth 30 g L⁻¹ and agar 20 g L⁻¹ was used for the growth of the fungal biomass which was preserved by refrigerating at 4°C. Starter culture was prepared by loop full inoculation of the cultivated fungus in 100 mL liquid medium (without agar) which was followed by 48 hrs incubation at 25 °C. Experimental culture was prepared using 250 mL of liquid medium inoculated with 5 mL of the starter culture. After incubation the biomass was stored for 25 days at 25°C. The growth media was then centrifuged at 7500 rpm for 30 min for separation of biomass. The residual biomass was then thoroughly washed with double distilled water number of times to ensure removal of residual growth and was followed by oven drying of the fungal biomass at 80 °C for 24 h, which was then grounded and sieved through a 100 mesh sieve. The dead cells of *Aspergillus oryzae* were used for immobilization on activated silica for preparation of the sorbent.

Exactly 100 mg, 150 mg, 200 mg of the biomass was homogenized with 1.0 g of activated silica and wetted with double distilled water. The paste was kept for drying in an

oven at 40, 60 and 80 °C for 1h. The wetting and drying step was repeated till *Aspergillus oryzae* got immobilized on silica. FTIR spectroscopy was used for characterization of this prepared sorbent. This AOAS sorbent was used for all studies.

General procedure

A glass column packed with 350 mg of the AOAS was pre-conditioned to the desired pH by double distilled water adjusted using dilute NH₃ and HCl. A sample solution containing 20 µg of Au(III) was adjusted to the appropriate pH and passed through the column. The sorbed Au(III) was eluted with 10.0 mL of 1:1 mixture (0.2 M HCl + 0.2 M thiourea) and its concentration was determined by FAAS.

Determination of Au(III) in Ayurvedic sample

Initially 10 powdered gold containing tablets were transferred into a platinum crucible and incinerated in a muffle furnace, gently at first, the temperature was then gradually increased to around 600 to 700 °C for three h to remove carbon from sample.³⁰ After cooling, remaining powder was dissolved in aqua regia to extract Au(III) and diluted to 250 mL with double distilled water.

Determination of Au(III) in dummy prepared sample

Separate solutions containing calcium (100 mg L⁻¹), potassium (1000 mg L⁻¹), sodium (1000 mg L⁻¹), chloride (1000 mg L⁻¹) and Au(III) (100 mg L⁻¹) were prepared. From above solutions 38 mL, 16.2 mL, 17.8 mL, 3.6 mL and 4.6 mL of Ca, K, Na, chloride and Au(III) respectively were taken, mixed to equilibrate and diluted up to in 250 mL.

Batch adsorption studies

A batch adsorption study was done using AOAS shaking with 100 µg ml⁻¹ solution on wrist action mechanical shaker. The effect of variables such as solution pH, contact time, initial adsorbate concentration and revolution per minutes (rpm) was studied. Equilibrium studies were conducted with 50 mg of AOAS sorbent, which was added to 50.0 mL aqueous solution of Au(III) (10-480 µg 50 mL⁻¹) in reagent bottles and pH adjusted to 2 at 31 °C. The solutions were agitated on a wrist action mechanical shaker for 15 min at 140 rpm. Desorption of Au(III) from the modified sorbent was done by shaking the sorbed resin after filtration, with 1:1 mixture of 0.2 M HCl + 0.2 M thiourea for 30 min at 180 rpm. After equilibration, the phases were filtered and analysed by FAAS.

Results and discussion

Characterization of AOAS

The immobilization of *Aspergillus oryzae* on activated silica and Au(III) sorbed on sorbent was checked by FTIR spectrum (Figure1). The peak observed at 1069.85 cm⁻¹ was assigned for Si–O–Si stretching. Another peak observed at 974.62 cm⁻¹ indicated the presence of Si–O–H stretching

vibrations of activated silica (Figure 1A),³¹ where as band observed at 947.46 cm^{-1} was unchanged during sorption-desorption. While, the spectrum of AOAS (Figure 1B) showed a band between $3600 - 3200\text{ cm}^{-1}$ due to $-\text{OH}$ groups and bands between $3000 - 2800\text{ cm}^{-1}$ were assigned to stretching vibrations of CH_2 and CH_3 groups. A peak observed at 1652.43 cm^{-1} was attributed to $\text{C}=\text{O}$ stretching in carboxyl or amide groups on the biomass. The spectrum also showed peaks at 1644.63 cm^{-1} and 1059.25 cm^{-1} which corresponds to the $-\text{N}-\text{H}$ deformation mode coupled with $\text{C}-\text{O}$ stretching from the amide groups present on the cell wall of biomass. A large band with several peaks between $1200 - 800\text{ cm}^{-1}$ may be attributed to the polysaccharide ring present on the biomass.³² A comparison of Figure 1A and B with Figure 1C, showed that peaks observed at 3564.11 , 1644.63 and 796.89 cm^{-1} indicated the immobilization of *Aspergillus oryzae* on activated silica. The spectra showed some variations after Au(III) sorbed on AOAS. As shown in Figure 1D, the peaks observed at 3259.06 cm^{-1} and 1644.63 cm^{-1} disappeared, which proved that the amide group of biomass was involved in the binding of Au(III).

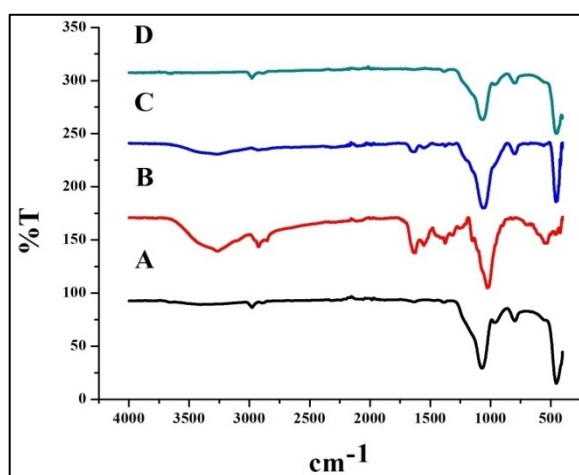


Figure 1. FTIR of (A) activated silica (B) *Aspergillus oryzae* (C) AOAS (D) Au(III) sorbed on AOAS.

Effect of amount of the sorbent and temperature on sorbent recovery

The amount of sorbent is an important parameter that affects the sorption and recovery of the analyte. Quantitative retention is affected when the amount of sorbent varies. For this purpose, different amounts of the sorbent (100–200 mg) were studied. The results showed that quantitative recoveries of the metal ions were obtained when the sorbent quantity was greater than 150 mg. With 100 mg of the sorbent, the lowest recovery was obtained, whereas 150 mg and 200 mg showed quantitative recoveries. Therefore 150 mg was chosen for further experiments.

Temperature is a parameter that affects the physical conditions of biomass. At $40\text{ }^{\circ}\text{C}$ reduction in the recovery of Au(III) was observed, whereas at $80\text{ }^{\circ}\text{C}$ color of the biomass changed which was not useful for further study. At $60\text{ }^{\circ}\text{C}$ temperature quantitative recoveries were obtained, hence this was chosen as the operative temperature.

Characterization of AOAS surface morphology

Scanning electron microscopy (SEM) was used to study the surface morphology of AOAS and for the evaluation of adsorbed Au(III) on AOAS. Figure 2a shows the high-resolution SEM images of AOAS surface while variation in Figure 2b indicated that Au(III) was adsorbed on AOAS. Irregular structure was observed in Figure 2b, indicating the adsorption of Au(III) on AOAS.

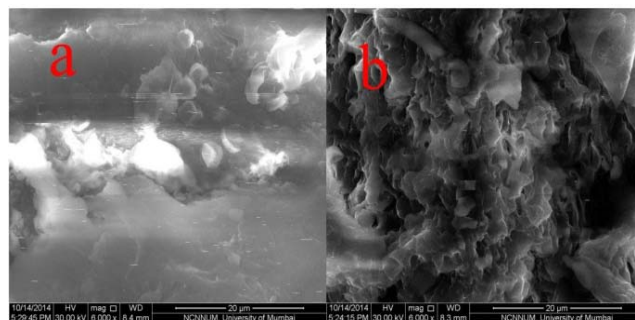


Figure 2. SEM images of (a) AOAS (b) Au(III) adsorbed on AOAS.

Effect of pH

pH is one of the most important parameter, because formation of strength of bond between the metal and microbial biomass varies with pH during the sorption of metal ions. Therefore, sorption of Au(III) on the columns containing AOAS sorbent were studied from pH 1.0 – 6.0 (Figure S1). pH range of 1 to 3 was studied with over ten digits, among which pH 2 showed maximum recovery with more than 99 % adsorption. Au(III) sorption increased with increase in pH on AOAS sorbent and it was quantitative ($99.7 \pm 0.2\%$) at pH 2.0. It was observed that only 45 % of Au(III) was sorbed on activated silica. It clearly indicated that, immobilization of the biomass on silica was necessary for complete sorption of Au(III). Hence, pH 2.0 was considered as the optimum pH used for further studies.

Sample flow rate and sample volume

The flow rate of sample solution has considerable influence on solid phase extraction, as high flow rates diminish the contact between the analyte and sorbent. Au(III) sorption was studied for sample flow rate of $1.0 - 4.0\text{ mL min}^{-1}$. Au(III) was quantitatively sorbed from $1.0 - 3.0\text{ mL min}^{-1}$ sample flow rate. While, flow rate $> 3.0\text{ mL min}^{-1}$ resulted in a decrease of Au(III) sorption. Hence, a sample flow rate of 1.0 mL min^{-1} was maintained in all experiments.

Sample volume is considered as one of the most important parameters studied for real sample analysis in solid phase extraction methods. Sample solution (25 - 1250 mL) containing $20\text{ }\mu\text{g}$ Au(III) at pH 2.0 was passed through the column. The recovery of Au(III) was done quantitatively even up to 1250 mL of sample solution. The eluent volume used was 10 mL. Hence, the pre-concentration factor achieved was 125.

Effect of eluent type and flow rate

The elution studies were performed in order to understand the recovery of Au(III) from AOAS sorbent column. Series of experiments were conducted using different concentrations of HCl and thiourea. Quantitative recovery was accomplished with 1:1 mixture of (0.2 M HCl + 0.2 M thiourea). This mixture was selected as an eluent since preliminary studies indicated that higher concentration of HCl damages biomass of the column.

Au(III) recovery was studied using 5.0 – 15.0 mL of mixture. It was found that 5.0 mL of mixture resulted in 84.3 ± 0.4 % recovery whereas; 10.0 mL and 15.0 mL of mixture gave quantitative recovery. Hence the effect of flow rate was investigated from 0.1 – 1.0 mL min⁻¹ with 10.0 mL mixture. Using of 0.1 mL min⁻¹ and 0.2 mL min⁻¹ flow rates the recovery was 99.4 ± 0.1 % and 98.3 ± 0.1 % respectively. While, at 1.0 mL min⁻¹ flow rate, the recovery decreased to 84.7 ± 0.1 %. Therefore, 10.0 mL of mixture at a flow rate of 0.2 mL min⁻¹ was used as an eluent for all subsequent studies.

Adsorption equilibrium isotherm

Adsorption equilibrium isotherm was studied in terms of following models.

Langmuir Adsorption Isotherm

Langmuir model represents the equilibrium distribution of metal ions between the solid and liquid phases.³³ The Langmuir model is valid for monolayer adsorption on the surface of a finite number of sites. Based upon these assumptions, Langmuir equation³⁴ is given eqn. (1) and (2).

$$\frac{C_a}{q_e} = \frac{1}{q_0 b} + \frac{C_a}{q_0} \quad (1)$$

$$R_L = \frac{1}{1 + bC_0} \quad (2)$$

where

C_e =equilibrium concentration of adsorbate (mg L⁻¹)

q_e =amount of metal adsorbed per gram of the adsorbent at equilibrium (mg g⁻¹),

q_0 =maximum monolayer coverage capacity (mg g⁻¹),

b =Langmuir isotherm constant (L mg⁻¹) and

R_L =separation factor.

The magnitudes of Langmuir constants can be determined from the linear plot of C_e/q_e versus C_e delineated in Figure 3a. Langmuir constant is related to the affinity of binding sites (mL mg⁻¹). It is a measure of energy of adsorption

indicating the adsorption nature to be either unfavorable if $R_L > 1$, linear if $R_L = 1$, favorable if $0 < R_L < 1$ and irreversible if $R_L = 0$. The data obtained indicated that Langmuir isotherm was favorable as value of b was greater than 0 but less than 1. Maximum monolayer coverage capacity (mg g⁻¹) from the Langmuir Isotherm model was obtained to be 9.5328 mg g⁻¹, b was 0.315 L mg⁻¹, R_L (the separation factor), as mentioned in Table S1, was calculated from above equation 2 and the R_L value calculated was 0.936 which indicated that the sorption data fitted well with the Langmuir Isotherm model.

Freundlich Adsorption Isotherm

The Freundlich model assumes a multilayer of adsorption of Au(III) on *Aspergillus oryzae* cell surface. According to Freundlich, the ratio of the amount of solute adsorbed on the biomass to the concentration of solute in the solution is not constant at different concentrations.³⁵ According to this theory, the empirical Freundlich equation based on sorption on a heterogeneous surface area is as follows:

$$q_e = K_f (C_e)^{\frac{1}{n}} \quad (3)$$

where

q_e is the amount of Au(III) adsorbed at equilibrium (mg g⁻¹),

C_e is the equilibrium concentration (mg L⁻¹).

K_f and n are Freundlich constants related to sorption capacity and adsorption intensity respectively.

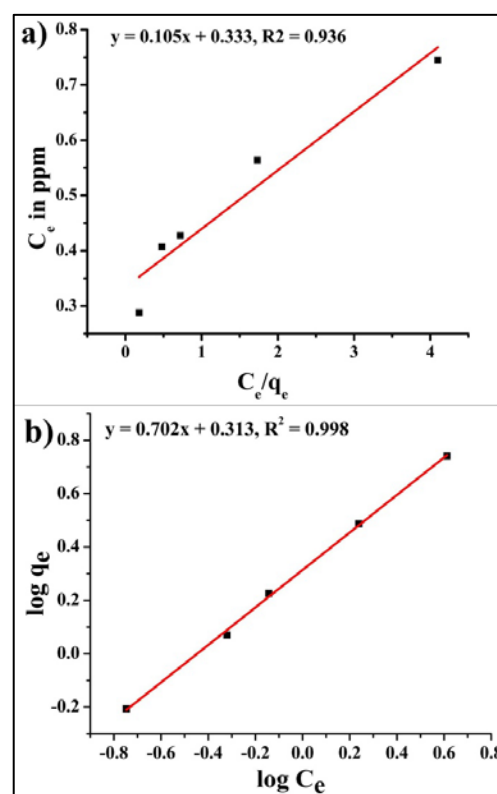


Figure 3. Adsorption isotherms for adsorption of Au (III) and AOAS (a) Langmuir (b) Freundlich.

Eqn. (3) can be linearized in logarithmic form as follows.

$$\log\left(\frac{x}{m}\right) = \log K_f + \left(\frac{1}{n}\right) \log C_e \quad (4)$$

where K_f and $1/n$ are capacity of the adsorbent for the adsorbate and adsorption intensity, respectively.

A linear regression plot of $\log q_e$ versus $\log C_e$ slope gives n value whereas intercept gives K_f value. The sorption capacity constant for Au(III) (K_f) and adsorption intensity of Au(III) (n) were found to be 0.5045 and 1.425 respectively. The value of n was observed to be between 1 to 10, indicating a favourable adsorption of Au(III) on AOAS. The correlation coefficient for the plot of $\log q_e$ vs. $\log C_e$ delineated in Figure 3b was found to be 0.998 indicating a very good fit of the experimental data.

Temkin adsorption isotherm

Temkin adsorption isotherm assumes that binding energy decreases linearly with increasing amount of metal bound to the surface of adsorbent.³⁶ Temkin isotherm has been applied in the form of Eqn. (5).

$$q_e = \frac{RT}{b} \ln A + \frac{RT}{b} \ln C_e \quad (5)$$

where

- b = Temkin constant related to heat of sorption (J mol^{-1}),
- A = the equilibrium binding constant (L g^{-1}),
- R = gas constant ($8.314 \text{ J mol}^{-1} \text{ K}^{-1}$) and
- T = absolute temperature (K).

As implied in the logarithmic form of the equation, uniform distribution of binding energies (up to some maximum binding energy) was carried out by plotting the quantity sorbed q_e against $\ln C_e$ delineated in Figure 4a and the constants were determined from the slope and intercept. The slope and intercept gives the value of Temkin constant related to heat of sorption and equilibrium binding constant respectively. In the present work, the values $A_T = 4.413 \text{ L g}^{-1}$, $RT/b = 3.574 \text{ J mol}^{-1}$ suggested a physical adsorption process whereas correlation coefficient (R^2) was found to be 0.911.

Dubinin–Radushkevich isotherm

Dubinin and Radushkevich (D–R) isotherm³⁷ commonly has been based on adsorption theory applied in the form of Eqn. (6) and its linear form can be shown in Eqn. (7).

$$q_e = q_{\max} \exp\left(-K_{DR} \varepsilon^2\right) \quad (6)$$

$$\log q_e = \log q_{\max} - K_{DR} \varepsilon^2 \quad (7)$$

where

K_{DR} ($\text{mol}^2 \text{ kJ}^{-2}$) is a constant related to the mean adsorption energy,

q_{\max} is the theoretical saturation capacity and ε is the Polanyi potential,

which can be calculated using the equation:

$$\varepsilon = RT \log\left(1 + \frac{1}{C_e}\right) \quad (8)$$

The intercept of the plot of $\log q_e$ versus ε^2 gives adsorption capacity, q_{\max} (mg g^{-1}) and the slope yields the K_{DR} ($\text{mol}^2 \text{ kJ}^{-2}$). R is the universal gas constant ($8.314 \text{ J mol}^{-1} \text{ K}^{-1}$) and T is the absolute temperature in Kelvin.

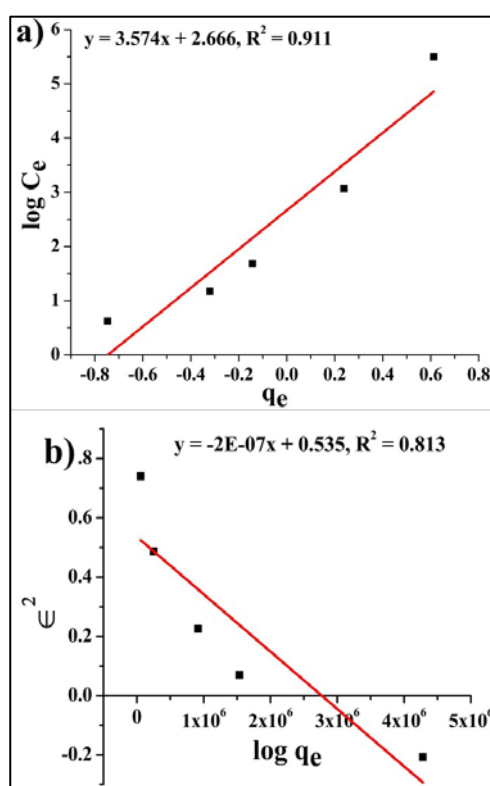


Figure 4. (a) Temkin (b) Dubinin and Radushkevich isotherms for adsorption of Au (III) and AOAS

The mean adsorption energy (E) can be calculated using the following relationship³⁷:

$$E = \frac{1}{\sqrt{-2K_{DR}}} \quad (9)$$

Some parameters were calculated theoretically from the D-R isotherm for Au(III) from Figure 4b. The theoretical saturation capacity (q_{\max}) was found to be 3.43 mg g^{-1}

Au(III) of AOAS, Constant K_{DR} obtained was $2 \times 10^{-7} \text{ mol}^2 \text{ kJ}^{-2}$, mean adsorption energy (E) calculated for Au(III) was 50 kJ mol^{-1} .

Harkin–Jura adsorption isotherm

The Harkin-Jura adsorption isotherm³⁸ can be expressed as eqn. (10).

$$\frac{1}{q_e^2} = \frac{B_2}{A} - \frac{1}{A} \log C_e \quad (10)$$

Harkin-Jura adsorption isotherm is applicable to multilayer adsorption which can be explained with the existence of a heterogeneous pore distribution, where B_2 is Harkin-Jura adsorption constant. Plot of $1/q_e^2$ vs. $\log C_e$ (Figure S2) gives slope and intercept which yields the value of A and B_2 respectively. For the present work the value obtained for $A = 2.3585$, $B_2 = 0.592$ and $R^2 = 0.740$. The lower value of correlation coefficient (0.740) indicated poor applicability of the H-J isotherm.

The adsorption isotherms such as Langmuir, Freundlich, Temkin, Dubinin and Radushkevich (D–R), Harkin-Jura were effectively followed (Table S2).

Mechanism for sorption and desorption of Au(III) on AOAS

During sorption mechanism, pH of the solution plays a major role for adsorption of Au(III) on sorbent. In first step of preparation of biomass activated on silica showed FTIR peak between $3600\text{--}3200 \text{ cm}^{-1}$ which get suppressed, confirming that -OH group is involved in bonding with fungal biomass. Whereas in the case of gold sorption on AOAS bonding was confirmed by SEM as well as disappearance of IR peak of 1644.63 cm^{-1} of amine group. During desorption, thiourea and HCl formed metal complex with gold where thiourea get linked to the central metal through the sulphur atom rather than nitrogen.³⁹ Hence gold shows +1 oxidation state rather than +3. The probable mechanism is shown in Figure 5.⁴⁰

Analytical performances of the method

The limit of detection (LOD) and limit of quantification (LOQ) of the proposed method for the determination of Au(III) was studied under the optimum experimental conditions. The limit of detection is defined as $\text{CLOD} = 3S_b/m$, where S_b is the standard deviation of replicate blank signals, and m is the slope of the calibration curve. The pre-concentration and limit of quantification based on ten times the standard deviations of the blank⁴¹ for Au(III) obtained were $0.88 \mu\text{g L}^{-1}$ and $2.93 \mu\text{g L}^{-1}$ respectively.

Real sample analysis

A tap water sample was analyzed for Au(III) using the standard addition method. The sample was spiked with different amount of Au(III) and passed through the AOAS sorbent packed column under the general procedure for

Au(III) determination. Good agreement was observed between the added and found amount of Au(III) (Table 1). The proposed method was also applied to determine Au(III) in a dummy sample (Table 1).

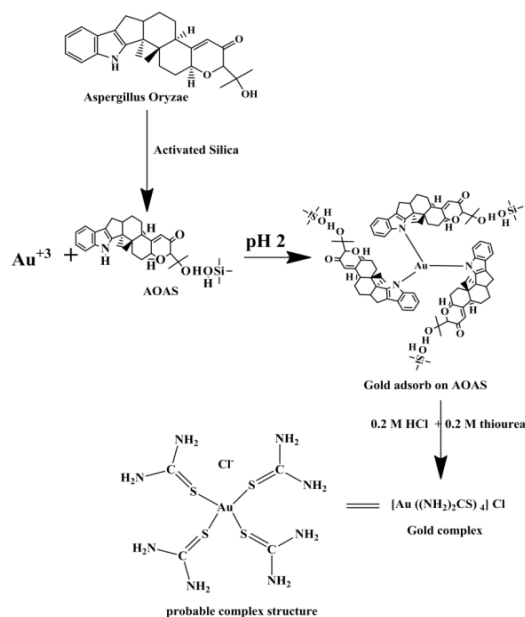


Figure 5. Probable mechanism for sorption and desorption of Au(III) on AOAS.

Table 1. Applications of AOAS method in the recovery of Au(III) in different samples.

Spiking of Au (III) in Tap Water sample			
Added amount	Found amount	Percent Recovery	
1.306± 0.12 mg	1.301± 0.18 mg	99.67± 0.07	
5.176± 0.15 mg	5.125± 0.22 mg	99.01± 0.32	
11.601± 0.11 mg	11.321± 0.30 mg	97.59± 0.40	
Spiking of Au (III) in Dummy sample			
Added volume	Added amount mg	Found amount mg	Percent Recovery
1 mL	0.424± 0.72	0.40± 0.62	94.42± 0.45
5 mL	2.087± 0.02	1.870± 0.85	89.79± 0.82
10 mL	4.027± 0.20	3.47± 0.61	86.25± 0.79
Determination of Au (III) in ayurvedic formulated product			
Item	ICP results mg	AOAS results mg	Percent Recovery
Baidyanath Swarnamalini Basat	84.34±0.025	83.73±0.039	98.09±0.05
Baidyanath Swog Chintumani	66.08±0.065	56.23± 0.311	85.09±0.35

During sorption, as the volume of dummy sample increases, matrix inserted in the sample was directly proportional to the volume of Au(III), which resulted in the decrease in recovery of Au(III). The data obtained with this method for the ayurvedic formulated product are presented in Table 1. The results of analysis of real samples indicated that the proposed method can be used for determination of Au(III) in different types of matrices.

Conclusions

An efficient method for determination of Au(III) adsorption on AOAS using SPE is reported. Preparation, characterization and adsorption properties have been studied. It is a simple, cost effective method which makes use of easily available and low cost biomass. The method is comparable with the procedure for limit of detection, pre-concentration factor and reusability. The reusability of the *Aspergillus oryzae* on activated silica for 29 cycles minimizes the waste generation. Application to the ayurvedic formulated product, dummy sample and tap water gave satisfactory results. The method can be applied for five different adsorption isotherms among that Langmuir and Freundlich were very well fitted.

Acknowledgements

The authors wish to thank for financial support from the University grant commission, New Delhi, India, and the Senior Research Fellowships of Basic Science Research (UGC-BSR).

References

- ¹Pyrzynska K., *Anal. Chim. Acta*, **2012**, 741, 9.
- ²Saranya, R., Rajendran, S., Krishnaveni, A., Jayasundari, J., *Eur. Chem. Bull.*, **2013**, 2, 6.
- ³Medved J., Bujdos M., Matus P., Kubova J., *Anal. Bioanal. Chem.*, **2004**, 379, 60.
- ⁴Behbahani M., Najafi F., Amini M. M., Sadeghi O., Bagheri A., Hassanlou P. G., *J. Ind. Eng. Chem.*, **2014**, 20, 2248.
- ⁵Behbahani M., Gorii T., Mahvari M., Salarian M., Bagheri A., Shaabani A., *Food. Anal. Method*, **2014**, 7, 957.
- ⁶Salarian M., Ghanbarpour A., Behbahani M., Bagheri S., Bagheri A., *Microchim. Acta*, **2014**, 181, 999.
- ⁷Li Y., Qi L., Shena Y., Ma H., *Anal. Chim. Acta*, **2014**, 811, 36.
- ⁸Abolhasani J., Behbahani M., *Environ. Monit. Assess.*, **2015**, 187, 1.
- ⁹das Gracas M., Korn A., Andrade J. B., de Jesus D. S., Lemos V. A., Bandeira M. L. S. F., Santos W. N. L., Bezerra M. A., Amorim F. A. C., Souza A. S., Ferreira S. L. C., *Talanta*, **2006**, 69, 16.
- ¹⁰Turker A. R., *Clean*, **2007**, 35, 548.
- ¹¹Afzali D., Daliri Z., Taher M. A., *Arabian J. Chem.*, **2014**, 7, 770.
- ¹²Sabermahani F., Taher M. A., Bahrami H., *Arabian J. Chem.*, 2012 doi:10.1016/j.arabjc.2012.04.053.
- ¹³Mladenova E., Dakova I., Karadjova I., Karadjov M., *Microchem. J.*, **2012**, 101, 59.
- ¹⁴Liang P., Zhao E., Ding Q., Du D., *Spectrochim. Acta Part B*, **2008**, 63, 714.
- ¹⁵Moawed E. A., El-Shahat M. F., *Anal. Chim. Acta*, **2013**, 788, 200.
- ¹⁶Bagheri M., Mashhadizadeh M. H., Razee S., *Talanta*, **2003**, 60, 839.
- ¹⁷Syed S., *Hydrometallurgy*, **2012**, 115-116, 30.
- ¹⁸Lesmana S. O., Febriana N., Soetaredjoa F. E., Sunarsob J., Ismadjia S., *Biochem. Eng. J.*, **2009**, 44, 19.
- ¹⁹Veglio F., Beolchini F., *Hydrometallurgy*, **1997**, 44, 301.
- ²⁰Khoo K. M., Ting Y. P., *Biochem. Eng. J.*, **2001**, 8, 51.
- ²¹Kottea P., Yuna Y. S., *Polym. Degrad. Stab.*, **2014**, 109, 424.
- ²²Zhang L., Li Z., Hu Z., Chang X., *Spectrochim. Acta Part A*, **2011**, 79, 1234.
- ²³Veronica A., Jason P.G., Martha L.L., Jose P.-V. R., Miguel J.-Y., Jorge G.-T. L., *Nanotechnology* **2009**, 20 (10), 105607.
- ²⁴Kuyuck N., Volesky B., *Biotechnol. Lett.*, **1988**, 10(2), 137.
- ²⁵Sag Y., *Sep. Purif. Methods*, **2001**, 30, 1.
- ²⁶Tan T. and Cheng P., *Appl. Biochem. Biotech.*, **2003**, 104, 119.
- ²⁷Svecova L., Spanelova M., Kubal M., and Guibal E., *Sep. Purif. Technol.*, **2006**, 52, 142.
- ²⁸Vogel A.I., *A textbook of Quantitative Inorganic Analysis*, 3rd ed., Longman, London, **1962**.
- ²⁹Cui Y., Chang X., Zhu X. and Zou X., *Int. J. Environ. Anal. Chem.*, **2008**, 88, 857.
- ³⁰Indian Pharmacopoeia, Volume I (2.3.19), **2010**, Gov. of India, Ministry of Health and Family Welfare, p. 82.
- ³¹Hajko P., Pokorny M., Radez I., Vesel T., EP 0702679 B1.
- ³²Kotte P., Yun Y. S., *Polym. Degrad. Stab.*, **2014**, 109, 424.
- ³³Malarvizhi T.S., Santhi T. and Manonmani S., *Res. J. Chem. Sci.*, 2013, 3, 44.
- ³⁴Langmuir I., *J. Am. Chem. Soc.*, **1918**, 40, 1361.
- ³⁵Freundlich H. M. F., *J. Phys. Chem.*, **1906**, 57, 385.
- ³⁶Johnson R. D., Arnold F. H., *Biochim. Biophys. Acta*, **1995**, 1247, 293.
- ³⁷Deepa K., Chandran P., Sudheer Khan S., *Ecol. Eng.*, **2013**, 58, 207.
- ³⁸Iyer K. P. D. Kunju A. S., *Colloids Surf.*, **1992**, 63, 235.
- ³⁹Andreazza P., Jossa D., Lafancheux F., Robert M. C., Zyss J., *Phys. Rev. B*, **1992**, 45, 7640.
- ⁴⁰Dhandapani M., Kandhaswamy M. A. Srinivasan V., *Cryst. Res. Technol.*, **2005**, 40, 805.
- ⁴¹Skoog, D. A., F. J. Holler, Nieman, T. A., *Principles of Instrumental Analysis*, 5th ed. Harcourt Brace and Company, Florida, **1998**, p. 13.

Received: 19.05.2016.

Accepted: 06.08.2016.



CONVENIENT SYNTHESIS OF NEW 7-METHYLTETRAZOLO[1,5-A]QUINOLINE-4-CARBALDEHYDE DERIVATIVES

Ibrahim Ali M. Radini^[a]

Keywords: Tetrazolo[1,5-a]quinoline-4-carbaldehyde, hydrazonoyl chlorides, thiazole, chromene.

7-Methyltetrazolo[1,5-a]quinoline-4-carbaldehyde (**1**) was reacted with thiosemicarbazide to give the appropriate thiosemicarbazone (**2**). Compound (**2**) was reacted with different α -halocarbonyl compounds such as phenacyl bromide, hydrazonoyl chlorides and α -chloroacetic acid to afford thiazoles (**4**), aryldiazanylthiazoles (**6**), and thiazolidin-4-one (**8**), respectively. A series of 7-methyltetrazolo[1,5-a]quinoline derivatives, such as 2-imino-2*H*-chromene (**11**), arylacrylohydrazides (**13**), (**15**) and (**17**) and (heteroarylethylidene) acrylohydrazides (**19**), (**21**) and (**23**) has been synthesized. The structures of the newly synthesized compounds have been confirmed by spectral and elemental analyses.

* Corresponding Authors

Phone: +966566444196

E-Mail: iradini44@gmail.com

[a] Chemistry Department, Faculty of Science, Jazan University, Jazan 2097, Saudi Arabia

Introduction

Quinoline derivatives are an important class of heterocyclic compounds.^{1,3} Several quinoline derivatives have various biological activities, such as antimicrobial,^{4,5} antiproliferative,⁶ antimycobacterial,⁷ antimalarial,⁸ antitumor,⁹ anti-inflammatory,¹⁰⁻¹³ and antiparasitic,¹⁴ anti-HIV,¹⁵ insecticidal,¹⁶ antidyslipidemic and antioxidant.¹⁷

The tetrazole group has been considered analogous to carboxylic group as a pharmacophore.¹⁸ Several substituted tetrazoles show pronounced activities including antimicrobial, antimycobacterial, antiproliferative, anticancer and multi-drug resistance etc.¹⁹ The most prominent pharmaceutical application of tetrazoles is as angiotensin II receptor antagonists for the treatment of high-blood pressure.²⁰ The fusion of quinoline to the tetrazole ring is known to increase the biological activity.²¹ In particular, tetrazolo[1,5-a]quinoline-4-carbaldehyde serves as a key synthetic intermediate for the synthesis of novel medicinally valuable compounds.²² Encouraged by these observations and in continuation of our previous work,²³⁻²⁵ we have synthesized, by facile methods, newer quinoline derivatives, using 7-methyltetrazolo[1,5-a]quinoline-4-carbaldehyde as a synthon.

Experimental

Melting points were determined on digital Gallen-Kamp MFB-595 instrument using open capillary tubes and are uncorrected. IR spectra were recorded on Shimadzu FTIR 440 spectrometer using KBr pellets. Mass spectra were performed at 70 eV on an MS-50 Kratos (A.E.I.) spectrometer provided with a data system. ¹H NMR (500

MHz or 400 MHz) and ¹³C NMR (125 MHz or 100 MHz) spectra were recorded on a Bruker model Ultra Shield NMR spectrometer in DMSO-d₆ using tetramethylsilane (TMS) as an internal standard, chemical shifts are reported as δ ppm units. The elemental analyses (% C, H, N) were done at the Microanalytical Center, Cairo University, Cairo, Egypt. Solvents were dried by standard techniques. The monitoring of the progress of all reactions and homogeneity of the synthesized compounds was carried out by TLC using aluminum sheets silica gel 60 F₂₅₄ (Merck).

Synthesis of 2-((7-Methyltetrazolo[1,5-a]quinolin-4-yl)methylene)hydrazinecarbothioamide (**2**)

To a solution of 2-cyanoacetylhydrazide (0.91 g, 10 mmol) in absolute ethanol (30 mL) containing two drops of glacial acetic acid, 7-methyltetrazolo[1,5-a]quinoline-4-carbaldehyde (**1**) (2.12 g, 10 mmol) was added. The reaction mixture was heated under reflux for 2 h then left to cool. The solid product obtained was collected by filtration and recrystallized from EtOH-DMF as green powder, m.p. >300 °C, Yield, 83 %; IR (KBr, cm⁻¹): ν = 3412 (NH), 3251, 3161(NH₂), 1598 (C=N) cm⁻¹. ¹H NMR (500 MHz, DMSO-d₆): δ = 2.68 (s, 3H, CH₃), 7.43 (d, 1H, *J* = 8, quinoline-H), 7.56 (d, 1H, *J* = 8, quinoline-H), 7.62 (s, 1H, quinoline-H), 7.88 (s, D₂O exchangeable, 2H, NH₂), 8.24 (s, 1H, CH=N), 8.48 (s, 1H, quinoline-H), 10.92 (s, D₂O exchangeable, 1H, NH); ¹³C NMR (125 MHz, DMSO-d₆): δ = 19.78 (CH₃), 121.85, 126.64, 128.12, 128.62, 131.12, 134.15, 136.38, 143.56, 147.17, 149.14, 175.11 (C=S). EI-MS: *m/z* (%): 285 [M⁺, 85]; Anal. Calcd. for C₁₂H₁₁N₇S (285.32): C, 50.51; H, 3.89; N, 34.36 %; Found: C, 50.34; H, 3.90; N, 34.17 %.

General procedure for the preparation of compound (**4**)

To a suspension of thiosemicarbazone **2** (0.285g, 1 mmol) in EtOH (20 mL), the appropriate 1-aryl-2-bromoethanones (**3a** or **3b**) (0.01 mol) was added and heated under reflux for 4 h (TLC), then left to cool, the formed solid product was filtered off, washed with ethanol, dried, and crystallized from EtOH-DMF to afford (**4a**) or (**4b**).

4-(4-Bromophenyl)-2-(2-((7-methyltetrazolo[1,5-a]quinolin-4-yl)methylene)hydrazinyl)thiazole (4a)

Brown powder, m.p. 288 °C, Yield, 83 %; IR (KBr, cm^{-1}): $\nu = 3248$ (NH), 1612, 1581 (C=N) cm^{-1} . ^1H NMR (500 MHz, DMSO- d_6): $\delta = 2.67$ (s, 3H, CH_3), 7.538 (s, 1H, thiazole-H), 7.618-7.635 (dd, 4H, $J = 7$, $J = 2$, Ar-H), 7.803-7.848 (m, 3H, quinoline-H), 8.159 (s, D_2O exchangeable, H, NH), 8.476 (s, 1H, CH=N), 8.589 (s, 1H, quinoline-H). ^{13}C NMR (125 MHz, DMSO- d_6): $\delta = 20.87$ (CH_3), 105.56, 116.29, 119.72, 120.62, 123.89, 127.54, 127.82, 129.32, 131.65, 132.76, 134.15, 138.18, 143.55, 145.86, 147.45, 148.14, 168.32. EI-MS: m/z (%): 463 [M^+ , 100], 465 [$(\text{M}^+ + 2)$, 98]. Anal. Calcd. for $\text{C}_{20}\text{H}_{14}\text{BrN}_7\text{S}$ (464.34): C, 51.73; H, 3.04; N, 21.12 %; Found: C, 51.34; H, 2.89; N, 20.91 %.

3-(2-(2-((7-Methyltetrazolo[1,5-a]quinolin-4-yl)methylene)hydrazinyl)thiazol-4-yl)-2H-chromen-2-one (4b)

Yellow crystals, m.p. 279 °C, Yield, 81 %; IR (KBr, cm^{-1}): $\nu = 3194$ (NH), 1707 (C=O), 1593 (C=N); ^1H NMR (500 MHz, DMSO- d_6): 2.69 (s, 3H, CH_3), 7.52-7.930 (m, 7H, coumarin-H and quinoline-H), 8.663 (s, 1H, thiazole-H), 8.013 (s, 1H, coumarin-H), 8.159 (s, D_2O exchangeable, H, NH), 8.526 (s, 1H, CH=N), 8.689 (s, 1H, quinoline-H); ^{13}C NMR (125 MHz, DMSO- d_6): $\delta = 21.70$ (CH_3), 111.30, 112.31, 115.86, 118.96, 120.19, 124.93, 128.33, 128.41, 129.55, 129.61, 131.53, 131.65, 132.40, 138.07, 143.59, 145.37, 145.53, 146.07, 146.29, 152.20, 158.44, 163.54. EI-MS: m/z (%): 453 [M^+ , 5]. Anal. Calcd. for $\text{C}_{23}\text{H}_{15}\text{N}_7\text{O}_2\text{S}$ (453.47): C, 60.92; H, 3.33; N, 21.62 %; Found: C, 60.09; H, 3.15; N, 21.31 %.

General procedure for the preparation of compound (6)

Equimolar amounts of thiosemicarbazone (**2**) (0.285g, 1 mmol) and either oxo-*N'*-phenylpropanehydrazonoyl chloride (**5a**) or *N'*-(4-bromophenyl)-2-oxopropane hydrazonoyl chloride (**5b**) (1 mmol) in absolute ethanol (30 mL) in the presence of few drops of triethylamine as a catalyst was heated under reflux for 3 h (TLC), then left to cool. The solid formed was isolated by filtration, washed with ethanol, dried, and recrystallized from EtOH-DMF (2:1) to afford (**6a**) or (**6b**).

4-Methyl-2-(2-((7-methyltetrazolo[1,5-a]quinolin-4-yl)methylene)hydrazinyl)-5-(phenyldiazenyl)thiazole (6a)

Red crystals, m.p. >300 °C, Yield, 85 %; IR (KBr, cm^{-1}): $\nu = 3251$ (NH), 1558, 1539 (C=N) cm^{-1} ; ^1H NMR (400 MHz, DMSO- d_6): $\delta = 2.75$ (s, 3H, CH_3), 2.65 (s, 3H, CH_3), 7.018-7.665 (m, 8H, Ar-H), 8.570 (s, 1H, CH=N), 8.790 (s, 1H, quinoline-H), 11.56 (s, D_2O exchangeable, H, NH); ^{13}C NMR (100 MHz, DMSO- d_6): $\delta = 15.40$, 21.70, 106.36, 121.49, 123.45, 124.77, 127.80, 128.43, 129.55, 131.30, 131.68, 133.38, 145.23, 145.49, 146.06, 149.11, 150.33, 154.43, 164.42. EI-MS: m/z (%): 427 [M^+ , 30]. Anal. Calcd for $\text{C}_{21}\text{H}_{17}\text{N}_9\text{S}$ (427.48): C, 59.00; H, 4.01; N, 29.49 %; Found: C, 58.77; H, 3.97; N, 29.05 %.

5-((4-Bromophenyl)diazenyl)-4-methyl-2-(2-((7-methyl tetrazolo[1,5-a]quinolin-4-yl)methylene)hydrazinyl)thiazole (6b)

Red crystals, m.p. 285 °C, Yield 85 %; IR (KBr, cm^{-1}): $\nu = 3251$ (NH), 1556, 1544 (C=N) cm^{-1} ; ^1H NMR (500 MHz, DMSO- d_6): $\delta = 2.73$ (s, 3H, CH_3), 2.64 (s, 3H, CH_3), 7.60-7.937 (m, 7H, Ar-H), 8.60 (s, 1H, CH=N), 8.91 (s, 1H, quinoline-H), 11.98 (s, D_2O exchangeable, H, NH); ^{13}C NMR (125 MHz, DMSO- d_6): $\delta = 15.40$, 21.70, 116.15, 119.66, 124.01, 128.04, 129.10, 133.04, 134.25, 136.40, 138.26, 145.23, 145.49, 146.06, 149.11, 150.33, 154.43, 164.01, 178.61. EI-MS: m/z (%): 505 [M^+ , 33], 507 [$(\text{M}^+ + 2)$, 31]. Anal. Calcd for $\text{C}_{21}\text{H}_{16}\text{BrN}_9\text{S}$ (506.38): C, 49.81; H, 3.18; N, 24.89 %; Found: C, 49.37; H, 2.97; N, 24.46 %.

Synthesis of 2-((7-methyltetrazolo[1,5-a]quinolin-4-yl)methylene)hydrazono)thiazolidin-4-one (8)

A mixture of thiosemicarbazone (**2**) (0.285g, 1 mmol) and chloroacetic acid (**7**) (0.1 g, 1 mmol) in glacial acetic acid (30 mL) containing anhydrous sodium acetate (0.33 g, 4 mmol) was heated under reflux for 6 h (TLC). The reaction mixture was cooled; the formed solid product was filtered off, washed with ethanol, dried, and recrystallized from AcOH to afford (**8**). Brown, m.p. 290 °C (charing), yield, 89 %; IR (KBr, cm^{-1}): $\nu = 3222$ (NH), 1648 (C=O) cm^{-1} ; ^1H NMR (500 MHz, DMSO- d_6): $\delta = 2.65$ (s, 3H, CH_3), 3.97 (s, 2H, CH_2), 7.85 (d, 1H, $J = 8.5$, quinoline-H), 8.16 (s, 1H, quinoline-H), 8.53 (d, 1H, $J = 8.5$, quinoline-H), 8.59 (s, 1H, CH=N), 8.84 (s, 1H, quinoline-H), 11.20 (s, D_2O exchangeable, H, NH); ^{13}C NMR (125 MHz, DMSO- d_6): $\delta = 21.73$, 33.6, 123.50, 126.26, 128.33, 128.76, 131.31, 135.26, 136.68, 147.49, 149.21, 164.42, 173. EI-MS: m/z (%): 325 [M^+ , 73]. Anal. Calcd for $\text{C}_{14}\text{H}_{11}\text{N}_7\text{O}_2\text{S}$ (325.34): C, 51.68; H, 3.41; N, 30.14 %; Found: C, 51.36; H, 3.21; N, 29.85 %.

Synthesis of 2-cyano-*N'*-((7-methyltetrazolo[1,5-a]quinolin-4-yl)methylene)acetohydrazide (9)

To a solution of 2-cyanoacetohydrazide (0.99 g, 10 mmol) in absolute ethanol (30 mL), (**1**) (2.12 g, 10 mmol) was added in the presence of two drops of glacial acetic acid. The reaction mixture was heated under reflux for 1-2 h then left to cool. The solid product formed was collected by filtration and recrystallized from MeOH-DMF (1:1). Yellowish green, m.p. 272-274 °C, Yield, 85 %; IR (KBr, cm^{-1}): $\nu = 3284$ (NH), 2260 (CN), 1691 (C=O) cm^{-1} . ^1H NMR (400 MHz, DMSO- d_6) $\delta = 2.68$ (s, 3H, CH_3), 3.98 (s, 2H, CH_2), 7.28-7.92 (m, 4H, Ar-H), 8.90 (s, 1H, CH=N), 11.88 (s, 1H, NH, D_2O exchangeable). EI-MS: m/z (%): 293 (M^+ , 42). Anal. Calcd. for $\text{C}_{14}\text{H}_{11}\text{N}_7\text{O}$ (293.28): C, 57.33; H, 3.78; N, 33.43 %; Found: C, 57.04; H, 3.47; N, 33.05 %.

Synthesis of Compounds (11), (13), (15) and (17)

Equimolecular mixture of **9** (0.293 g, 1 mmol) and appropriate aldehyde (1 mmol), [2,4-dihydroxy benzaldehyde (**10**) in case of (**11**), 4-(dimethylamino) benzaldehyde (**12**) in case of (**13**), 2-chloroquinoline-3-car-

aldehyde (**14**) in case of (**15**) and 7-methyltetrazolo[1,5-a]quinoline-4-carbaldehyde (**16**) in case **17**] in anhydrous methanol (20 mL) containing piperidine (0.50 mL) was heated under reflux for 3-5 h (TLC). The formed solid was collected by filtration and recrystallized from methanol to gave compounds (**11**), (**13**), (**15**) and (**17**).

7-Hydroxy-2-imino-N'-((7-methyltetrazolo[1,5-a]quinolin-4-yl)methylene)-2H-chromene-3-carbohydrazide (**11**)

Brown powder, m.p. >300 °C, Yield, 85 %; IR (KBr, cm^{-1}): ν 3396.6 (OH), 3284 (NH), 1678 (C=O) cm^{-1} ; $^1\text{H NMR}$ (500 MHz, DMSO-d_6): δ = 2.69 (s, 3H, CH_3), 4.37 (s, H, NH, D_2O exchangeable), 6.53-8.57 (m, 8H, Ar-H), 8.51 (s, 1H, CH=N), 9.04 (s, 1H, OH, D_2O exchangeable), 11.98 (s, H, NH, D_2O exchangeable); EI-MS: m/z (%): 413 [M^+ , 25]. Anal. Calcd. for $\text{C}_{21}\text{H}_{15}\text{N}_7\text{O}_3$ (413.12): C, 61.01; H, 3.66; N, 23.72 %; Found: C, 60.87; H, 3.49; N, 23.32 %.

2-Cyano-3-(4-(dimethylamino)phenyl)-N'-((7-methyltetrazolo[1,5-a]quinolin-4-yl)methylene)acrylohydrazide (**13**)

Orange crystals, m.p. 290-291 °C, Yield, 87%; IR (KBr, cm^{-1}): ν 3205 (NH), 2202 (CN), 1660 (C=O); $^1\text{H NMR}$ (500 MHz, DMSO-d_6): δ 2.73 (s, 3H, CH_3), 3.10 (s, 6H, 2CH_3), 6.87-8.55 (m, 8H, Ar-H), 8.65 (s, 1H, CH=C), 9.09 (s, 1H, CH=N), 12.16 (s, 1H, NH, D_2O exchangeable) ppm; EI-MS: m/z (%): 424 [M^+ , 33]. Anal. Calcd. for $\text{C}_{23}\text{H}_{20}\text{N}_8\text{O}$ (424.17): C, 65.08; H, 4.75; N, 26.40; Found C, 64.87; H, 4.59; N, 26.05.

3-(2-Chloroquinolin-3-yl)-2-cyano-N'-((7-methyltetrazolo[1,5-a]quinolin-4-yl)methylene)acrylohydrazide (**15**)

Yellow crystals, m.p. 290-292 °C, Yield, 89%; IR (KBr, cm^{-1}): ν 3234 (NH), 2202 (CN), 1660 (C=O); $^1\text{H NMR}$ (500 MHz, DMSO-d_6): δ_{H} 2.68 (s, 3H, CH_3), 6.96-8.22 (m, 9H, Ar-H), 8.47 (s, 1H, CH=C), 8.68 (s, 1H, CH=N), 12.08 (s, 1H, NH, D_2O exchangeable) ppm; EI-MS: m/z (%): 466 [M^+ , 33], 468 [M^+ + 2, 11]. Anal. Calcd. for $\text{C}_{24}\text{H}_{15}\text{ClN}_8\text{O}$ (466.88): C, 61.74; H, 3.24; N, 24.00; Found C, 61.11; H, 2.99; N, 23.78.

2-Cyano-3-(7-methyltetrazolo[1,5-a]quinolin-4-yl)-N'-((7-methyltetrazolo[1,5-a]quinolin-4-yl)methylene)acrylohydrazide (**17**)

Yellow crystals, m.p. 266-267 °C, Yield, 85 %; IR (KBr, cm^{-1}): ν = 3237 (NH), 2214 (CN), 1667 (C=O) cm^{-1} ; $^1\text{H NMR}$ (500 MHz, DMSO-d_6): δ = 2.83 (s, 6H, 2CH_3), 6.99-8.28 (m, 8H, Ar-H), 8.51 (s, 1H, CH=C), 8.72 (s, 1H, CH=N), 12.05 (s, 1H, NH, D_2O exchangeable); EI-MS: m/z (%): 487 [M^+ , 16]. Anal. Calcd. for $\text{C}_{25}\text{H}_{17}\text{N}_{11}\text{O}$ (487.47): C, 61.60; H, 3.52; N, 31.61 %; Found: C, 61.34; H, 3.43; N, 31.22 %.

Synthesis of compounds (**19**) and (**21**)

Equimolecular mixture of (**1**) (0.221 g, 1 mmol) and appropriate hydrazones (**18**) and (**20**) (1 mmol) in anhydrous methanol (20 mL) containing piperidine (0.5 mL) was heated under reflux for 3-5 h (TLC). The formed solid was collected by filtration and recrystallized from methanol to gave compound (**19**) and (**21**).

2-Cyano-3-(7-methyltetrazolo[1,5-a]quinolin-4-yl)-N'-((1-(thien-2-yl)ethylidene)acrylohydrazide (**19**)

Brown powder, m.p. >300 °C, Yield, 81 %; IR (KBr, cm^{-1}): ν = 3197 (NH), 2205 (CN), 1619 (C=O) cm^{-1} ; $^1\text{H NMR}$ (500 MHz, DMSO-d_6): δ = 2.33 (s, 3H, CH_3), 2.90 (s, 3H, CH_3), 7.16-8.50 (m, 7H, Ar-H), 8.64 (s, 1H, CH=C-), 11.33 (s, 1H, NH, D_2O exchangeable); EI-MS: m/z (%): 401 [M^+ , 43]. Anal. Calcd. for $\text{C}_{20}\text{H}_{15}\text{N}_7\text{OS}$ (401.44): C, 59.84; H, 3.77; N, 24.42 %; Found: C, 59.51; H, 3.47; N, 24.13 %.

2-Cyano-N'-((1-(fur-2-yl)ethylidene)-3-(7-methyltetrazolo[1,5-a]quinolin-4-yl)acrylohydrazide (**21**)

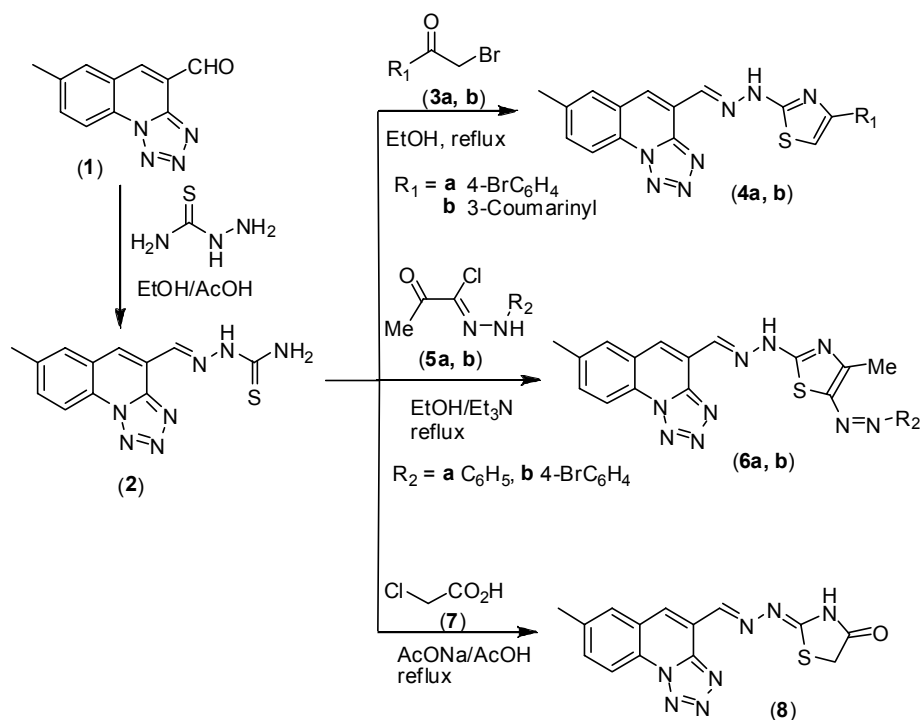
Yellow crystals, m.p. 296 °C, Yield 79 %; IR (KBr, cm^{-1}): ν = 3124 (NH), 2200 (CN), 1610 (C=O) cm^{-1} ; $^1\text{H NMR}$ (500 MHz, DMSO-d_6): δ = 2.29 (s, 3H, CH_3), 2.89 (s, 3H, CH_3), 6.49-7.15 (m, 3H, furan-H), 7.65-8.60, (m, 4H, quinoline-H), 8.76 (s, 1H, CH=C-), 11.60 (s, 1H, NH, D_2O exchangeable); EI-MS: m/z (%): 385 [M^+ , 43]. Anal. Calcd. for $\text{C}_{20}\text{H}_{15}\text{N}_7\text{O}_2$ (385.37): C, 62.33; H, 3.92; N, 25.44 %; Found: C, 62.03; H, 3.61; N, 25.16 %.

Results and Discussion

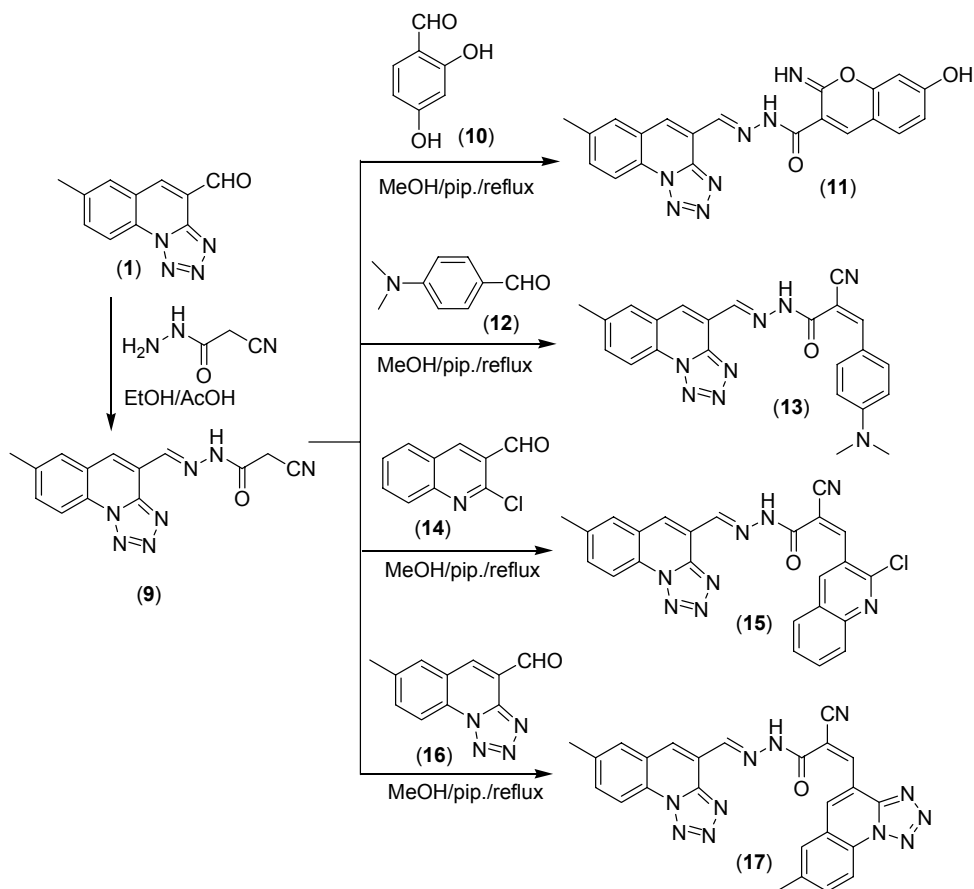
The synthetic procedures adopted to obtain the target compounds are depicted in Schemes 1-3. The starting material (**1**) was prepared according the literature procedures.¹⁴

Reaction of (**1**) with molar amount of thiosemicarbazide in boiling absolute ethanol containing few drops of acetic acid for 2 h, afforded 2-((7-methyltetrazolo[1,5-a]quinolin-4-yl)methylene) hydrazinecarbothioamide (**2**) in a good yield.

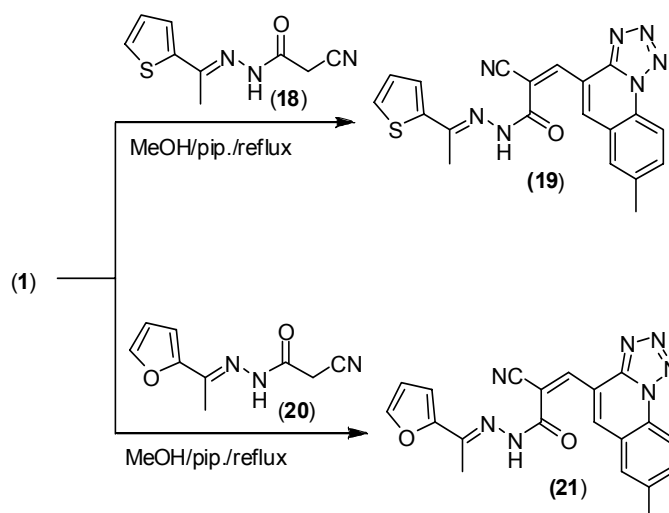
The reaction of compound (**2**) with equivalent amount of α -haloketones, for example, 4-bromophenacyl bromide (**3a**) and 3-bromoacetyl coumarin (**3b**), was performed in refluxing ethanol to yield (**4a**) and (**b**) in good yields. Also, (**2**) was reacted with hydrazonoyl chlorides, e.g. (**5a**) and (**5b**), in boiling ethanol in the presence of catalytic amount of triethyl amine to give thiazoles (**6a**) and (**6b**) in good yields.



Scheme 1. Synthesis of compounds (4), (6) and (8).



Scheme 2. Synthesis of compounds (11), (13), (15) and (17).



Scheme 3. Synthesis of compounds (19), and (21).

Similarly, 2-((7-methyltetrazolo[1,5-a]quinolin-4-yl)methylene)hydrazono)thiazolidin-4-one (8) was obtained from the reaction of (2) with chloroacetic acid in acetic acid in the presence of sodium acetate at reflux temperature.

Spectroscopic data (IR, ^1H NMR, and MS) and elemental analysis of compounds (4), (6), and (8) confirmed their structures. The IR spectra of compounds (4), (6), and (8) revealed the absence of absorption bands of NH_2 and $\text{C}=\text{S}$ functions. In addition ^1H NMR of these compounds indicates the disappearance of NH_2 signal. Also, $\text{C}=\text{S}$ signals was disappeared in ^{13}C NMR spectrum. Thus clearly indicating the carbothioamide moiety was involved in cyclization reaction to afford thiazole ring. The mass spectra of compounds (4), (6), and (8) was showed the molecular ion peaks which were in an agreement with the calculated masses (c.f. experimental section).

Reaction of compound (1), with molar amount of 2-cyanoacetohydrazide in boiling absolute ethanol containing few drops of acetic acid for 2 h, afforded 2-cyano-N'-((7-methyltetrazolo[1,5-a]quinolin-4-yl)methylene)acetohydrazide (9) in a good yield. Condensation of (9) with equimolar amounts of different aldehydes, namely 2,4-dihydroxybenzaldehyde (10), 4-(dimethylamino)benzaldehyde (12), 2-chloroquinoline-3-carbaldehyde (14), and 7-methyltetrazolo[1,5-a]quinoline-4-carbaldehyde (16) in methanol in the presence of few drops of piperidine at reflux temperature gave 7-hydroxy-2-imino-N'-((7-methyltetrazolo[1,5-a]quinolin-4-yl)methylene)-2H-chromene-3-carbohydrazide (11), 2-cyano-3-(4-(dimethylamino)phenyl)-N'-((7-methyltetrazolo[1,5-a]quinolin-4-yl)methylene)acrylohydrazide (13), 3-(2-chloroquinolin-3-yl)-2-cyano-N'-((7-methyltetrazolo[1,5-a]quinolin-4-yl)methylene)acrylohydrazide (15), 2-cyano-3-(7-methyltetrazolo[1,5-a]quinolin-4-yl)-N'-((7-methyltetrazolo[1,5-a]quinolin-4-yl)methylene)acrylohydrazide, respectively (Scheme 2). The formation of (11) probably takes place through condensation of the aldehydic group with the active methylene function followed by nucleophilic attack of the hydroxyl group on the neighboring nitrile residue eventually giving the target compound.

The structures suggested for compounds (9), (11), (13), (15), and (17) are in a good agreement with their analytical and spectroscopic data. The ^1H -NMR spectrum of (9) indicated the presence of a singlet signal at $\delta = 3.98$ ppm, assignable for the active methylene group ($-\text{COCH}_2\text{-CN}$). The IR spectrum of (11) revealed the absence of the nitrile group this confirmed the cyclization process. Also, mass spectrum of (11) contains a molecular ion peak at m/z 413, which supports the structure of compound (11).

On the other hand, Knoevenagel condensation reaction of (1) with 2-cyano-N'-((1-(thien-2-yl)ethylidene)acetohydrazide (18) and 2-cyano-N'-((1-(fur-2-yl)ethylidene)acetohydrazide (20) in refluxed methanol containing few drops of piperidine afforded 2-cyano-3-(7-methyltetrazolo[1,5-a]quinolin-4-yl)-N'-((1-(heteroaryl)ethylidene)acrylohydrazide (19) and (21), respectively. The structures of compounds (19) and (21) are in a good agreement with their analytical and spectroscopic data (c.f. experimental section).

References

- Elderfield, R. C., Kremer, C. B., Kupchan, S. M., Birstein, G., Cortes, G., *J. Am. Chem. Soc.*, **1947**, *69*, 1258-1260.
- Meth-Cohn, O., Narine, B., *Tetrahedron Lett.*, **1978**, *19*, 2045-2048.
- Ali, M. M., Rajanna, K. C., Prakash, P. K. S., *Synlett.*, **2001**, 51-253.
- Shah, N. K., Shah, N. M., Patel, M. P., Patel, R. G., *Chin. Chem. Lett.*, **2012**, *23*, 454-457.
- Khidre, R. E., Abu-Hashem, A. A., El-Shazly, M., *Eur. J. Med. Chem.*, **2011**, *46*, 5057-5064.
- Zieba, A., Sochanik, A., Szurko, A., Rams, M., Mrozek, A., Cmoch, P., *Eur. J. Med. Chem.*, **2010**, *45*, 4733-4739.
- Carta, A., Palomba, M., Briguglio, I., Corona, P., Piras, S., Jabes, D., Guglielame, P., Molicotti, P., Zanetti, S. *Eur. J. Med. Chem.*, **2011**, *46*, 320-326.
- Dominguez, J. N., Gamboa, N., Rodrigues, J. R., Angel, J. E., *Lett. Drug Design Discov.*, **2007**, *4*, 49-54.
- Abdou, W. M., Khidre, R. E., Kamel, A. A., *Arch. Pharm. Chem. Life Sci.*, **2012**, *345*, 123-136
- Chen, Y.-L., Chen, I.-L., Lu, C.-M., Tzeng, C.-C., Tsao, L.-T., Wang, J.-P., *Bioorg. Med. Chem.*, **2004**, *12*, 387-392.
- Bawa, S., Kumar, S., *Indian J. Chem.*, **2009**, *48B*, 142-145.
- Khidre, R. E., Abdel-Wahab, B. F., Badria, F. A.-R., *Lett. Drug Design Discov.*, **2011**, *8*, 640-648.
- Abdou, W. M., Khidre, R. E., Shaddy, A. A., *J. Heterocycl. Chem.*, **2013**, *50*, 33-41.
- Kouznetsov, V. V., Méndez, L. Y. V., Leal, S. M., Cruz, U. M., Coronado, C. A., Gómez, C. M. M., Bohórquez, A. R. R., Rivero, P. E., *Lett. Drug Design Discov.*, **2007**, *4*, 293-296.
- Luo, Z. G., Zeng, C. C., Yang, L. F., He, H. Q., Wang, C. X., Hu, L. M., *Chin. Chem. Lett.*, **2009**, *20*, 789-792.
- Wu, Q. L., Li, Y. Q., Yang, X. L., Ling, Y. *Chin. J. Org. Chem.*, **2012**, *32*, 747-754.
- Sashidhara, K. V., Kumar, A., Bhatia, G., Khan, M. M., Khanna, A. K., Saxena, J. K., *Eur. J. Med. Chem.*, **2009**, *44*, 1813-1818.

- ¹⁸Lei, P., Yuchuan, L., Yuzhang, Y., Wei, L., Xuejiao, Z., Siping, P., *Chin. J. Org. Chem.*, **2012**, *32*, 667-676.
- ¹⁹Adamec, J., Beckert, R., Weib, D., Waisser, K., Möllmann, U., Kaustová, J., Buchta, V., *Bioorg. Med. Chem.*, **2007**, *15*, 2898-2906.
- ²⁰Wexler, R. R., Greenlee, W. J., Irvin, J. D., Goldberg, M. R., Prendergast, K., Smith, R. D., Timmermans, P. B. M. W. M., *J. Med. Chem.*, **1996**, *39*, 625-656.
- ²¹Mukharjee, A., Akhater, M. S., Sharma, V. L., Seth, M., Bhaduri, A. P., Agnihotri, A., Mehrotra, P. K., Kamboj, V. P., *J. Med. Chem.*, **1989**, *32*, 2297-2300.
- ²²Bekhit, A. A., El-Sayed, O. A., Aboulmagd, E., Park, J. Y., *Eur. J. Med. Chem.*, **2004**, *39*, 249-255.
- ²³Radini, I. A. M., Elsheikh, T. M. Y., El-Telbani, E. M., Khidre, R. E., *Molecules*, **2016**, *21*, 909-921.
- ²⁴Radini, I. A. M., Abdel-Wahab, B. F., Khidre, R. E., *Phosphorus Sulfur Silicon Relat. Elem.*, *2016*, *191*, 844-856
- ²⁵Radini, I. A. M., Abd El-Wahab, A. H. F., *Eur. J. Chem.*, **2016**, *7*, 230-237.

Received: 16.07.2016

Accepted: 07.08.2016.



PHYTOTOXICITY OF CARBON NANOTUBES IS ASSOCIATED WITH DISTURBANCES OF ZINC HOMEOSTASIS

Olga Zaytseva^{[a]*} and Günter Neumann^[a]

Keywords: soybean, common bean, maize, seedling development, nutrient availability, multi-walled carbon nanotubes, nanomaterials.

Effects of short-term seed treatments with multi-walled carbon nanotubes (MWCNTs) on seedling development in soil culture and of root-exposure in hydroponics were studied on soybean, considered as model plant system. At 8 days after sowing and in later stages of seedling development, stunted growth and poor fine root production were detected. More detailed investigations revealed zinc (Zn) deficiency as a major growth-limiting factor. The growth of affected plants was recovered by foliar application of ZnSO₄ or by cultivation in nutrient solution supplied with soluble ZnSO₄. Since Zn is an important co-factor of enzymes involved in detoxification of reactive oxygen species (ROS), such as copper-zinc superoxide dismutases, stunted plant growth in response to MWCNTs treatments may be related to oxidative damage associated with lipid peroxidation and excessive oxidative degradation of auxin as growth hormone important for lateral root formation and leaf expansion.

* Corresponding Authors

E-Mail: olga.zaytseva@uni-hohenheim.de

[a] Institute of Crop Science (340h), Faculty of Agriculture, University of Hohenheim, Stuttgart, 70593, Germany

Introduction

Carbon nanotubes (CNTs) are currently among the most important additives for composite materials with a predicted market increase up to USD 5.91 billion by 2018.¹ During manufacturing, utilization and disposal, these materials are intentionally or by chance released into the environment.²⁻⁶ Due to a very high volume to surface ratio, nanomaterials can exhibit novel properties leading to yet unknown environmental interactions,⁷⁻⁹ complicating predictions on the fate of engineered nanoparticles released into environmental compartments, such as soil, air, and water. There are still controversial discussions whether nanoparticles exert beneficial or adverse effects on living organisms, on their ability to penetrate living tissues/barriers, and incorporation into food chains.¹⁰⁻¹² Accordingly, in the recent past, various studies addressed the impact of metal-based^{13,14} as well as carbon-based nanomaterials¹⁵⁻²¹ also on germination and early growth of higher plants. The resulting findings are frequently controversial, with positive as well as negative effects of CNTs, depending on plant species, source of CNTs, their physico-chemical properties, applied concentrations of nanotubes and the culture systems.

The effects of MWCNTs on seed germination and seedling development were studied in various plant species, such as tomato (*Solanum lycopersicum* L.),^{15,16} radish (*Raphanus sativus* L.), rapeseed (*Brassica napus* L.), ryegrass (*Lolium perenne* L.), lettuce (*Lactuca sativa* L.),² maize (*Zea mays* L.), cucumber (*Cucumis sativus* L.),¹⁷ zucchini (*Cucurbita pepo* L.)¹⁸ and others. In some cases MWCNTs did not affect germination rates but in different ways influenced further seedling development. Ghodake et al.¹⁹ reported no effect of MWCNTs at 10–40 mg L⁻¹ on germination of mustard (*Brassica juncea* L.) and gram (*Vigna mungo* (L.) Hepper) but root elongation of mustard seedlings was doubled as compared to the control at 20 mg L⁻¹, while higher concentrations had inhibitory effects

on root hair formation. In the majority of studies, which focused on the influence of nanoparticles on seedling development, artificial growth media or hydroponic culture systems where employed but experiments with soil-grown plants are rare. Begum et al.,²⁰ Begum and Fugetsu²¹ and Stampoulis et al.¹⁸ reported negative effects of MWCNTs added to a Hoagland nutrient solution in concentrations up to 2000 mg L⁻¹ on the development of various plant species, namely red spinach (*Amaranthus tricolor* L.), lettuce, cucumber and zucchini, while chili (*Capsicum annum* L.), okra (*Abelmoschus esculentus* (L.) Moench) and soybean (*Glycine max* (L.) Merr) remained unaffected.

From the eco-toxicological point of view it is very important to uncover the mechanisms of interactions between nanomaterials and plants, since plants are an important component of ecosystems, exhibiting close interactions with other living organisms as well as with inorganic components such as air, soil and water. Moreover, numerous applications are under development using nanomaterials for the development of novel plant growth stimulators, fertilisation and plant protection.²² Therefore, investigation of genotypic differences and identification of the most MWCNT-sensitive plant species and cultivars, as well as determination of toxic thresholds under different environmental conditions is urgently needed. However, the high variability of reported results and a wide range of different types of CNTs, makes comparisons difficult.

In a previous pilot study²³, we have investigated the responses of three crop species (soybean; common bean, *Phaseolus vulgaris* (L.); and maize) to short-term seed exposure (36 h) of a defined industrial MWCNT batch applied at a low (50 µg seed⁻¹) and high (500 µg seed⁻¹) dosage in a standardised germination test under controlled environmental conditions according to the rules of the International Seed Testing Association (ISTA).²⁴ MWCNT treatments increased germination percentage and reduced the proportion of abnormal seedlings²⁴ particularly in soybean associated with a reduction in the speed of water uptake during imbibition. However, early development of seedling was affected particularly by inhibition of root growth (fine root production) in all plant species first detectable at 8 days after sowing (DAS).

In the present study the consequences of these treatment effects on early growth were monitored in different culture systems (hydroponics, soil culture) with contrasting availability of water and nutrients.

Experimental

MWCNTs and preparation of MWCNT suspensions

Industrial multi-walled carbon nanotubes, MWCNTs (NanoTechCenter Ltd., Tambov, Russia) were used for the experiments. The MWCNTs have a minimum length of 2 μm , an external diameter of 20–70 nm and an internal diameter of 5–10 nm. The material was produced by chemical vapor deposition with purity above 98% (Appendix A). The selected concentrations of the MWCNT working suspensions used in the experiments (50, 100, 500 and 1000 mg L^{-1}) were in the range previously employed for various other studies on plant effects of MWCNTs.^{15,19-21} For preparation of working suspensions, MWCNTs were mixed directly with deionized (DI) water and dispersed by ultrasonification (SONOREX SUPER RK 510 H; 35 KHz, Bandelin Electronic, Berlin, Germany) for 30 min.

Test plants

For the experiments three plant species were used: soybean (*Glycine max.* (L.) Merr cv. BR16 Conquista, Embrapa, Brazil), common bean (*Phaseolus vulgaris* L. cv. Bohnen maxi, Baywa AG, Germany) and maize (*Zea mays* L. cv. Surprise, Saaten Union GmbH, Rastatt, Germany).

Seed treatments

Suspension of MWCNTs in DI water was used in a concentration of 1000 mg L^{-1} corresponding to a dose of 500 $\mu\text{g seed}^{-1}$. Deionized (DI) water was used as a control. Five mL of MWCNTs suspensions or DI water were added to plastic Petri dishes (diameter 96 mm, Greiner, Nürtingen, Germany) with 3 layers of filter paper (Blue ribbon MN 640d, Macherey und Nagel, Düren, Germany) at the bottom, and ten soybean seeds were evenly distributed per Petri dish and homogeneously moistened with the treatment solutions. The Petri dishes were covered with lids and placed into an incubator (BD 115, Binder, Tuttingen, Germany) at 25 °C for 36 h in the dark before emergence of the radicles, and subsequently transferred to different growth mediums without MWCNTs addition: (a) in filter paper rolls wetted with DI water for 10 days, (b) in filter paper rolls wetted with DI water for 3 days, then into rhizoboxes with silty loam soil for 10 days, (c) in filter paper rolls wetted with DI water for 6 days, then into hydroponic culture with fill nutrient solution for 9 days, (d) into pots with loess subsoil for 38 days and (e) into pots with loess subsoil and foliar Zn application for 33 days (Figure 1, experimental set-up 1). The rhizobox experiment was performed additionally with maize and common beans.

Seed vitality staining

Seed vitality staining was performed after 36 h of MWCNTs treatments according to ISTA rules.²⁴ Seeds were stained with 1% (w/v) 2, 3, 5-triphenyltetrazolium chloride (TTC) (pH 6.5–7.5) for 18 h. After rinsing the seeds with DI water, they were cut lengthwise with a razor blade and staining intensity of seed organs was evaluated under a binocular microscope (Stemi 2000-C, Zeiss, Germany). In metabolically active cells, TTC is reduced by dehydrogenases, forming red formazan and therefore, color intensity reflects the degree of metabolic activity in the stained tissues. Finally, embryos were excised, and formazan was quantitatively extracted with 2 M KOH/DMSO (1:1.16 v/v) using mortar and pestle. After removal of solid material by centrifugation, absorption of the supernatant was measured spectrophotometrically at 485 nm.

Seedling growth in filter rolls

As a pre-culture for hydroponic and rhizobox experiments seedlings were germinated in filter paper rolls: one sheet of filter paper (58×58 cm, MN710, Macherey und Nagel, Düren, Germany) was folded lengthwise four times and was wetted with 60 ml of DI water. Ten treated with MWCNTs seeds were placed along the edge of the paper which was subsequently folded, forming a paper roll with the seeds inside. The paper rolls were placed in upright position into a plastic germination box (30×20×10 cm), the lids of the box was opened and it was placed for 3–6 d (until rootlets reach 2.0–2.5 cm) into a climate chamber with a 14 h light period and an average temperature of 23 °C with regular additions of 25 ml DI water per filter roll to compensate for evaporation.

Hydroponic culture

Hydroponic culture was employed to investigate the impact of the MWCNTs on seedling development of soybean under full, freely available nutrient supply. Seed treatments with MWCNTs (1000 mg L^{-1}) and pre-culture in filter rolls were performed as described above. Seedlings with a root length of 2.0–2.5 cm were transferred from filter rolls to pots with 2.5 L nutrient solution, aerated with an aquarium pump and containing 2 mM $\text{Ca}(\text{NO}_3)_2$, 100 μM KH_2PO_4 , 0.7 mM K_2SO_4 , 0.1 mM KCl, 0.5 mM MgSO_4 , 10 μM H_3BO_3 , 0.5 μM MnSO_4 , 0.5 μM ZnSO_4 , 0.2 μM CuSO_4 , 0.01 μM $(\text{NH}_4)_6\text{Mo}_7\text{O}_{24}$, and 20 μM Fe(III)-EDTA, which was replaced in 3 day-intervals. In each pot, 8 seedlings were fixed with foam strips in perforated lids with 4 replicates per treatment. Cultivation was performed in a climate chamber with a 14 h light period (200 $\mu\text{mol m}^{-2}\text{s}^{-1}$) at 23 °C. After a culture period of 16 d, seedlings were harvested for biomass and root length determination. Alternatively, non-treated seeds were pre-cultured in moist filter rolls, and thereafter exposed for 6 days to nutrient solution amended with MWCNTs (50, 100, 500 mg L^{-1}) and subsequently cultivated in nutrient solution without MWCNTs supply for 7 days (Figure 1, experimental set-up 2).

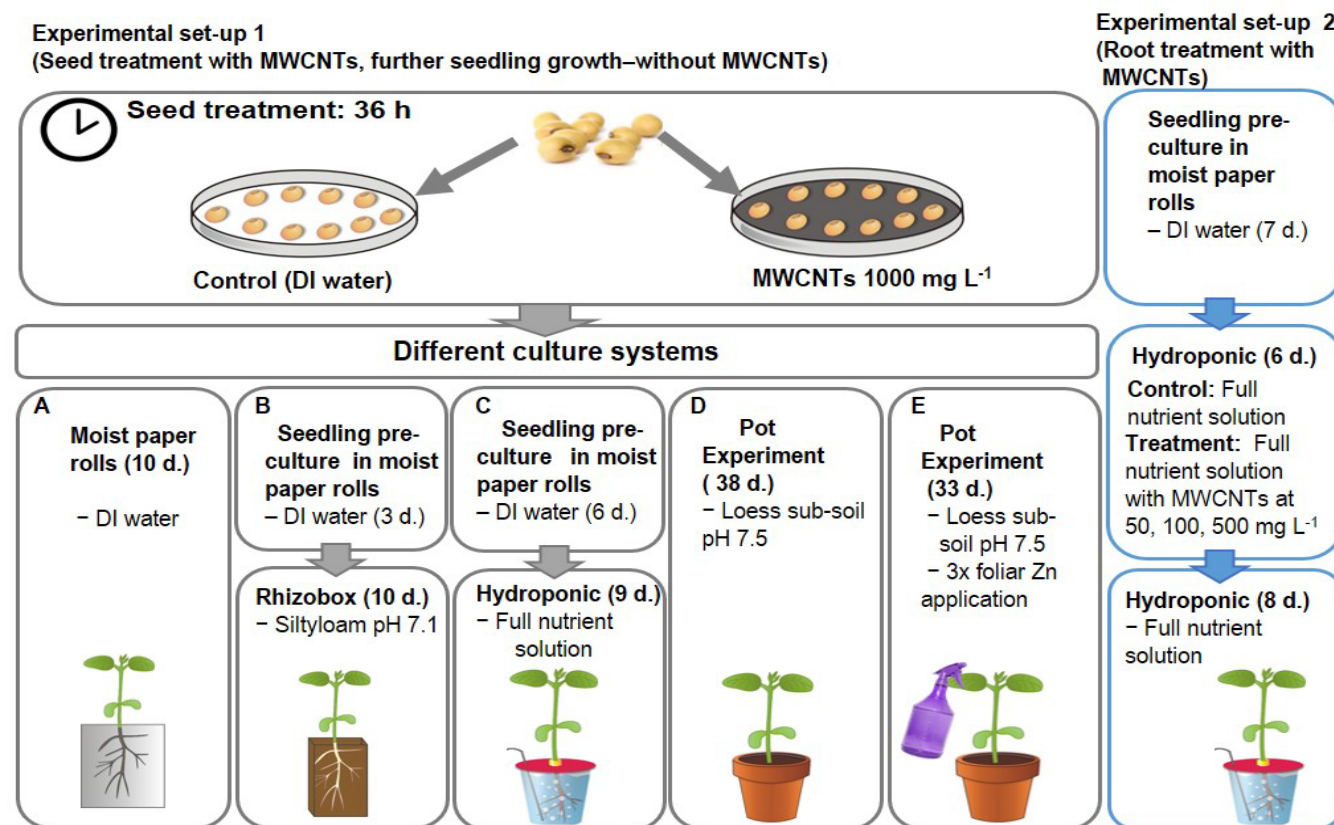


Figure 1. Schematic representation of the performed experiments: experimental set-up 1 and 2.

Soil culture - seedling growth in rhizoboxes

A rhizobox experiment was performed to monitor root development in soil culture. Seed treatments in Petri dishes, and pre-culture in filter rolls were performed as described above. Each of two seedlings with a root length of 2.0–2.5 cm were transferred into rhizoboxes equipped with transparent root observation windows²⁵ filled with 0.5 kg of a clay loam field soil (pH 7.1) taken from the Heidfeldhof experimental station in Hohenheim (Stuttgart, Germany). During the culture period, soil moisture was adjusted gravimetrically to 20% (w/w) by supplying DI water via holes on the backside of the boxes. Cultivation was performed in a climate chamber with a 14 h light period ($200 \mu\text{mol m}^{-2} \text{s}^{-1}$) at 23 °C. After a culture period of 15 days, the seedlings were harvested for biomass and root length determination.

Soil culture - pot experiments

Pot experiments were conducted to investigate the effects of short-term MWCNTs seed treatment and foliar Zn application on early growth of soybean on a soil substrate with limited nutrient solubility. A calcareous loess subsoil low in available P (P CAL 5 mg kg^{-1}), total N (0.02%), calcium chloride-diethylenetriaminepentaacetic acid (CAT) extractable micronutrient concentrations (mg kg^{-1} soil): Mn, 15; Fe, 7.8; Zn, 0.6; B, 0.2; organic matter (0.1 %), pH 7.6 was used for the experiments. Each pot was filled with 1 kg of a mixture of loess subsoil and quartz sand (50 % w/w). Basal fertilization for the substrate comprised of N (100 mg kg^{-1}) as $\text{Ca}(\text{NO}_3)_2$; K (150 mg kg^{-1}) as K_2SO_4 , Mg (50 mg kg^{-1}) as MgSO_4 , P (80 mg kg^{-1}) as $\text{Ca}(\text{H}_2\text{PO}_4)_2$. Seed

treatment with MWCNTs (1000 mg L^{-1} ; 36 h) was performed as described above. Thereafter, 4 seeds per pot were sown at depth of 1 cm and the pots were cultivated in a climate chamber with a 14 h light period ($200 \mu\text{mol m}^{-2} \text{s}^{-1}$) at 23 °C. During the culture period the moisture content of the substrate was adjusted gravimetrically in to 20% (w/w) by regular supply of DI water. At 10 DAS thinning was performed to final number of two seedlings per pot with 10 replicates per treatment. Harvests were performed at 26 DAS and 38 DAS for each 5 replicates for the determinations of biomass, root length and nutritional status.

Plant analysis in the first experiment revealed a critical Zn-nutritional status associated with growth depressions for soybean plants, developed from MWCNT-treated seeds. Therefore, in a second experiment, after unfolding of the 1st trifoliate leaves (15 DAS) foliar Zn applications were applied once a week with 0.5 mM or 5 mM ZnSO_4 or DI water as negative control (8 replicates per treatment). Final harvest was performed at 33 DAS for the determination of leaf area (young fully developed leaf) plant height, biomass and root length.

Mineral analysis of plant tissues

For mineral nutrient analysis, dried shoots of soybean plants were ground to a fine powder and each 250 mg of dry plant material were ashed in a muffle furnace at 500 °C for 4 h. After cooling, the samples were extracted twice with 2.5 mL of 3.4 M HNO_3 and evaporated to dryness to precipitate SiO_2 . The ash was dissolved in 2.5 mL of 4 M HCl , subsequently diluted ten times with hot deionized water, and boiled for 2 min. After cooling, the solutions

were adjusted to 25 ml with DI water and passed through blue ribbon filters (Macchery & Nagel, Düren, Germany). Zinc concentrations in the extracts were determined by atomic absorption spectrometry (iCE 300 Series, Thermo Fisher Scientific, United Kingdom).

Analysis of leaf area and root morphology

Fresh root samples, stored in 30% (v/v) ethanol were carefully separated on transparent Perspex trays and subsequently digitalised with an Epson Expression 10000XI scanner (Epson, USA) which was also used for scanning of leaves. Analysis was performed using the WinRHIZO software (Regent Instruments, Quebec, Canada).

Statistical analysis

All experiments were performed in a completely randomized design. Statistical analysis was conducted with the SigmaPlot 11.0 software package using the Student t-test for comparison of two treatments and one-way ANOVA for comparison of multiple treatments. The level of significance was determined at a P value ≤ 0.05 . All results in tables and graphs are presented as mean values \pm SE (standard error of a mean).

Results and Discussion

It has been already reported that short-term seed exposure (36 h) medium ($50 \mu\text{g seed}^{-1}$) and high ($500 \mu\text{g seed}^{-1}$) dosages of MWCNTs even prior to radicle emergence can induce significant effects on germination and early seedling development.²³ In a pilot study with three crop species (soybean, *Glycine max*; common bean, *Phaseolus vulgaris*; and maize, *Zea mays*), germination rate was increased, associated with reduced formation of abnormal seedlings according to the ISTA classification²⁴ particularly in soybean. This effect could be attributed to a reduction in the speed of water uptake, detectable already during the first 12 h of seed imbibition. However, during later seedling development, inhibition of root growth (mainly fine root production) was recorded in seedlings of all plant species, first detectable at 8 DAS, and associated with a reduced metabolic activity of the root tissue. A minimum time period of 36 h MWCNT seed-exposure was required for induction of root damage.²³

The results of the present study confirmed penetration of MWCNTs and its localization in the embryonic axis (Figure 2 E) even in non-germinated seeds, as has been described for other plant species also.^{15,26} This was associated with a reduced metabolic activity of the embryonic tissue detected by 2,3,5-triphenyltetrazoliumchloride staining (Figure 2 B, C) at 36 h of seed imbibition, and most probably causing the inhibition of root growth during later seedling development.²³ In this context, a closer look to the effective dosage of MWCNTs shows that only an extremely small proportion of the applied MWCNT dose (e.g. $500 \mu\text{g seed}^{-1}$ supplied in a treatment suspension with a concentration of 1000 mg L^{-1}) was really in contact with the seed surface, since the majority of the applied MWCNTs was sticking to the germination paper (Figure 2 A). A quantitative

evaluation of the MWCNT proportion finally taken up into the seeds and interacting with the plant metabolism would require incubation experiments with radioactively-labeled MWCNT tracers as previously described by Larue et al.²⁷ However, even without the availability of exact quantitative data on MWCNT uptake it is obvious that even trace amounts MWCNTs entering the seeds exhibit a high metabolic activity with the ability to induce both, positive and negative effects on plant development.

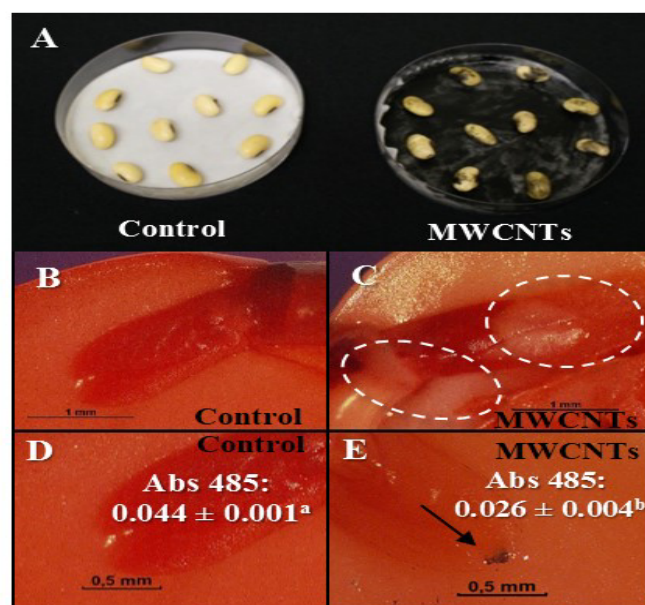


Figure 2. (A) Soybean seed treatment in Petri dishes: control (DI water) and MWCNTs (1000 mg L^{-1}) variants; (B–E) Embryos of MWCNT-treated and non-treated soybean seeds (2 DAS), stained with 1% 2,3,5-triphenyl tetrazolium chloride for 18 h. The weakly-stained regions highlighted in (C) indicate embryo tissues with a low metabolic activity. The numeric values in (D) and (E) represent absorption intensity of tetrazolium extracted from the embryos after photometric determination (means \pm SEM). Different letters (a, b) indicate significant differences between the treatments (Student t-test, $P \leq 0.05$). The black arrow in (E) indicates MWCNTs accumulation next to the embryo. DI–deionised water, MWCNTs–multi-walled carbon nanotubes, DAS–days after sowing.

Interestingly, the further development of plants grown from MWCNT-treated seeds was strongly dependent on the culture conditions. Cultivation of soybean seeds, identified as most sensitive to MWCNT treatments²³, in a hydroponic culture system with all essential plant nutrients provided in sufficient and freely available amounts, induced a complete recovery of root growth in plants grown from MWCNT-treated seeds within three weeks of the culture period, without any growth differences to control plants (Table 1, Figure 3 A). This finding suggests that nutrient limitation of the seedlings was a major problem induced by the MWCNT treatments, which could be supplemented by freely available nutrient supply in the hydroponic culture system. However, root growth inhibition was maintained even in nutrient solution with unlimited nutrient supply when the presence of MWCNTs was not restricted to the imbibition stage and MWCNTs were applied during plant growth in nutrient solution exerting inhibitory effects already at low concentrations of 50 mg L^{-1} (Table 1). By contrast, shoot growth remained unaffected (Table 1).

Table 1. Growth characteristics of soybean plants: (I) developed from seeds treated for 36 h with MWCNTs (1000 mg L⁻¹) and DI water (Control), pre-germinated in filter paper rolls without MWCNTs for 6 d and subsequently grown in full nutrient solution without MWCNTs for 9 d (see Figure 1, experimental set-up 1 C); (II) developed from non-treated seeds, pre-germinated in filter paper rolls for 7 d, grown in nutrient solution amended with MWCNTs (50, 100, 500 mg L⁻¹) for 6 d and finally grown in nutrient solution without MWCNTs for 8 d (see Figure 1, experimental set-up 2).

Treatment	Plant height, cm	Shoot dry matter, g	Root dry matter, g	Root length, cm	Root diameter, mm
(I) Seed treatment (36 h)					
Control	24.6 ± 0.3 a	0.17 ± 0.01 a	0.03 ± 0.00 a	268.9 ± 23.3 a	0.50 ± 0.01 a
MWCNTs 1000 mg L ⁻¹	25.0 ± 0.5 a	0.17 ± 0.00 a	0.02 ± 0.00 a	244.8 ± 4.0 a	0.51 ± 0.01 a
(II) Root treatment in hydroponics (6 days)					
Control	39.3 ± 1.5 a	0.29 ± 0.03 a	0.04 ± 0.00 a	609.3 ± 33.2 a	0.35 ± 0.01 a
MWCNTs 50 mg L ⁻¹	41.2 ± 0.9 a	0.32 ± 0.01 a	0.03 ± 0.00 a	493.3 ± 29.5 b	0.40 ± 0.02 a
MWCNTs 100 mg L ⁻¹	40.6 ± 0.2 a	0.31 ± 0.01 a	0.03 ± 0.00 a	457.6 ± 31.2 b	0.42 ± 0.02 b
MWCNTs 500 mg L ⁻¹	40.3 ± 0.7 a	0.31 ± 0.01 a	0.03 ± 0.00 a	497.3 ± 24.6 b	0.42 ± 0.00 b

Note: Results represent mean values ± SEM of four replicates. Different letters (a, b) indicate significant difference between treatments (Student t-test for the (I) seed treatment experiment, $P \leq 0.05$; one-way ANOVA, Tukey test for the (II) root treatment in hydroponics experiment, $P \leq 0.05$). MWCNTs—multi-walled carbon nanotubes.

Table 2. Growth characteristics of soybean, common bean and maize seedlings, developed from seeds treated for 36 h with MWCNTs (1000 mg L⁻¹) and subsequently grown in soil culture in rhizoboxes.

Treatment	Plant height, cm	Shoot dry matter, g	Root dry matter, g	Root length, cm	Root diameter, mm
Soybean (<i>Glycine max</i> (L.) Merr), 15 DAS					
Control	15.4 ± 0.6 a	0.11 ± 0.00 a	0.03 ± 0.00 a	350.7 ± 25.3 a	0.85 ± 0.01 b
MWCNTs 1000 mg L ⁻¹	14.3 ± 1.1 a	0.11 ± 0.01 a	0.02 ± 0.00 a	264.1 ± 17.5 b	0.89 ± 0.02 a
Common bean (<i>Phaseolus vulgaris</i> L.), 17 DAS					
Control	8.6 ± 0.5 a	0.14 ± 0.01 a	0.06 ± 0.00 a	922.9 ± 92.0 a	0.32 ± 0.01 a
MWCNTs 1000 mg L ⁻¹	8.7 ± 0.7 a	0.14 ± 0.01 a	0.04 ± 0.01 a	575.9 ± 98.4 b	0.36 ± 0.02 a
Maize (<i>Zea mays</i> L.), 14 DAS					
Control	24.9 ± 1.0 a	0.08 ± 0.01 a	0.09 ± 0.01 a	618.1 ± 46.5 a	0.81 ± 0.01 b
MWCNTs 1000 mg L ⁻¹	21.5 ± 2.4 a	0.06 ± 0.01 a	0.08 ± 0.01 b	452.6 ± 48.7 b	0.86 ± 0.01 a

Note: Results represent mean values ± SEM of five replicates. Different letters (a, b) indicate significant difference between treatments (t-student test, $P \leq 0.05$). DAS—days after sowing, MWCNTs—multi-walled carbon nanotubes.

Apparently, the freely available nutrient supply in hydroponics was sufficient to maintain normal shoot growth even with a smaller root system affected by the MWCNTs treatments. Root growth effects of MWCNTs have been documented also in previous studies with different plant species, and responses ranged from growth inhibition, no effects and even growth stimulation particularly at lower MWCNT concentrations.^{18,20,21}

In an additional experiment, further development of soybean seedlings was monitored in soil culture on a clay loam field soil (pH 7) and a calcareous Loess subsoil pH 7.6 with full macronutrient (N, P, K, Mg) fertilizers, carried out in rhizoboxes, equipped with root observation windows for monitoring of root growth effects and in pot experiments. In contrast to the experiment in hydroponic culture, inhibitory effects of short-term MWCNTs treatments during seed imbibition on root growth, persisted in soil culture up to 6 weeks after sowing even in absence of further root contact with MWCNTs. The effects were not only detectable in soybean (Figure 3 B), but similarly also in common bean and maize (Table 2), affecting mainly root length development. Typical symptoms comprised of reduction of average root length, associated with increased average root diameter in the plants developed from MWCNT-treated seeds (Table 2), which could be attributed to a reduction in

lateral and fine root production (Figure 4). This was associated with stunted shoot growth, inhibited leaf expansion, and chlorosis of young leaves (Figure 5 A, B) as a typical indicator for zinc deficiency (little leaf syndrome²⁸). In accordance with the visual symptoms, shoot nutrient analysis revealed critically low zinc levels at final harvest of plants exposed to MWCNT-seed treatments, reaching less than 20 % of the Zn concentrations of untreated control (Figure 5 C). No comparable effect could be observed for other nutrients such as phosphate (P) or potassium (K) (data not shown). A critical role particularly of Zn as limiting nutrient in MWCNT-treated soybeans was further confirmed by the observation that depressions of root and shoot growth could be restored by repeated foliar Zn applications throughout the culture period (Figure 4). Zinc limitation can induce oxidative stress since certain superoxide dismutases involved in detoxification of free radicals require Zn as a co-factor.^{29,30} Apart from lipid peroxidation of membranes³¹ Zn limitation may also promote oxidative degradation of indole acetic acid (IAA). The resulting low IAA levels have been discussed as a cause for limited leaf expansion and may be similarly responsible also for limited lateral fine root production observed in MWCNT-treated plants.^{32,33} Exposure of plants to MWCNTs can induce increased formation of reactive oxygen species (ROS)²¹ and the related oxidative stress may be responsible for the inhibition of root growth already in young seedlings (10 DAS).

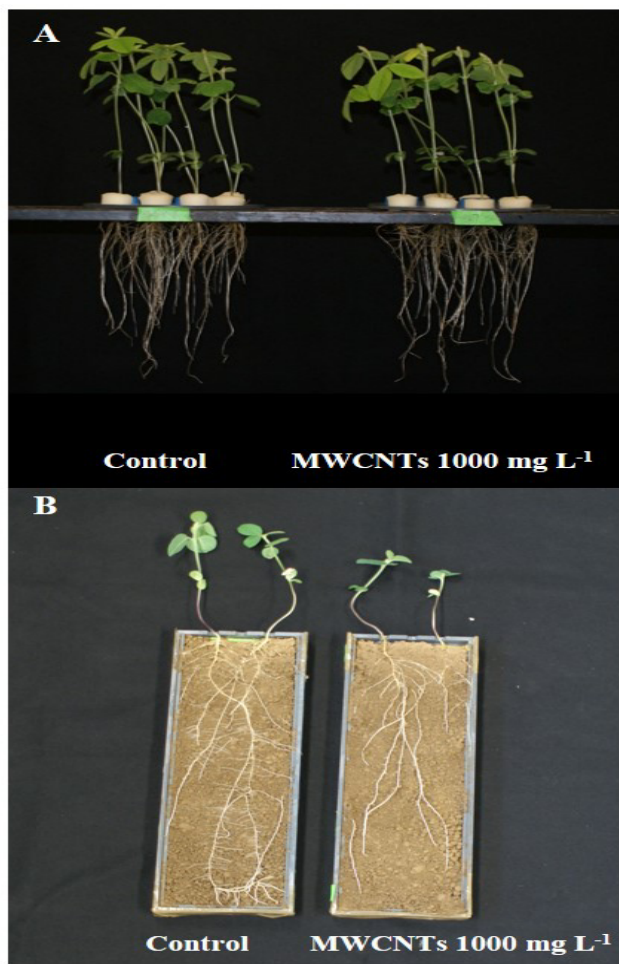


Figure 3. (A) Absence of growth effects after short-term MWCNTs seed treatment (36 h; 1000 mg L⁻¹) of soybean, subsequently grown in hydroponic culture with full nutrient supply (16 DAS); (B) negative influence of short-term MWCNTs seed treatment (36 h; 1000 mg L⁻¹) on root and shoot development of soybean seedlings in soil culture (15 DAS). DAS—days after sowing, MWCNTs—multi-walled carbon nanotubes.

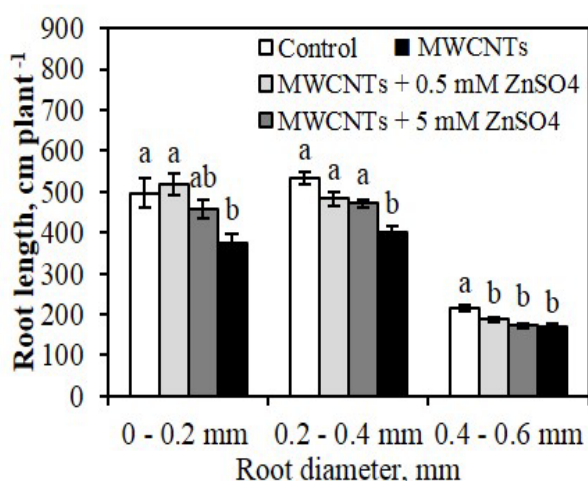


Figure 4. Effects of short-term MWCNTs seed treatments (36 h; 1000 mg L⁻¹) and 3x-foliar Zn application (0.5 and 5 mM) on development of fine roots (different diameter classes) of soybean plants in soil culture (33 DAS). Results represent mean values \pm SEM of eight replicates. Different letters (a, b) indicate significant difference between treatments (one-way ANOVA, Tukey test, $P \leq 0.05$). DAS—days after sowing, MWCNTs—multi-walled carbon nanotubes.

Whether this effect is already linked with zinc deficiency, remains to be established. When these seedlings are supplied with high amounts of freely available nutrients e.g. in hydroponic culture, sufficient nutrients are taken up even by the smaller root systems of MWCNT-treated plants finally leading to a compensation of the inhibitory effects on plant growth. In soil culture, sparingly soluble nutrients and particularly Zn are obviously not acquired in sufficient amounts by the stunted root systems and the Zn demand can only be covered by additional foliar Zn application.

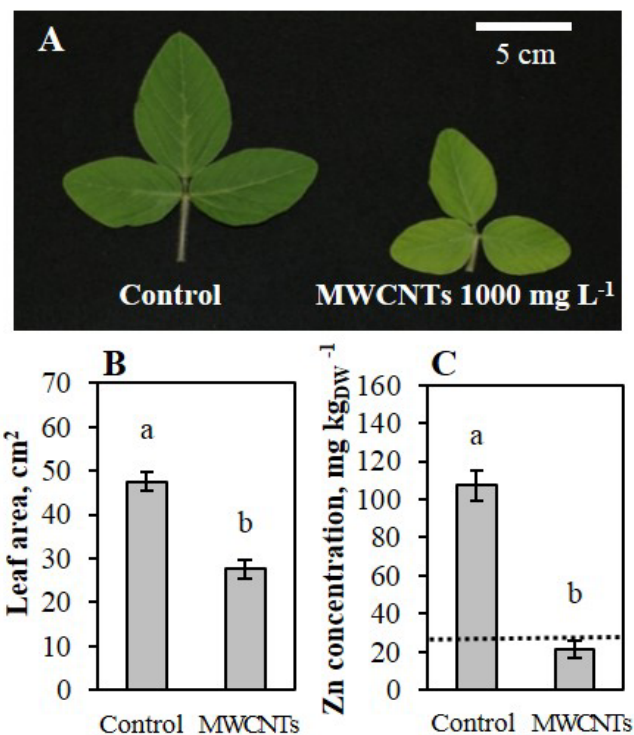


Figure 5. (A) First fully developed leaves of soybean plants with and without short-term MWCNTs seed treatment (38 DAS). Leaf chlorosis (pale-green color) and inhibited leaf expansion (little-leaf syndrome) in the MWCNTs variant as a typical symptom of Zn deficiency. (B) Effect of short-term seed treatments with MWCNTs on surface area of the first fully developed leaf of soybean plants (38 DAS). (C) Zinc concentration of the soybean shoots (38 DAS). The dotted line indicates the level of zinc deficiency.³⁴ Results represent mean values \pm SEM of five replicates. Different letters (a, b) indicate significant difference between treatments (Student t-test, $P \leq 0.05$). DAS—days after sowing, MWCNTs—multi-walled carbon nanotubes.

Conclusions

Our findings suggest that short-term exposure to small amounts of MWCNTs during germination can induce long lasting inhibitory effects during the development of soybean plants. Moreover, the expression of effects strongly depends on the culture conditions and application time. This may at least partially explain the high variability of responses reported in the literature, comprising both stimulatory and inhibitory effects. Different concentrations and types of applied MWCNTs have been discussed as additional factors. The close link of MWCNTs applications with production of ROS²¹ may provide an explanation for the expression of both, positive and negative effects. The formation of ROS

has been discussed as a physiological base for hormesis effects at low concentrations by stimulation of seed germination³⁵ and plant defence mechanisms and for negative effects induced by oxidative stress at higher concentrations. In this context also the sensitivity of plants may vary during their ontogenesis and in response to the environmental conditions. However the physiological base of MWCNTs effects on plant metabolism and potential relationships with oxidative stress responses still require a more detailed characterisation. This is of particular importance in face of agricultural applications of MWCNTs currently under development or already on the market.^{36,37}

Acknowledgments

The author (O. Zaytseva) is grateful to the Ministry of Science, Research and the Arts of Baden-Württemberg (Germany) and the Education, Audiovisual and Culture Executive Agency of the European Union for financial support. Furthermore, the authors would like to thank Dr. T. E. Hartmann for proof reading of the article.

The authors declare that they have no conflict of interest.

References

- ¹Nanocomposites (Carbon Nanotubes, Polymer Metal Fiber, Nanofibers, Graphene, Nanoplatelet and Others) Market for Automotive, Aviation, Electronics, Energy, Construction, Healthcare, Plastics, Military, Consumer Goods and Other Applications - Global Industry Analysis, Size, Share, Growth, Trends and Forecast, 2012–2018. Transparency Market Research. 08.04.2015.
- ²Sun, T. Y., Gottschalk, F., Hungerbühler, K. and Nowack, B., *Environ. Pollut.*, **2014**, *185*, 69–76.
- ³Som, C., Wick, P., Krug, H. and Nowack, B., *Environ Int*, **2011**, *37*(6), 1131–1142.
- ⁴Som, C., Berges, M., Chaudhry, Q., Dusinska, M., Fernandes, T. F., Olsen, S. I. and Nowack, B., *Toxicology*, **2010**, *269*(2-3), 160–169.
- ⁵Petersen, E. J., Zhang, L., Mattison, N. T., O'Carroll, D. M., Whelton, A. J., Uddin, N., Nguyen, T., Huang, Q., Henry, T. B., Holbrook, R. D. and Chen, K. L., *Environ. Sci. Technol.*, **2011**, *45*(23), 9837–9856.
- ⁶Nowack, B., Ranville, J. F., Diamond, S., Gallego-Urrea, J. A., Metcalfe, C., Rose, J., Horne, N., Koelmans, A. A. and Klaine, S. J., *Environ. Toxicol. Chem.*, **2012**, *31*(1), 50–59.
- ⁷Yang, K. and Lin, D.-H., *Journal of Zhejiang University: Science A*, **2014**, *15*(8), 547–551.
- ⁸Wiesner, M. R., Lowry, G. V., Alvarez, P., Dionysiou, D. and Biswas, P., *Environ. Sci. Technol.*, **2006**, *40*(14), 4336–4345.
- ⁹Smita, S., Gupta, S. K., Bartonova, A., Dusinska, M., Gutleb, A. C. and Rahman, Q., *Environmental Health: A Global Access Science Source*, **2012**, *11*(SUPPL.1).
- ¹⁰Sarma, S. J., Bhattacharya, I., Brar, S. K., Tyagi, R. D. and Surampalli, R. Y., *Critical Reviews in Environmental Science and Technology*, **2015**, *45*(9), 905–938.
- ¹¹Singh, N., Manshian, B., Jenkins, Gareth J S, Griffiths, S. M., Williams, P. M., Maffei, Thierry G. G., Wright, C. J. and Doak, S. H., *Biomaterials*, **2009**, *30*(23-24), 3891–3914.
- ¹²Rico, C. M., Majumdar, S., Duarte-Gardea, M., Peralta-Videa, J. R. and Gardea-Torresdey, J. L., *J. Agric. Food Chem.*, **2011**, *59*(8), 3485–3498.
- ¹³Watson, J.-L., Fang, T., Dimkpa, C. O., Britt, D. W., McLean, J. E., Jacobson, A. and Anderson, A. J., *BioMetals*, **2015**, *28*(1), 101–112.
- ¹⁴Kim, B. and McBride, M. B., *J. Environ. Qual.*, **2009**, *38*(6), 2253–2259.
- ¹⁵Khodakovskaya, M., Dervishi, E., Mahmood, M., Xu, Y., Li, Z., Watanabe, F. and Biris, A. S., *ACS Nano*, **2009**, *3*(10), 3221–3227.
- ¹⁶Morla, S., Rao, C. Ramachandra S. V. and Chakrapani, R., *J. Chem., Biol. Phys. Sci.*, **2011**, *1*(2), 328.
- ¹⁷Lin, D. and Xing, B., *Environ. Pollut.*, **2007**, *150*(2), 243–250.
- ¹⁸Stampoulis, D., Sinha, S. K. and White, J. C., *Environ. Sci. Technol.*, **2009**, *43*(24), 9473–9479.
- ¹⁹Ghodake, G., Seo, Y. D., Park, D. and Lee, D. S., *J. Nanoelectron. Optoelectron.*, **2010**, *5*(2), 157–160.
- ²⁰Begum, P., Ikhtari, R., Fugetsu, B., Matsuoka, M., Akasaka, T. and Watari, F., *Appl. Surf. Sci.*, **2012**, *262*, 120–124.
- ²¹Begum, P. and Fugetsu, B., *J. Hazard. Mater.*, **2012**, *243*, 212–222.
- ²²Zaytseva O. and Neumann G., *Chem. Biol. Technol. Agric.*, **2016**, *3*, 17.
- ²³Zaytseva, O., Neumann, G., *Eur. Chem. Bull.*, **2016**, *5*(5), 202–210.
- ²⁴The International Seed Testing Association (ISTA), *ISTA Rules Full Issue*, **2015**.
- ²⁵Luster, J.; Brunner, I. Livio, *Handbook of methods used in rhizosphere research*, Swiss Federal Research Institute WSL, **2006**.
- ²⁶Lahiani, M. H., Dervishi, E., Chen, J., Nima, Z., Gaume, A., Biris, A. S. and Khodakovskaya, M. V., *ACS Appl. Mater. Interfaces*, **2013**, *5*(16), 7965–7973.
- ²⁷Larue, C., Pinault, M., Czarny, B., Georgin, D., Jaillard, D., Bendiab, N., Mayne-L'Hermite, M., Taran, F., Dive, V. and Carrière, M., *J. Hazard. Mater.*, **2012**, *227-228*, 155–163.
- ²⁸Marschner, H. (ed.), *Mineral nutrition of higher plants*, Academic Press, London, GB, **1995**.
- ²⁹Baek, K.-H. and Skinner, D. Z., *JACEN*, **2012**, *01*(01), 34–40.
- ³⁰Cakmak, I., *New Phytol.*, **2000**, *146*(2), 185–205.
- ³¹Cakmak, I. and Marschner, H., *J. Plant Physiol.*, **1988**, *132*(3), 356–361.
- ³²Cakmak, I., Marschner, H. and Bangerth, F., *J. Exp. Bot.*, **1989**, *40*(3), 405–412.
- ³³Du, H., Liu, H. and Xiong, L., *Front. Plant Sci.*, **2013**, *4*.
- ³⁴Bergmann W., *Ernährungsstörungen bei Kulturpflanzen*, VEB Gustav Fischer Verlag, Jena, Germany, **1988**.
- ³⁵Ishibashi, Y., Koda, Y., Zheng, S.-H., Yuasa, T. and Iwaya-Inoue, M., *Ann. Bot.*, **2013**, *111*(1), 95–102.
- ³⁶Lewis G., *Carbon nanotube production method to stimulate soil microorganisms and plant growth produced from the emissions of internal combustion (WO 2013110202 A1)*.
- ³⁷Biris, A. S. and Khodakovskaya, M. V. *Method of using carbon nanotubes to affect seed germination and plant growth (US2012233725 (A1))*.

Received: 12.06.2016.

Accepted: 08.08.2016.



QUALITY ASSESSMENT OF TWO WATER RESOURCES IN MUNICIPALITY OF KAMENICA (KOSOVO)

Fatbardh Gashi^[a], Naser Troni^{[a]*}, Fatmir Faiku^[a], Sylejman Kryeziu^[a], Anilë Gashi^[a] and Jeton Shabani^[a]

Keywords: Quality assessment, well water, outliers, Kamenica, UV-VIS spectrometry.

In this study the assessment of water quality of two water resources (depth 10-50 meters) in the municipality of Kamenica have been investigated. Concentrations of some ions are determined using UV-VIS spectrometry. Statistical studies have been carried out by calculating of basic statistical parameters and anomalies (extremes and outliers). By comparing with available results of three similar water -samples in Kosovo, it can be summarized that water quality of two water-samples in the municipality of Kamenica is similar to the well waters of Mirosala. From the results of field work and laboratory analyses it was found out that the well water does not fulfil the criteria set by the WHO. The high value of Fe, Mn and turbidity pollutants indicated pollution by natural pollutants and from anthropogenic sources like waste waters.

* Corresponding Authors

E-Mail: naser_troni@yahoo.com

[a] Department of Chemistry, Faculty of Natural Sciences, St. Mather Teresa 10, University of Prishtina, Kosovo

Introduction

Drinking water is supposed to be pure enough to be consumed or used with low risk of immediate or long term harm.¹ Well water represents an important source of drinking water and its quality is currently threatened by a combination of overexploitation and microbiological and chemical contamination. More than four billion cases of diarrhea cause 2.2 million deaths, mostly of children under the age of five.² The sources of physico-chemical contamination are numerous and include the land disposal of sewage effluents, sludge and solid waste, septic tank effluent, urban runoff and agricultural, mining and industrial practices.^{3,4} Decomposition of organic matter and pollution due to anthropogenic activity are the main sources of pollution of water.⁸ Therefore, multidisciplinary collaborative research is essential for understanding the pollution processes. As reported by Brils⁹, adequate water quality in Europe is one of the most eminent concerns for the future. Good management of natural and environmental waters will give results if leading institutions constantly monitor information about environmental situation. Therefore, seeing it as a challenge for environmental chemists, our goal is to determine the amount and nature of pollutants in the environment. Heavy metals are significant environmental pollutants, and their toxicity is a problem of increasing significance for ecological, evolutionary, nutritional and environmental reasons.⁹

Potable and safe water is gradually becoming a scarce commodity, due to mixing up of huge contaminants through natural process like soil and rock weathering and anthropogenic activities such as industrial effluents, domestic sewage, garbage, over mining activity, explosive population etc.^{17,18}

Mainly there are four main approaches that can be used to assess the water quality of a water body: (1) water quality index approach, (2) trophic status index approach, (3) statistical analysis approaches of the water quality data such as correlation analysis and (4) biological analysis approaches such as Genetic Algorithms method and other different biological indices.²² Literature has also shown that multivariate statistical methods have been proved to be one of the most useful tools for extracting meaningful information from data sets. For example applied cluster analysis (CA) to delineate monitoring sites of surface/drinking water quality while used CA and discriminant analysis (DA) to identify significant parameters and optimize monitoring network of ground water quality data.²³⁻²⁶

Until recently, the waters of Kosovo have been poorly investigated. Gashi et al.²⁷ performed first step with investigation of the rivers Drini i Bardhë, Morava e Binçës, Lepenc and Sitnica, which are of supra-regional interest. As Drenica River is the most important tributary of Sitnica River, the current investigation represents next step in detailed investigation and monitoring of Sitnica river watershed, which is most polluted river system in Kosovo.

Experimental

Study area

The aim of the current work is to perform, a systematic research of two water resources in Municipality of Kamenica (Figure 1). Kamenica is a town and municipality (district of Gjilane) in the eastern part of Kosovo.³⁴ Although there are more than 50 water quality parameters available, only 14 parameters are selected for our investigation. These parameters are water temperature, conductivity, pH, consumption of KMnO₄, concentration of ammonia, nitrites, nitrates, etc. The results are interpreted using modern statistical methods that can be used to locate

pollution sources. The levels of some physico-chemical parameters of well waters are compared with the World Health Organization standards for drinking water.^{35,36} Finally some parameters of the present sample were compared with values of 3 well-waters in Kosovo.



Figure 1. Location of the study area and positions of sampling stations.

Sampling and sample preparation

For chemical analysis water samples are collected in July, 2015. The storage vessels were previously rinsed three times with sampled water and labelled with the date and the name of the sample. These samples are transferred to refrigerator (at 4° C) for analysis in the laboratories. All tests are performed at least thrice to calculate the average value. Sampling, preservation and experimental procedure for the water samples are carried out according to the standard methods for examination of water.³⁷⁻³⁹ Samples are preserved in refrigerator after treatment.

Chemical Characterization

Double distilled water was used in all experiments. All instruments are calibrated according to manufacturer's

recommendations. Temperature of water was measured immediately after sampling. TDS and pH measurements were performed using pH/ion-meter of Hanna Instruments.

Turbidity was measured using Turbidimeter HI 93703. Electrical conductivity was measured by Hanna Tetra-con 96 conductometer.

Chemical consumption of KMnO_4 was determined by Thiemann Küebel volumetric method of boiling in acidic environment. Concentration of calcium and chloride ion was determined by volumetric titration. Concentrations NO_2^- (at 507 nm), NO_3^- (at 500 nm) and NH_4^+ (at 655 nm) were determined by UV-VIS spectrometry method, using Agilent 8452, Spectrophotometer. Concentrations Fe^{2+} (at 510 nm) and Mn^{2+} (at 525 nm) were determined by UV-VIS spectrometry, using Spectroquant NOVA 60 photometer (Merck, Germany).

Statistical Methods

Program Statistica 6.0⁴⁰ was used for the statistical analysis of data in this work, such as descriptive statistics, distribution histograms and box plot diagrams for determination of anomalies i.e. extremes and outliers.

RESULTS

The value of physico-chemical parameters from 10 water samples (at the depth of 10, 20, 30, 40 and 50 m) of two resources, i.e. water temperature, EC, pH, Turbidity, TDS, consumption of KMnO_4 , hardness, and concentrations of Cl^- , NH_4^+ , NO_2^- , NO_3^- , Ca^{2+} , Fe^{2+} and Mn^{2+} are presented in tables 1 and 2. The descriptive statistical summary of the selected variables at water samples are presented in table 3. For each variable, the values are given as arithmetic mean, geometric mean, median, minimal and maximal concentration, variance and standard deviation. Scatter box plot diagrams of 15 measured variables are presented in Figures 2 and 3 Using experimental data and box plot approach of Tukey,⁴¹ anomalous values (extremes and outliers) of 14 variables were determined.

Table 1. Physico-chemical parameters of water samples from two resources.

Parameter	S ₁ -10m	S ₁ -20m	S ₁ -30m	S ₁ -40m	S ₁ -50m	S ₂ -10m	S ₂ -20m	S ₂ -30m	S ₂ -40m	S ₂ -50m
Water temp. °C	10.8	10.8	10.9	10.8	10.8	10.7	10.8	10.8	10.8	10.9
EC, at 20 °C μscm^{-1}	530	530	520	490	510	500	500	510	500	500
pH	7.18	7.17	7.2	7.19	7.2	7.55	7.63	7.65	7.5	7.61
Turbidity NTU	2.32	1.66	1.88	10.5	7.42	12.88	11.73	10.39	15.9	15.8
TDS mg L^{-1}	260	260	260	260	250	250	250	260	250	250
Hardness °dH	12.19	12.75	12.61	12.89	12.05	8.83	8.83	8.69	8.83	8.81
KMnO_4 consumed mg L^{-1}	11.7	12.96	12.01	11.06	11.7	5.69	6.95	6.32	7.21	7.23
Cl^- mg L^{-1}	10.28	10.28	10.28	7.44	8.5	9.22	9.22	8.51	4.61	4.61
NH_4^+ mg L^{-1}	0.31	0.32	0.37	0.48	0.38	0.41	0.33	0.22	0.18	0.19
NO_2^- mg L^{-1}	0.0045	0.0082	0.0031	0.0034	0.0032	0.0012	0.0015	0.0012	0.005	0.001
NO_3^- mg L^{-1}	1.12	1.29	1.28	0.7	0.7	0.35	0.32	0.32	0.32	0.2
Fe^{2+} mg L^{-1}	2.14	2.35	2.12	1.42	1.27	0.13	0.17	0.12	0.14	0.14
Mn^{2+} mg L^{-1}	1.28	1.32	1.29	1.02	1.11	0.15	0.17	0.16	0.12	0.11
Ca^{2+} mg L^{-1}	17.94	18.74	18.74	19.14	19.4	13.95	13.95	13.95	13.95	14.2

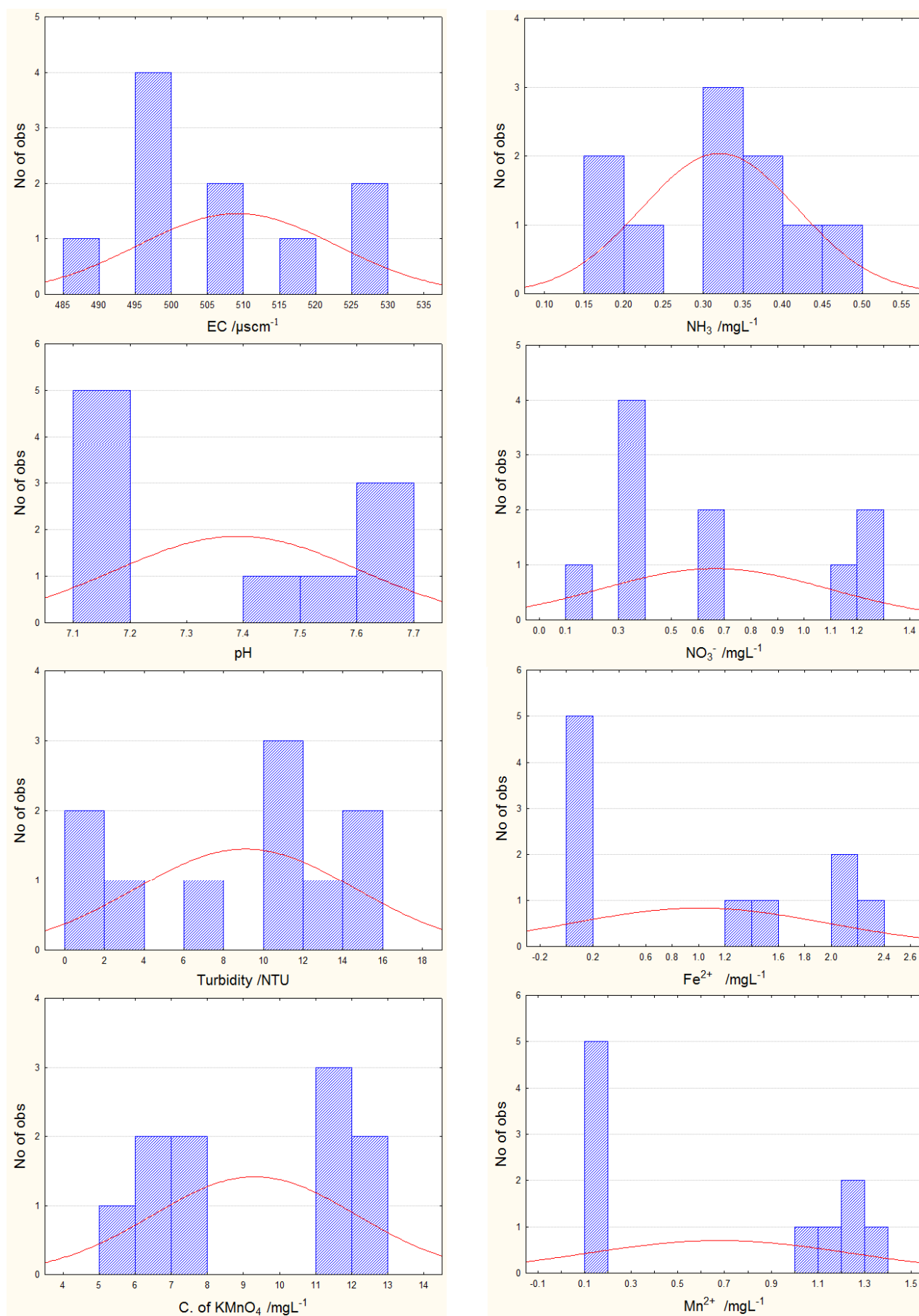


Figure 2. Frequency histograms of 8 measured variables.

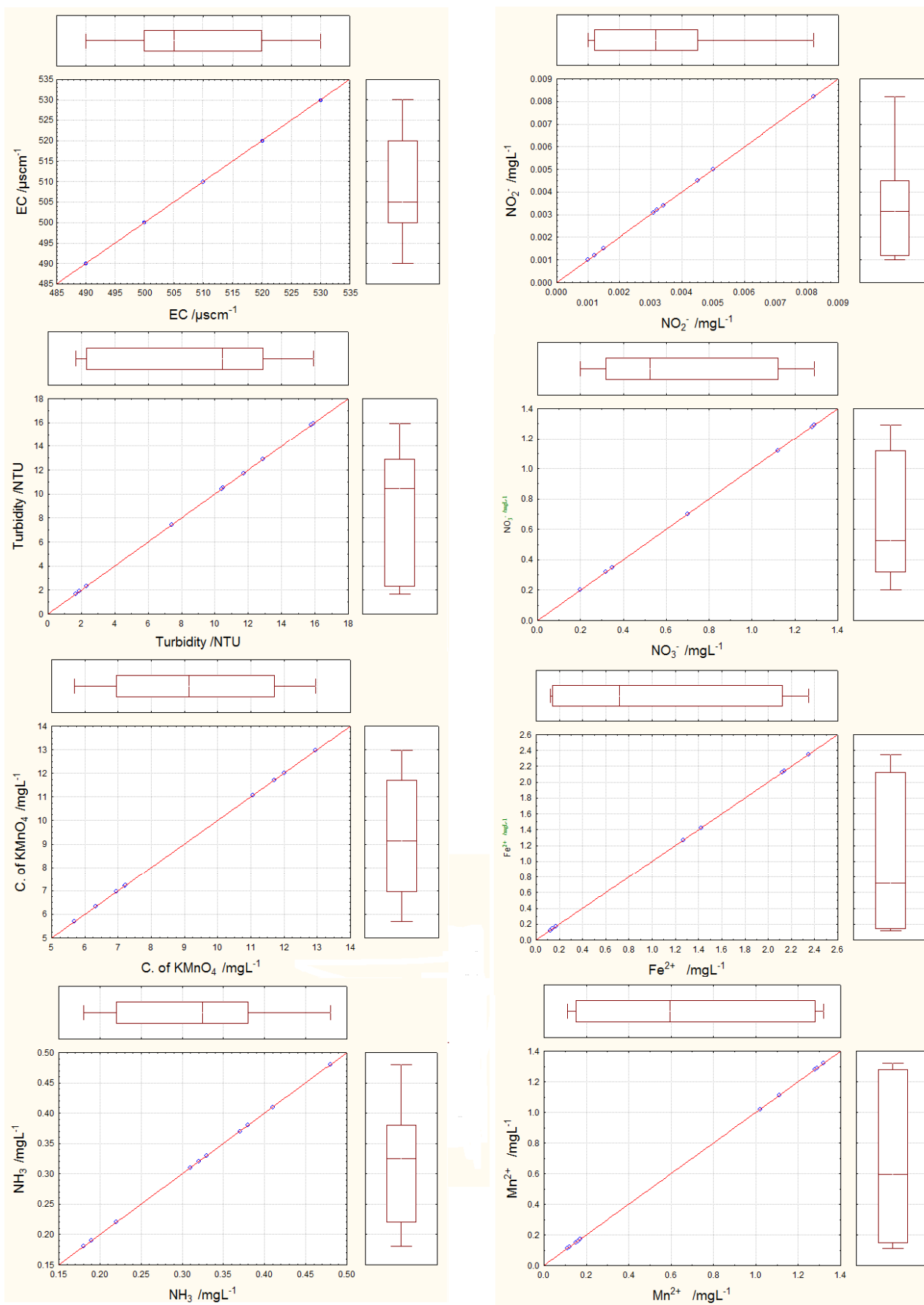


Figure 3. Frequency histograms of some measured variables.

DISCUSSION

In the present study, the temperature of 10 water samples in two resources varied from 10.7–10.9 °C, with a low standard deviation of 0.0032, an usual behavior of most of well waters. As thermostat adjustment of the instrument for conductivity measurement wasn't done, temperature of water sample was measured and with approximate correction factor, f , which for water, in temperature range from 10 to 25 °C, is 0.02 °C⁻¹, it was calculated to temperature of 20 °C. The electrical conductivity (EC) of water samples varied from 490–530 μScm^{-1} as a sign of natural pollution, and are higher than the values for Izbicak karstic spring on the slopes of Mt. Biokovo in Croatia (362.5 μScm^{-1}), which is known to be under the significant anthropogenic influence.⁴² Turbidity values in all water samples varied from 1.66 to 15.90 NTU and its value in samples S_1 at the depths 40 m and 50 m, and in all samples from S_2 exceeded recommended WHO norms for drinking waters. TDS values in all water samples varied from 250 to 260 mg L^{-1} and no sample exceeded the recommended WHO norms of 1500 mg L^{-1} for drinking waters. pH values varied from 7.17–7.76 and it could be because of the composition of rocks in that area. Total hardness was ranging from 8.69 to 12.89 °dH and were found to be well below the recommended standards for drinking water (30 °dH). Increased hardness on those locations is of natural origin, due to presence of gravel, sand, sandy clay and tuffs deposits.⁴³ Consumption of KMnO_4 ranged from 5.69 to 12.9 mg L^{-1} and the value in all the samples were found to be within the recommended norms for drinking water. Similarly, concentrations of calcium, chlorides, ammonia, nitrites and nitrates in all the samples were found to be within recommended WHO standards for drinking water. The concentration of iron in all the samples exceeded the recommended WHO norms of 0.3 mg L^{-1} for drinking waters. Similarly, manganese in all the water samples from S_1 , exceed recommended WHO norms of 0.1 mg L^{-1} for potable water.

Table 3. Statistical analysis of 14 variables of water from two resources.

Variable	Mean	Geometric	Median	Minimum	Maximum	Variance	Std. Dev.
Temp. °C	10.8100	10.8099	10.8000	10.7000	10.9000	0.0032	0.05676
EC $\mu\text{s cm}^{-1}$	509.0000	508.8352	505.0000	490.0000	530.0000	187.7778	13.70320
pH	7.3880	7.3852	7.3500	7.1700	7.6500	0.0462	0.21498
Turbidity NTU	9.0480	6.8348	10.4450	1.6600	15.9000	30.2450	5.49955
TDS mg L^{-1}	255.0000	254.9510	255.0000	250.0000	260.0000	27.7778	5.27046
Hardness °dH	10.6480	10.4842	10.4400	8.6900	12.8900	3.8628	1.96540
KMnO_4 consumed mg L^{-1}	9.2830	8.8862	9.1450	5.6900	12.9600	7.9380	2.81745
Cl^- mg L^{-1}	8.2950	7.9869	8.8650	4.6100	10.2800	4.6122	2.14760
NH_3^- mg L^{-1}	0.3190	0.3043	0.3250	0.1800	0.4800	0.0096	0.09803
NO_2^- mg L^{-1}	0.0032	0.0026	0.0032	0.0010	0.0082	0.0000	0.00225
NO_3^- mg L^{-1}	0.6600	0.5392	0.5250	0.2000	1.2900	0.1834	0.42825
Fe^{2+} mg L^{-1}	1.0000	0.5012	0.7200	0.1200	2.3500	0.9250	0.96178
Mn^{2+} mg L^{-1}	0.6730	0.4096	0.5950	0.1100	1.3200	0.3213	0.56682
Ca^{2+} mg L^{-1}	16.3960	16.2169	16.0700	13.9500	19.4000	6.5200	2.55343

Table 2. Mean values of some physico-chemical parameters of water from two resources.

Parameter	WHO standard	Resource (mean value)	
		1	2
Temp. °C	8-12	10.84	10.84
EC μscm^{-1}	1000	516	498
pH	6.5-8.5	7.18	7.58
Turbidity NTU	5	13.34	4.75
TDS mg L^{-1}	1500	258	258
Hardness °dH	<30	12.498	8.798
KMnO_4 consumed mg L^{-1}	250	13.86	6.5
Cl^- mg L^{-1}	30	9.35	7.23
NO_3^- mg L^{-1}	50	1.018	0.298
NO_2^- mg L^{-1}	3	0.0042	0.00198
NH_3 mg L^{-1}	0.5	0.37	0.26
Fe^{2+} mg L^{-1}	0.3	1.86	0.14
Mn^{2+} mg L^{-1}	0.1	1.2	0.142
Ca^{2+} mg L^{-1}	200	18.74	14

Basic statistical parameters for the 14 parameters analyzed in water samples from two water resources are presented in Table 3. Based on the frequency histograms (Figure 2) and two dimensional scatter box plot diagrams (Figure 3), anomalous values (extremes and outliers) were not registered.

When values of 10 selected measured parameters in waters of Kamenica are compared with similar well waters in Kosovo (Table 4), following facts can be observed: EC and concentrations of NH_3 , NO_2^- , NO_3^- , Ca^{2+} , Fe^{2+} and Mn^{2+} , water resources of Kamenica were approximately the same with well waters of Mirošala.

EC is significantly lower than that of the well waters of Lipjan and pH is approximately the same with well waters of Sprig and well waters of Istog, but higher than that in well waters of Lipjan. pH is significantly lower than that in the well waters of Mirosala. Consumption of KMnO_4 were significantly lower than that in the well waters of Lipjan and Mirosala.

Concentrations of NH_3 , NO_2^- , NO_3^- and Ca^{2+} of waters of Kamenica were significantly lower than in spring and well water of Istog. Concentration of Fe^{2+} in waters of Kamenica is approximately similarly with spring and well water of Istog. Concentrations of Mn^{2+} were significantly higher than in spring and well water of Istog. The distribution of Fe and Mn pollutants indicated natural pollutions and this may be a direct impact from geological constitution of rocks i.e. marlstone, claystone, sandstone, partly tuffstone, lignite, gravel, sand, sandy clay and tuffs deposits.

Table 4. Comparison of properties of water of Kamenica wells with those of water in similar wells in Kosovo.

Parameter	Kamenica well	Istog well ⁴⁴	Lipjan well ⁴⁵	Mirosala well ⁴⁶
EC $\mu\text{S cm}^{-1}$	490-530	696.3	1029.1	475.5
pH	7.17-7.65	7.2	6.86	7.98
KMnO_4 consumed mg L^{-1}	6.5-13.86	-	78.512	10.7133
NH_3 mg L^{-1}	0.26-0.37	2.372	-	-
NO_2^- mg L^{-1}	0.00198-0.0042	0.0617	-	0.0218
NO_3^- mg L^{-1}	0.298-1.018	19.04	-	0.2133
Cl^- mg L^{-1}	7.23-9.35	24.63	736.78	16.2593
Ca^{2+} mg L^{-1}	14-18.74	85.313	23.72	39.4033
Fe^{2+} mg L^{-1}	0.14-1.86	0.5287	-	16.858

CONCLUSIONS

Generally, waters of Kosovo wells are enriched in dissolved solids, as the consequence of aquifer lithology and residence time of ground water. In this study the assessment of water quality of water resources in Kamenica were investigated. In comparison with available results of three similar well waters in Kosovo, it can be summarized that water quality of resources in Kamenica were approximately the similarly with well waters of Mirosala. Results from physico-chemical analyses were used to compare the obtained value of the selected parameters with the WHO existing criteria of drinking water. Turbidity from the first well water (S_1), generally appeared to be significantly high, and exceed recommended WHO norms for drinking waters. The concentration of iron from the first well water (S_1), also appeared to be significantly high and exceed recommended WHO norms from 0.3 mg L^{-1} for drinking waters. The concentration of manganese in both well waters appeared to be significantly high and exceed recommended WHO norms of 0.1 mg L^{-1} for drinking waters. From the results of field work and laboratory analyses it was found out that the water from two well of Kamenica not fulfill the World Health Organization criteria set for drinking waters and can not be used as potable water.

From the results of field work and laboratory analyses it was found out that well water not fulfill the criteria set by the World Health Organization and the distribution of pollutants indicated anthropogenic sources of pollutants, waste waters and small rivers in suburb. The distribution of Fe and Mn pollutants indicated natural pollutions and this may be a direct impact from geological constitution of rocks: marlstone, claystone, sandstone, partly tuffstone, lignite, gravel, sand, sandy clay and tuffs deposits.

ACKNOWLEDGMENTS

This paper is a part of M. Sc. thesis of Sylejman Kryeziu, defended at the University of Prishtina, in July 2015 (supervisor Dr. Fatbardh Gashi). The study was financially supported by University of Prishtina. Measurements were performed at laboratory of The Institute of Public Health in Gjilan. Colleagues from the Department of Chemistry, University of Prishtina are thanked for their assistance.

References

- Angulo, F. J., Tippen, S., Sharp, D. J., Payne, B. J., Collier, C. *Am. J. Public Health*, **1997**, *87*, 580-584.
- http://www.unicef.org/media/media_21423.html
- Close, M., Dann, R., Ball, A., Pirie, R., Savill, M. and Smith, Z., *New Zealand J. Water Health*, **2008**, *6(1)*, 83-98.
- Keswick, B. H. (1984): *Groundwater Pollution Microbiology*. New York, John Wiley and Sons. 39-64.
- Thompson, T., Fawell, J., Kunikane, S., Jackson, D., Appleyard, S., Callan, P., Bartram, J. and Kingston, P., *Chemical safety of drinking-water: Assessing priorities for risk management*, World Health Organization. **2007**, Geneva.
- Chirila, E., Bari, T. and Barbes, L., *Ovidius Univ. Ann. Chem.*, **2010**, *21*, 87-90.
- Hamilton, L. S., *Food and Agriculture Organization of the United Nation*, 1st Ed., Rome, **2008**, 78.
- Montgomery, J. M., *Water Treatment, Principles and Design*. John Wiley & Sons, New York, **1996**, 474.
- Brils, J., *Ann. Inst. Superiore Sanita*, **2008**, *44*, 218-223.
- Lenntech water treatment and air purification. Water treatment. Lenntech*, Rotterdamseweg, **2004**, Netherlands (<http://www.excelwater.com/thp/filters/Water-Purification.htm>).
- Mildvan, A. S., *Metal in enzymes catalysis*. In: Boyer DD (ed) *The enzymes*, Academic Press, London, **1970**, *11*, 445-536.
- El Khalil, H., El Hamiani, O., Bitton, G., Ouazzani, N. and Boularbah, A., *Environ. Monit Assess.*, **2008**, *163*, 147-160.
- Lăcătușu, R., Cîtu, G., Aston, J., Lungu, M. and Lăcătușu, A. R., *Carpath J. Earth Environ Sci*. **2009**, *4*, 39-50.
- Higuera, P., Oyarzun, R., Oyarzún, J., Maturana, H., Lillo, J. and Morata, D., *Appl. Geochem.*, **2004**, *19*, 1855-1864.
- Zhai, L., Liao, X., Chen, T., Yan, X., Xie, H., Wu, B. and Wang, L., *J. Environ. Sci.*, **2008**, *20 (6)*, 696-703.
- Habashi, F., *Environmental issues in the metallurgical industry progress and problems, Environmental issues and Waste Management in Energy and Mineral Production*, Balkama, Rotherdam, **1992**, 1143-1153.
- Kebata-Pendias, A. and Pendias, H., *Trace elements in soils and plants*, CRC Press, Boca Raton, Florida, **1986**, p. 315.

- ¹⁷Pandey, S. and Tiwari S., *Nature and Science*, **2009**, 7(1), 17-20.
- ¹⁸Altman, S. J. and Parizek, R. R., *J. Environ. Quality*, **1995**, 24, 707-718.
- ¹⁹Jinwal, A. and Dixit, A., *Asian J. Exp. Sci.*, **2008**, 22(3), 311-316.
- ²⁰Järup, L., *Brit. Med. Bull.*, **2003**, 68, 167-182.
- ²¹Bruins. M. R., Kapil, S. and Oehme F. W., *Environ. Saf.*, **2000**, 45, 198-207.
- ²²Elshemy, M. and Meon, G., Climate change impacts on water quality indices of the southern part of aswan high dam reservoir, lake Nubia, 15th *Int. Water Tech. Conf.*, Alexandria, Egypt, **2011**, p.17.
- ²³Astel, A., Biziuk, M., Przyjazny, A. and Namiesnik, J., *Water Research*, 2006, 8, 1706-1716.
- ²⁴Simeono, V., Stratis, J. A., Samara, C., Zachariadis, G., Voutsas, D. and Anthemidis, A., *Water Research*, **2003**, 37, 4119-4124.
- ²⁵Singh, K. P., Malik, A., Singh, V. K., Mohan, D. and Sinha, S., *Anal. Chim. Acta*, **2005**, 550, 82-91.
- ²⁶Shrestha, S. and Kazama F., *Env. Modell. Software*, **2007**, 22, 464-475.
- ²⁷Gashi, F., Franciskovic-Bilinski S. and Bilinski, H., *Fres. Env. Bull.*, 2009, 18, 1462-1471.
- ²⁸Gashi, F., Frančičković-Bilinski, S., Bilinski, H., Troni, N., Bacaj, M. and Jusufi, F., *Environ. Monit. Assess.*, **2011**, 175, 279-289.
- ²⁹Gashi, F., Troni, N., Faiku, F., Laha, F., Haziri, A., Kastrati, I., Beshtica, E. and Behrami, M., *Am. J. Environ. Sci.*, **2013**, 9(2), 142-155.
- ³⁰Gashi, F., Troni, N., Hoti, R., Faiku, F., Ibrahim, R., Laha, F., Kurteshi, K., Osmani S. and Hoti, F., *Fres. Env. Bull.*, **2014**, 23(1), 91-97.
- ³¹Gashi, F., Stanislav Frančičković-Bilinski, S., Bilinski, H. and Kika, L., *Environ. Earth Sci.*, **2016**, 75, 801.
- ³²Gashi, F. Frančičković-Bilinski, S., Bilinski, H., Haziri, A., Gashi, S., *Arabian J. Geosci.*, **2016**, 9(6), 1-11.
- ³³Troni, N., Faiku, F., Gashi, F., Hoti, R., Teneqja, V., Laha F. and Berisha, R., *Int. J. Green Herbal Chem.*, **2013**, 2(2), 203-207.
- ³⁴<https://sq.wikipedia.org/wiki/Kamenica>
- ³⁵World Health Organization. *Guidelines for Drinking-water Quality*, 3rd ed. Vol. 1. Geneva, **2004**.
- ³⁶World Health Organization. *Guidelines for Drinking-water Quality*, 4th ed. Geneva, **2011**.
- ³⁷APHA, AWWA and WEF. Standard Method for the Examination of water and waste water. 20th ed. *Am. Pub. Health. Ass.*, Washington D.C. **1998**.
- ³⁸Baba, A., Kaya, A. and Birsoy, K. Y., *Water, Air Soil Pollut.*, **2003**, 149, 93-111.
- ³⁹Dalmacija, B., Water Quality Control in Towards of Quality Management, Faculty of Sciences, in serbian, Novi Sad, **2000**
- ⁴⁰Stat Soft. Inc. Statistica (data analysis software system), ver. 6. <http://www.statsoft.com>, **2001**.
- ⁴¹Tukey, J. W. *Exploratory data analysis*. Addison-Wesley, **1977**:
- ⁴²Matić, N., Maldini, K., Cuculić, V., Frančičković-Bilinski, S., *Chemie der Erde – Geochem.*, **2012**, 72, 179-190.
- ⁴³Independent Commission for Mines and Minerals / Komisioni i Pavarur për Miniera dhe Minerale/Nezavisna Komisioni za Rudnike i Geological map of Kosovo, Prishtinë. Minerale, **2006**.
- ⁴⁴Gashi, F., Frančičković-Bilinski, S., Bilinski, H., Shala A. and Haziri, A., Municipality (Kosovo). submitted to *Chemie der Erde. Geochem.*, **2016**
- ⁴⁵Gashi, F., Faiku, F., Hetemi, S., Bresa, F., and Gashi, S., *Moroccan J. Chem.*, **2016**, 4(1), 187-196.
- ⁴⁶Gashi, F., Troni, N., Faiku, F., Thaqi, A. and Gashi, A., *Eur. Chem. Bull.*, **2016**, 5(2), 63-68.

Received: 08.06.2016.

Accepted: 09.08.2016.



CHARACTERIZATION OF THE PHYSICO-CHEMICAL PROPERTIES OF THE MASERU MUNICIPAL WASTEWATER SLUDGE FOR POTENTIAL APPLICATION IN AGRICULTURAL SOILS AS AN ORGANIC-MINERAL AND SOIL MODIFIER

Emmanuel B. Tanor^{[a]*}, Mosotho J. George^{[a]#}, Phakisane J. Mohase^[a], Makhale E. Khesa^[a] and Lekunutu A. Khesa^[b]

Keywords: Waste water sludge, chemical toxicity, nutrient content, bio-fertilizer, soil application, Lesotho.

The indiscriminate land disposal of wastewater sludge in Lesotho poses an environmental and health concern since sludge typically contains a myriad of hazardous chemicals. This study characterised the physico-chemical properties of the sludge generated at the Ratjomose Wastewater Treatment Plant in Maseru, the capital city of Lesotho and its chemical safety for application on land as an organic fertilizer. The sludge was slightly acidic and had considerable amounts of macronutrients. The heavy metal concentrations are less than the maximum limits recommended by the Food and Agricultural Organization and the South African standards for sludge applied to agricultural land and are slightly higher than those recommended in the national industrial effluent discharge standards in Lesotho. Principal component analysis did not reveal any major differences between the different cells used in the treatment plant. Since the nutrients and chemical composition of this sludge match the guidelines for an organic-mineral soil conditioner, it can be concluded that this sludge is safe for use in agricultural soils with no expected negative effects.

* Corresponding Authors

Fax: +266 2234 0000

* E-Mail: eb.tanor@nul.ls or eb.tanor@gmail.com

E-mail: jm.george@nul.ls or maluti2005@gmail.com

[a] Department of Chemistry and Chemical Technology, National University of Lesotho, P.O. Roma 180, Roma, Lesotho

[b] Quality Control Laboratory, Production Division, Water and Sewerage Company, Maseru, Lesotho

Introduction

The sludge is a solid end-product of wastewater treatment, whose composition depends on the source and type of the wastewater influent entering the treatment plant as well as the treatment processes employed therein.¹ Wastewater sludge typically contains about 50 % organic matter and significant amounts of plant macronutrients that are generally not present in conventional chemical fertilizers.² These factors make the application of sludge as a fertilizer and soil conditioner in agriculture a more attractive option than the conventional disposal in landfills.³ The application of sludge to agricultural land ranges from as low as 0.06 % to as high as 70 % of the total sludge generated.^{4,5} Primarily, sludge application to the land recycles the essential plant nutrients and organic matter into the soil, which improves the productivity of the soil and increases crop yields with yield enhancement reportedly as high as 20 %.^{6,7} It improves the physical and chemical properties of soils; such as the organic matter content and electrical conductivity of soils that increase considerably,⁸ lowered erosion rates, even before vegetation covers the soil surface,⁹ the bulk density decreases aggregate stability increases, all of which result in increasing water retention, aeration and permeability of some soils,^{10,11} especially when the sludge is applied in the form of dewatered sludge cake.¹²

The other advantage includes the reduction in the use and costs of synthetic chemical fertilizers with savings as high as 40 % being reported when inorganic chemical fertilizers are

supplemented with wastewater sludge.⁷ It has also been argued that the recycling of organic matter through the soil-plant system in the form of sludge, compost and manure will reduce the amount of carbon in the atmosphere.¹³ Generally, municipal wastewater sludge contains toxic pollutants both of chemical and biological origin.^{14,15} The bioavailability of sludge-borne metals in soils is influenced by the physical and chemical properties of the soil of which the pH, the cation exchange capacity and the organic matter content become the major influential factors over the long-term.^{16,17} This therefore emphasizes the need for comprehensive characterization of sludge to mitigate the potential environmental and health impacts such as the potential risk of accumulation of toxic metals^{18,19} and some high parasite concentrations²⁰ in soil and hence a necessity to determine the appropriate loading rates and application frequency in order to protect farmers and farm workers, soils, crops and the environment^{21,22}. In view of these potential risks, application of sewage sludge to agricultural land is not accepted in many countries due to heightened public awareness and perception of risk as direct consequences of sludge application on land.²³

In Lesotho, as in most other developing countries, sanitation focuses largely on the treatment of the wastewater and little attention is given to the management of the sludge generated, due to the high cost of treatment and disposal.⁴ Sludge treatment, handling and disposal may be up to 50 % of the total costs for wastewater treatment. A large proportion of the sludge produced in Maseru, the capital of Lesotho, is generated at the Ratjomose Wastewater Treatment Plant (RWTP), the largest sewage treatment plant in Lesotho, capable of handling of 20 million cubic meters of wastewater per day. The municipal wastewater is treated using a combination of conventional and waste stabilization ponds methods. However, the guidelines for the management of the sludge generated are still at the drafting stage. Consequently, a large proportion of sludge generated

at wastewater treatment plants is disposed of indiscriminately in the abandoned quarries or recycled into agricultural land by individual subsistence farmers to improve soil fertility for crop production.²⁴ The current status favours the wastewater treatment company, because it is relieved of the burden and cost of further treatment and disposal of the sludge.

This study examined the physical and chemical characteristics of municipal wastewater sludge generated at the RWTP for its suitability for application on agricultural land, and compared the concentrations of nutrients and some common pollutants with South African standards and the FAO guidelines.²⁵ The data will also help to avoid the practice in most developing countries where effluent and sludge disposal standards are either too stringent because they are based on standards from developed countries or too relaxed so as to attract foreign industrial capital and therefore they do not guarantee the safety of the intended use of water and reuse of sludge in agriculture.²⁶

Experimental

The selection of parameters for the study was guided by either the beneficial or detrimental effects on soil and on plant growth, potential environmental and health impacts.^{21,27} The parameters selected for determination are pH, electrical conductivity, organic matter, macronutrients – nitrates and phosphates, calcium, potassium, magnesium and sodium; micronutrients - iron, manganese, copper and zinc and seven potential toxic metals arsenic, cadmium, chromium, cobalt, lead, mercury and nickel.

Sample collection, preparation and analyses

Sludge samples were collected from the RWTP and stored in the refrigerator at 4 °C till further use. Prior to analysis, the samples were air-dried at room temperature to a constant mass. Portions of the air-dried sludge were crushed and sieved through a 2-mm mesh to restrict particle size. These fractions were used to determine the physical and chemical parameters. To determine electrical conductivity (EC) and pH the sludge samples were blended in water (1:10 w/w) at 25 °C. The pH was measured using pH meter InoLab pH Level-1 (Germany), while conductivity was measured with conductivity meter, Condi-330i (Germany).

For other determinations, the representative samples were weighed and dried to a constant weight at 80±5 °C. A portion of the air-dried sludge samples was ground and sieved through a 1.0-mm mesh. This fraction was used to determine the total organic matter, nutrients, and the total content of potential toxic metals. Total organic carbon (TOC) was determined according to literature.²⁸ Organic matter (OM) was determined by wet digestion method. Nitrate-nitrogen and total phosphorous were determined according to the Hach methods 8039 and 8187.²⁹

Solutions for the determination of metals were prepared by acid digestion of the sludge samples according to US-EPA Method 3050B.²¹ Metals bound to organic carbon were released with 30 % H₂O₂ and HNO₃ at pH 2.0 and 85 °C.³⁰ Sodium, potassium, lead and zinc were determined by AAS

FS-220 flame atomic absorption spectrophotometer (Varian, California, USA). The other metals were determined using LIBERTY AX Sequential ICP-AES spectrophotometer (Varian, California, USA). Standard solutions for the analysis were prepared according to the Varian AAS 1998 Handbook. All chemicals used were of analytical reagent grade (Merck and BDH) and all solutions were prepared using de-ionized water.

Multi-variate statistics, specifically, principal component analysis was carried out using MINITAB Version 14 for the inter-cell variation as well as analysis of the differences between the analytes.

Results and Discussion

Nutrient content of the sludge

The results for the nutrient content and some physical properties of the sludge are shown in Table 1. The sludge is moderately acidic, the pH values of all the samples are within the range from 5.45 to 7.25 with a mean pH of 6.05. Sludge pH is very crucial in determining the rates of application on land as it has a direct effect on the pH of the soil and the bioavailability of micronutrients and metal ions to plants.^{31,32} An increase in sludge acidity could result in increase in the solubility of most metal ions like Pb, Cr, Cd, Cu, Ni and Zn and hence their bioavailability and uptake by plants.³³ The pH range for most agricultural practices is 6.5 to 7.5. Within this pH range most metal ions are bound to soil particles and therefore not accessible to plants.³⁴ In the untreated form, the sludge from the RWTP is only suitable for application to alkaline soils so as to neutralize the alkalinity rather than as a mere bio-fertiliser.

Table 1. The major nutrient contents and some physical properties of the sludge samples.

Parameter	Cell 1	Cell 2	Cell 3	Cell 4
pH	6.01	5.45	5.50	7.25
Conductivity, $\mu\text{S cm}^{-1}$	703	784	776	277
Total organic matter, g kg^{-1}	520	350	548	554
Total organic carbon, g kg^{-1}	1660	1733	1656	2871
TDS, g kg^{-1}	566	522	554	770
Organic-nitrogen, g kg^{-1}	15.8	19.2	13.6	47.4
Nitrate-nitrogen, g kg^{-1}	32.6	26.4	38.2	51.6
Total N, g kg^{-1}	48.4	45.6	21.8	99.0
Total P, g kg^{-1}	24.5	5.7	28.5	13.4
Ca, g kg^{-1}	31.5	35.2	25.3	24.7
Mg, g kg^{-1}	6.2	9.4	8.3	5.3
K, g kg^{-1}	1.8	4.3	2.6	2.4
Na, g kg^{-1}	3.2	4.5	2.1	1.8

EC is a surrogate measure of total dissolved solids (TDS) and also has a direct correlation with salinity, which is the total concentration of dissolved ionic salts in the soil solution. Therefore, it is expected that the total dissolved solids would correlate positively with the electrical conductivity, but the relationship is not direct because the mobility of ionic species in solution is variable and depends

on the nature and type of ions in the solution. The EC value for the fourth drying cell is half its value for TDS, which indicate that the dissolved solids were both ionic and non-ionic in nature. Salinity is an important parameter of soil and high salinity has toxic effects.³⁵ Thus the application of sludge with high levels of salts could ultimately affect the growth of plants.³⁶

The organic matter content of the sludge is in the range 350 to 554 g kg⁻¹ of dry weight, which translates to 35.0 to 55.4 %, which is typical of municipal wastewater sludge.³⁷ The overall effect of the changes brought by the sludge could be the reduced amounts of runoff and soil erosion,⁶ which will be very beneficial to farmers in Lesotho where soil erosion is major problem.

Regarding the major nutrients shown in Table 1, the total nitrogen content, determined as the sum of the organic and inorganic nitrogen, fell in the range 2.2-9.9 % while total phosphorous fell within 0.6-2.9 %. These values compare very well with those of some common organic manure and provide similar fertilizing properties (see Table 2). Nitrogen is an integral component of chlorophyll and therefore essential for photosynthesis and is important in periods of rapid plant growth. It is also a vital component of proteins, which control the metabolic processes required for plant growth. An adequate supply of nitrogen is associated with vigorous vegetative growth and a plant's dark green colour. Nitrogen deficiency is characterized by reduced plant growth and a pale green or yellow colour.³⁸

Phosphorus is a critical component of nucleic acids and plays a vital role in plant reproduction and it is essential to seed formation. Phosphorus is essential for the biological energy transfer processes that are vital to life and growth³⁹. Phosphorus deficiency is indicated by reduced plant growth, delayed maturity, and small fruit set. The availability of phosphorous is very sensitive to the soil pH with the uptake rate by higher plants being at the highest between pH 5.0 and 6.0 where H₂PO₄⁻ predominates in soil solution.⁴⁰ The sludge contains significantly higher amounts of total nitrogen than that in cattle, poultry and sheep manures (Table 2). The phosphate content is higher than that of cattle and sheep manure, but lower than phosphate content of poultry manure.

The concentrations of exchangeable bases are in the range of 1.80-9.40 g kg⁻¹ of the dried mass. The lowest value was recorded for Na⁺ while the highest value was for Ca²⁺. These values are much higher than the concentrations determined for cattle and sheep manures (Table 2), but are lower than the concentrations in poultry manure. However, the nutrient contents are lower than those of synthetic inorganic fertilizers on the market. Most nitrogenous fertilizers contain 15-40 % total nitrogen, phosphate fertilizers contain 14-30 % of phosphates, which may be in the water soluble form or citrate soluble form and potash fertilizers contain 22-60 % of water soluble potash.⁴¹ Though the nutrients contents are low, relative to chemical fertilizers, the sludge can be a good alternative as a soil conditioner because land application reduces or eliminates the cost of disposal and use of synthetic mineral fertilizers.

The comparison of the values from cell to cell did not seem to follow any trend as can be seen from Figure 1. Some parameters showed a decrease from cell 1 to 4, some do not show any trend.

Table 2. Comparison of nutrients content of used sludge sample and some common organic manure.

Manure	Average nutrient content (% by weight)				
	Total-N	P ₂ O ₅	K ₂ O	CaO	MgO
Poultry*	2.20	1.80	1.10	2.40	0.70
Cattle*	1.20	0.17	0.11	0.35	0.13
Sheep*	1.55	0.31	0.15	0.46	0.15
Maseru	8.50	1.20	0.34	3.01	0.75
Sludge		(PO ₄ ³⁻)	(K)	(Ca)	(Mg)

*Source: SRI-CSIR, 1997 Soil Research Institute (SRI). 1998. The 1997 Annual Report. Accra.

Heavy metal content

The presence of toxic heavy metals in sludge makes its use as an organic fertilizer or soil amendment a matter of concern. Furthermore, the uptake of these metals by plants and their subsequent bioaccumulation along the food chain poses a potential threat human health. The total concentrations of the heavy metals in the sludge are shown in Table 3.

Table 3. Metal contents of sewage sludge from Ratjomose Wastewater Treatment Plant.

Metal	Total conc. mg kg ⁻¹	Bound to organic carbon,		Maximum limit*, mg L ⁻¹
		mg kg ⁻¹	%	
Al	37.5	21.4	57.1	NA
As	13.5	8.50	65.4	0.5
Cd	8.5	7.34	86.4	0.05
Co	172.2	29.3	17.0	NA
Cr (total)	7.4	4.31	58.2	0.5
Cu	85.0	65.3	76.8	1.0
Fe	1424	1121	78.7	NA
Hg	4.2	3.76	89.5	0.02
Ni	18.0	8.60	47.8	NA
Pb	25.8	0.8	3.1	0.1
Zn	4438	843.6	19.7	5.0

*National Environment Secretariat, Wastewater Discharge Standards, First Draft, Maseru, 1997; NA – not included in draft standards.

The higher concentrations of these heavy metals in the sludge could only originate from the textile industries, since there are no other chemical industries in Maseru. These industries discharge their effluents into the sewer systems with minimum pre-treatment.⁴¹ Textile industries effluents contain heavy metal ions from metal containing dyes.^{42,43} In general all the sludge samples contain relatively higher amounts of all the target metals.

It was observed that the sludge sample with the higher organic matter content has a higher proportion of the heavy metals bound to organic carbon. Most of the metals have a high proportion bound to organic matter in a decreasing order: Hg (89.5 %) > Cd (86.4 %) > Cu (76.8 %) > As (65.4 %) > Cr (58.2 %) > Ni (47.8 %) > Zn (19 %) > Co (17 %) > Pb (3.1 %).

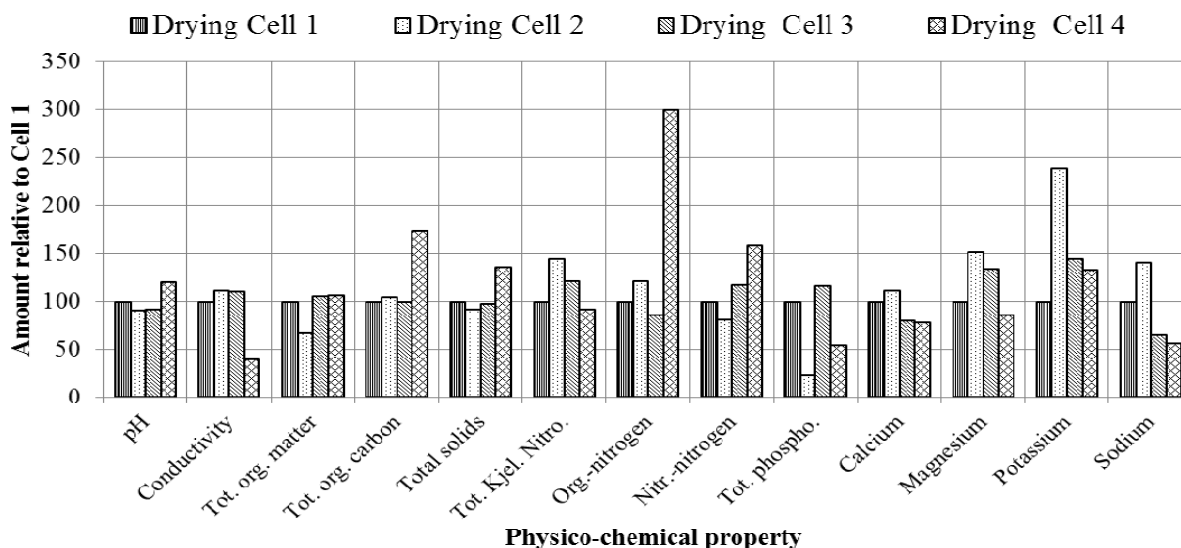


Figure 1. Some physico-chemical properties of sludge of in different cells relative to those in cell 1.

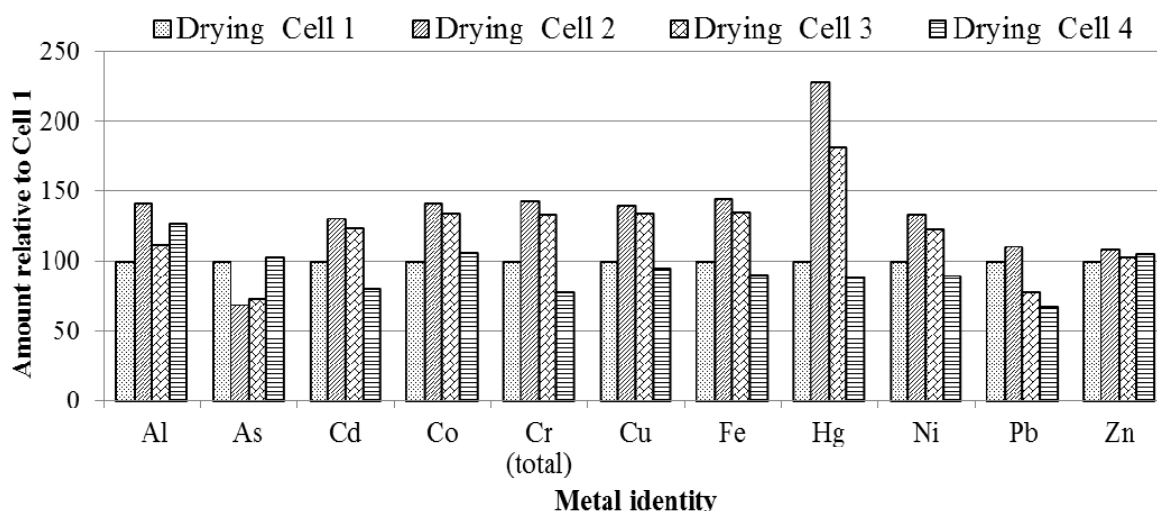


Figure 2. Relative abundances of some heavy metals measured relative to cell 1.

This suggests that these metals may have formed stable insoluble complexes with the organic fraction or they are strongly bound to the organic matter, limiting their solubility and potential bioavailability in soil.¹⁵ Depending on the pH of the soil, these organic-bound metals may be slowly released and become bioavailable to plants.⁴⁴ This assertion agrees with the slight increases in metal concentrations with increasing acidity of the sludge. All the sludge samples exhibited elevated levels of the metals, higher than the maximum limits set out in the draft wastewater and industrial effluent discharge standards for Lesotho.⁴⁵

Interestingly, it was observed that the concentrations of the metals increase slightly with the increasing acidity, i.e. decreasing pH of the sludge.

Figure 3 is a plot of relative abundances of individual ions (relative to pH 7.25, near neutral measured pH) against the actual pH of the media.

The metal concentrations were compared with the South African sludge standards and the FAO recommended guidelines for sludge application on land, as shown in Table 4 because there are no national standards in Lesotho. In all the sludge samples, only the concentration zinc (4438 mg kg^{-1} dry weight) exceeded the maximum permissible value of 3000 mg kg^{-1} dry weight of the South African standards, but lower than the 7500 mg kg^{-1} weight recommended by FAO. Heavy metals are a concern because they are non-biodegradable and over time they accumulate in the plough layer of the soil, where they are available to plants.

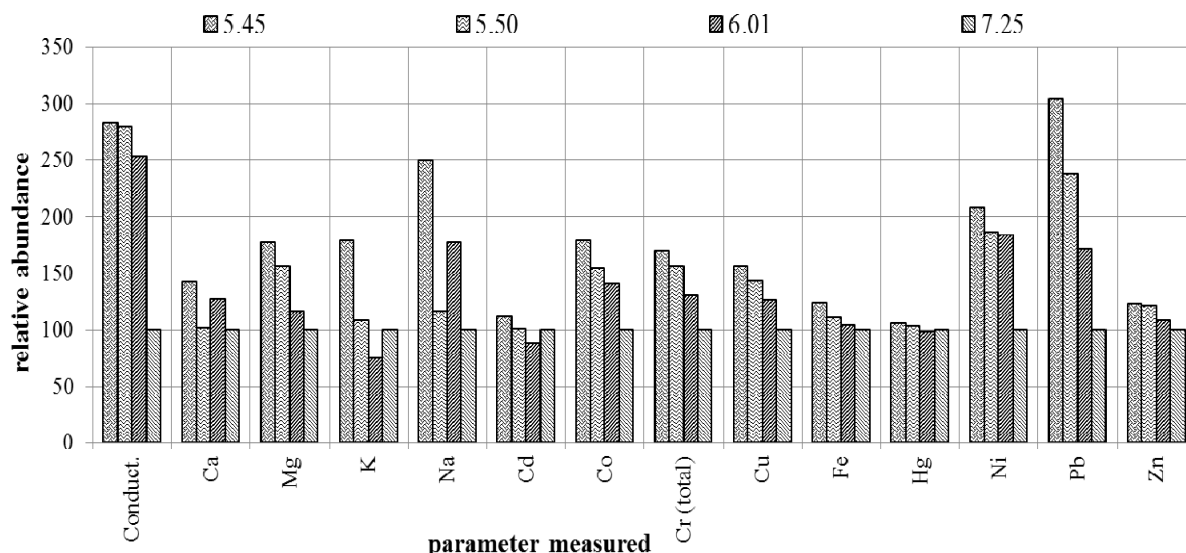


Figure 3. The pH dependence of the abundance of the metal ions from the sludge relative to pH 7.25.

Table 4. Comparison of heavy metals concentration in sewage sludge with international standards.

Metal	Amount, mg kg ⁻¹ (dry weight)		
	RWTP Sludge	South African Standards	FAO Guidelines
As	13.0	80	75
Cd	18.5	20	85
Co	56.4	-	-
Cr	7.4	1200	3000
Cu	85.0	1200	4300
Hg	4.2	25	57
Ni	18.0	200	420
Pb	25.8	1200	840
Zn	4438	3000	7500

Most heavy metals such as cadmium, build up in the soil with continued sludge applications can be toxic to soil micro-organisms and thus affecting soil fertility and physical structure.

The mean concentrations of the metals in the sludge samples are shown in Table 2. There is no general agreement concerning the maximum allowable concentrations of various metals in sewage sludge. The concentrations of all the metals are several times lower than the recommended maximum permissible contaminant levels (MCL) set by most regulations bodies. For example, the South African Standards (SAS) set the MCL for zinc at 4438 mg kg⁻¹ dry sludge while the US EPA set the value at 7500 mg kg⁻¹ dry sludge; both significantly higher than the obtained values of 3000 mg kg⁻¹.

With this comparison, it can be concluded that the sludge can be applied safely to the agricultural land. However, MCL values vary with the pH of the soil because it is known

that crop damage from phytotoxic elements is more likely to occur on acid soils. The MCL values for Zn are 200 mg kg⁻¹ dry sludge at pH 5.0-5.5; 250 mg kg⁻¹ dry sludge at pH 5.5-6.0; 300 mg kg⁻¹ dry sludge at pH 6.0-7.0 and 450 mg kg⁻¹ dry sludge at pH >7.0 (see Table 3). Thus, the pH of the sludge is very vital when deciding on the rate of application of sludge on land. The phytotoxicity from the sludge metals usually is not clearly apparent for most plants as long as the soil pH is maintained in the 6-7 range by lime amendment.

Analysis of the data with multivariate statistics

Multi-variate statistics is usually used to reveal some valuable information that may be hidden from the human eye at the same time reduce the complexity of the data to only few dimensions that could be easily identified. This technique was successfully applied recently in the profiling of the Caledon River along Maseru City where it demonstrated major contributors to the general water pollution in this important source of potable water to the municipality other than being an international border with South Africa, the only neighbour to Lesotho.⁴⁵ Figure 4 shows the scatter plot following the analysis of the data by principal component analysis.

As can be seen, the data shows that there is no considerable difference between the cells (PC1) but rather a larger difference occurred in between the trials (still along the PC1), a situation that is quite strange. This possibly implies that the samples may not have been homogenous enough to yield similar and comparable replicate results. This assertion is supported by the loadings plot (Figure 5) which reveals that a majority of these parameters are responsible for the shift in the PC1, while PC2 corresponds to the variation between the individual cells, which is usually the opposite. However Cell 4 seems to be the one that is slightly different from the rest of the cells with about 5 % variance (Figure 4) while Cells 1 and 3 are almost replicates.

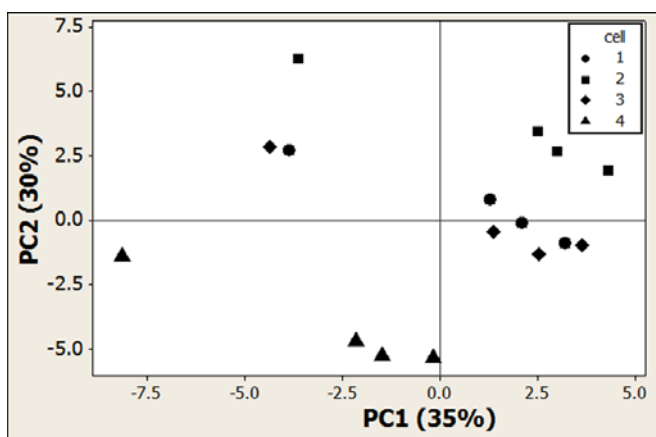


Figure 4. A scatterplot showing the variance between the cells and the replicates

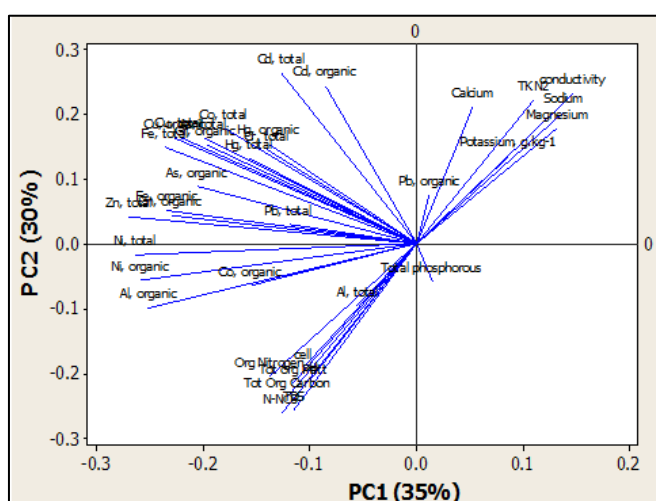


Figure 5. A loadings plot showing individual parameters that were measured in the study

The small difference observed between the cells was to be expected since the cells are used interchangeably, where the next cell is used when the previous gets emptied, and so on. The shift in the PC2 due to nitrogen content is clearly expressed in Figure 1 for Cell 4. This has thus rendered Cell 4 different from the other cells. However, overall, this difference in the cell is quite negligible. These results further demonstrate the applicability of multi-variate statistics in reducing the multiplicity of data into something manageable to screen for major contributors to the observed trends.

Conclusions

The sewage sludge produced at the Ratjomose Treatment Plant has been characterized for its physico-chemical properties. The results showed that the sludge can be a good source of organic matter, plant macro- and micro-nutrients. It has higher nutrient content than cattle, sheep and poultry manures, although these contents are still lower than the conventional NPK fertilizers. The pH varies in a very narrow range of pH 6.4 - 7.6, which is close to neutrality and ideal for most soils. However, the sludge contains some toxic heavy metals, but the levels are much lower than the

guideline values recommended by FAO, but higher than the recommended in the draft national standards. A high proportion of these metals is bound to organic carbon in the order: Hg (89.5 %) > Cd (86.4 %) > Cu (76.8 %) > As (65.4 %) > Cr (58.2 %) > Ni (47.8 %) > Zn (19 %) > Co (17 %) > Pb (3.1 %), and hence may not be readily available for plant uptake. There seems to be a direct relationship between high acidity and the release of these heavy metal ions from the organic matter. Besides the intra-trial differences, something considered a possibility of batch error; the four cells seem to have uniform compositions. It can thus be concluded that this sludge can be applied to agricultural soils with confidence as it contains very low levels of hazardous components. The presence of hazardous heavy metals, albeit at considerably low levels, requires some thought if this sludge would have to be regularly applied to the same field to avoid eventual accumulation of these ions.

References

- Wong, J. W. C., Li, K. L., Zhou, L. X., Selvam, A., *Geoderma*, **2007**, 137, 310
- Warman, R. P., Termeer, W. C., *Biosci. Technol.*, **2005**, 96(9), 1029
- Ramulu, J. S., *Reuse of municipal sewage and sludge in agriculture*. Scientific Publishers, **2002**, Jodhpur, India.
- Spinosa, L., *Wastewater sludge: a global overview of the current status and future prospects*. 2nd Rev. Ed., IWA Publishing, **2011**, London, United Kingdom.
- North East Biosolids and Residuals Association, *A national biosolids regulation, quality, end use and disposal survey*. **2007**, USA.
- Ojeda, G., Alcaniz, J. M., Ortiz, O., *Land Degrad. Dev.*, **2003**, 14(16), 563.
- Henning, B. J., *PhD Dissertation*. **2000**, University of Pretoria, South Africa.
- Mendoza, C., Assadien, N. W., Lindemann, W., *Chemosphere*, **2006**, 63(11), 1933.
- Sort, X, Alcañiz, J. M., *Land Degrad. Rehabil.*, **1996**, 7, 69.
- Singh, R. P., Agrawal, M., *Waste Manage.*, **2008**, 28, 347.
- Annabi, M., Le Bissonnais, Y., Le Villio-Poitrenaud, M., Houot, S., *Agric. Ecosyst. Environ.*, **2011**, 144, 382.
- Casado-Vela, J., Selle, S., Navarro, M. A., Bustamante, J., Mataix, C., Guerrero, J., Gomez, I., *Waste Manage.*, **2006**, 26, 946.
- Kotschi, J., Muller-Samann, K., *IFOAM*, Bonn, Germany. Retrieved on 24 June 2013 from www.ifoam.org/Neil:PATH.
- Smith, S. R., Riddell-Black, D., *Final Report to DEFRA*. **2007**. Retrieved on 01 February 2011 from http://randd.defra.gov.uk/Document.aspx?Document=SP054_7_7266_FRA.pdf.
- Smith, S. R., *Environ. Int.*, **2009**, 35, 142.
- Hue, N. V., Ranjith, S. A., *Water Air Soil Poll.*, **1994**, 72(1), 265.
- Sherene, T., *BFAIJ*, **2010**, 2(2), 112.
- Obrador, A., Mingot, J. I., Alvarez, J. M., Rico, M. I., *Sci. Total Environ.*, **1997**, 206, 117.
- Alvarez, A., Mochon, M. C., Sanchez, J. C. J., Rodriguez, M. T., *Chemosphere*, **2002**, 47(7), 765.
- Jimenez, B., Barrios, J. A., Mendez, J. M., Diaz, J., *Water Sci. Technol.*, **2004**, 49(10), 251.

- ²¹Environmental Protection Agency, Method 3050B, **1996**. Retrieved on 12 May 2014 from http://www.epa.gov/osw/hazard/testmethods/sw846/online/3_series.htm.
- ²²Herselman, J. E., Moodley, P., *Water Research Commission TT 350/09*. **2009**. Pretoria, South Africa.
- ²³Robinson, K. G., Robinson, C. H., Raup, L. A., Markum, T. R., *J Environ. Manage.*, **2012**, *98*, 29.
- ²⁴Water and Sewerage Company, *Sewage treatment and disposal – sludge handling*. **2007**. Maseru, Lesotho. Retrieved on 17 April 2013 from www.wasco.co.ls/water/treatment.php.
- ²⁵Food and Agriculture Organisation. *FAO Irrigation and Drawing Paper 47*. **1992**, Rome, Italy.
- ²⁶Ragas, A. M., Scheren, P. A., Konterman, H. I., Leuven, R. S., Vugteveen, P., Lubberding, H. J., Niebeek, G., Stortelder, P. B., *Water Sci. Technol.*, **2005**, *52(9)*, 133.
- ²⁷Achiba, W. B., Gabteni, N., Lakhdar, A., Liang, G. D., Verloo, M., Jedidi, N., Gallili, T., *Agric. Ecosyst. Environ.*, **2009**, *130*, 156.
- ²⁸European Standards. Draft European Standard, STD Version 2.1a, TC-WI 2004(E). **2004**.
- ²⁹Hach Company, DR/2000 Spectrophotometer Procedures Manual. 8th Edition. **1993**.
- ³⁰Tessier, A., Campbell, P. C. G., Bisson, M., *Anal. Chem.*, **1979**, *51(7)*, 844.
- ³¹Fytianos, K., Katsianis, G., Triantafyllou, P., Zachariadis, G., *Bull. Exp. Biol. Med.*, **2001**, *67*, 423.
- ³²Hinsinger, P., *Plant Soil*, **2001**, *237*, 173.
- ³³Singh, R. P., Agrawal, M., *Chemosphere*, **2007**, *67(11)*, 2229.
- ³⁴Gaskin, J., Risse, M., Segars, B., Harris, G., *Pollution Prevention and Assistance Division, Factsheet Series, Special Bulletin 27*, **2012**. University of Georgia.
- ³⁵Asia, I. O., Ekpo, K. E., Chuekwedu, M. E., *Afr. J. Biotechnol.*, **2008**, *7(14)*, 2434.
- ³⁶Murillo-Amador, B., Lopez-Aguilar, R., Kaya, C., Larringa-Mayoral, J., Florez-Hernandez, A., *J. Agron. Crop Sci.*, **2002**, *188(4)*, 235.
- ³⁷Mamta, I., Wani, K.A., Bhadauria, R., *World J. Agric. Sci.*, **2001**, *7(6)*, 643.
- ³⁸Chen, L. S., Wang, K., *J. Soil Sci. Plant Nutr.*, **2014**, *14(2)*, 382.
- ³⁹Hua, L., Wang, Y., Wu, W., McBride, M. B., *Water Air Soil Poll.*, **2008**, *188*, 225.
- ⁴⁰Furihata, T., Sakura, H., *Plant Cell Physiol.*, **1992**, *33*, 1151
- ⁴¹Vitosh, M. L. *Michigan State University Cooperative Extension Service, Extension Bulletin*, E-896. **1983**.
- ⁴²United Nations Environment Programme. *UNEP Technical Report 16*. **1994**. Paris, France.
- ⁴³Poornima, K., Vasudevan, K., Venkateshwarlu, M., *Elec. J. Environ. Sci.*, **2011**, *4*, 79.
- ⁴⁴Mullins, G. L., Sommers, L. E., *J. Environ. Qual.*, **1996**, *15*, 382.
- ⁴⁵National Environmental Secretariat. *Wastewater Discharge Standards - First Draft*. **1997**, Maseru, Lesotho
- ⁴⁶Tanor, E. B., Ts'enoli, S. B., George, M. J., *Eur. Chem. Bull.*, **2014**, *3(8)*, 776..

Received: 07.07.2016.

Accepted: 18.08.2016.



BENEFICIAL EFFECTS OF HYPOTHALAMIC PROLINE-RICH PEPTIDE-1 ON THE HEART FAILURE ASSOCIATED WITH EXPERIMENTAL PANCREATIC NECROSIS AND CRUSH SYNDROME

A. G. Guevorkyan^[a], N. Kh. Alchujyan^{[b]*}, H. M. Mikayelyan^[b], V. H. Barseghyan^[b], H. L. Hayrapetyan^[b], H. F. Khachatryan^[b], V.S. Grigoryan^[a], L. H. Melkonyan^[c], S. G. Chailyan^[b], G. A. Kevorkian^[b]

Keywords: Calcium binding proteins, cardiomyocytes, crush syndrome, hypothalamic proline rich peptide-1, pancreatic necrosis, sarcoplasmic reticulum.

Hypothalamic neurosecretory cytokine, proline-rich peptide-1 (PRP-1) may protect against myocardial dysfunction and hypocalcemia induced by experimental pancreatic necrosis (PN) and/or crush syndrome (CS). 24 and 48 h after initiation of experimental PN, effective doses of PRP-1 were administered to adult Wistar male rats divided into groups corresponding to early, reparative, chronic, and chronic recurrent stages of PN. Similarly age and sex matched rats were immediately administered PRP-1 after 2 h of compression injury. The PRP-1 normalized the histopathological changes in cardiac tissues in the dynamics of both PN and CS. Study of $^{45}\text{Ca}^{++}$ binding to the membrane proteins of cardiomyocyte sarcoplasmic reticulum (SR) showed that PRP-1 could prevent an impairment in the calcium binding ability of the Ca^{2+} depot proteins caused under pathological conditions. Besides, PRP-1 suppresses a PN and/or CS-induced compensatory manifestation the affinity to calcium of the 32-kDa SR membrane protein and restores its native properties. The results highlight new prospects over the functional implications of PRP-1 and its possible therapeutic potential for the treatment of patients at high risk of cardiovascular disease associated with different pathologies.

* Corresponding Authors

Fax: +(37410) 297343

E-Mail: alchujyan@mail.ru

[a] Yerevan State Medical University after M. Heratsi (YSMU)

[b] H. Buniatian Institute of Biochemistry NAS RA, 5/1 P. Sevak St., 0014, Yerevan, Republic of Armenia

[c] Gyumri State Pedagogical Institute after M. Nalbandyan (GSPI)

INTRODUCTION

It is generally accepted that the steady state of calcium flux balance is significantly necessary for myocardium.^{1,2} Hypocalcemia is one of the metabolic alterations involved in the hemodynamic changes and myocardial damage observed in clinical and experimental studies in acute pancreatitis, and its severe form, pancreatic necrosis (PN).³ It has been shown that traumatic muscle crush injury may also be a cause of cardiomyocyte specific injury.⁴ Our findings suggest that muscle crush injury induced crush syndrome (CS) accompanied by total intoxication causes a cardiac muscle injury at the early stage of decompression similar to the myocardial damage occurred in experimental PN.^{5,6} Moreover, we have demonstrated that both experimental acute pancreatitis and long-term compression injury are accompanied by a loss of ability to bind calcium of the membrane proteins of the cardiomyocyte sarcoplasmic reticulum (SR) that contributed to hypocalcemia which is involved in common cellular and molecular mechanisms of myocardial injury.^{6,7}

Plenty of evidence suggests the interplay between cardiac endocrine system and hypothalamic neurosecretory

hormones providing optimal functioning of brain and heart.^{8,9} Hypothalamic neurohormones are involved in the regulation of the intracellular calcium level and exert cardioprotective properties in acute pancreatitis.^{5,10} Proline-rich peptide-1 (PRP-1), one of the neurosecretory cytokines discovered and studied at H. Buniatian institute of Biochemistry NAS RA (acad. A.A. Galoyan) is implicated in the multiple mechanisms of neuroprotection, regulation of myelopoiesis, immune and stress response.¹¹ PRP-1 may also provide cardio-protective effects via regulation of phospholipids metabolism and their level in the cardiomyocyte membranes, and suppression of oxidative stress in heart tissues as it was demonstrated at cardiopulmonary insufficiency. We have shown that PRP-1 could upregulate the protein synthesis, stimulate a utilization of D-glucose, and prevent histopathological changes in tissues during CS.^{12,13} The aim of the present study was to extend our knowledge on the effects of PRP-1 on molecular mechanisms of myocardial damage particularly associated with a loss of the calcium binding ability of the cardiomyocyte proteins during experimental PN and/or CS.

EXPERIMENTAL

Materials and methods

Bovine serum albumin was from Carl Roth (GmbH, Karlsruhe). Solid-phase synthesis of proline-rich peptide-1 was performed at Moscow laboratory headed by acad. A.A. Galoyan. All other reagents were purchased from Sigma-Aldrich (USA).

Animals and study design

The experiments were carried out in accordance with the European Communities Council Directive (86/609/EEC) on care and use of animals for experimental procedures; protocols were approved by the respective Institutional Animal Care and Ethics Committee of the National Academy of Sciences the Republic of Armenia. Animals were housed six per cage at 12:12 h light/dark cycle (08.00–20.00 h) and had unrestricted access to a standard diet and tap water. Adult 6–7 month-old male Wistar rats weighing 180–220 g were randomly divided into groups ($n = 12/\text{group}$) and subjected to the experimental PN and/or compression injury under conditions of PRP-1 treatment. The PRP-1 preparation was dissolved in saline and filtered (0.22 μm) before use.

Experimental pancreatic necrosis was developed using previously established procedures.⁵ Briefly, pancreas was removed through a surgical incision, and a tail of the pancreas, which ends abutting the spleen was cooled by chloroethyl, and the frozen part was defrosted by fingers, returned to its place and incision was sutured. Rats were sacrificed at different stages of PN (marker enzyme, serum α -amylase determined by Reagent kits (ECOLab ZAO, Russia), 1, 7, 14 and 21 d after initiation of PN corresponding to early, reparative, chronic, and chronic recurrent stages of PN respectively. 24 and 48 h after initiation of the PN, PRP-1 (10^{-6} M) was injected to rats intraperitoneally.

Experimental crush syndrome was induced by application of a standardized mechanical pressure (10 kg/100 g body weight) applied to the femoris muscle of rat for two hours.¹³ Rats were sacrificed immediately after removal of the load, and at 2, 4, 24, and 48 h of decompression stages. Intraperitoneal administration of PRP-1 (10^{-6} M) was performed immediately at the end of compression and an hour later.

Age and sex matched intact rats serve as controls. Rats were anaesthetized with ester prior to surgical and/or compression procedures and/or decapitation.

Measurement of cardiac-specific Troponin I (cTnI) in the whole blood, a very sensitive and specific indicator of damage to the heart muscle was performed by test of i-STAT cTnI (cTnI; i-STAT, Princeton, NJ). cTnI could detect myocardial necrosis in complex clinical situations, where the usual enzymatic markers may be ineffective.¹⁴

Isolation of cardiomyocyte, and preparation of sarcoplasmic reticulum

After decapitation of animals under light anesthesia the heart was excised, attached to a Langendorff column, perfused with 0.15 M KCl, then crushed by a special press with micro-holes and homogenized in an ice-cold 20 mM HEPES buffer pH 7.4, containing 0.44 M sucrose and 1 mM EDTA, (1:10, w/v) using Potter homogenizer (1500 rpm for 3 min). The homogenate was centrifugated at 50 g for 3–5 min, and cardiomyocytes in the pellet were obtained, suspended in the 20 mM HEPES buffer pH 7.4, containing 300 mM sucrose, 1 mM PMSF, and 20 mM PIPES, and disrupted with a glass-glass homogenizer. The homogenates

were centrifuged at 500 g for 20 min, and the supernatant was subjected to sucrose gradient centrifugation. SR was presented by the densest fraction characterized with the highest $\text{K}^+/\text{Ca}^{2+}$ -ATPase activity, and the absence of the Na^+/K^+ -ATPase activity.¹⁵ Purity of the SR was confirmed also morphologically.

Polyacrylamide gel electrophoresis and isoelectric focusing

Prior to initiation of PN and/or CS, radioactive $^{45}\text{CaCl}_2$ was administrated to animals. Translocation of calcium ions was assessed by measuring the distribution of $^{45}\text{Ca}^{++}$ in the cardiomyocyte cellular compartments.¹⁶ SR membrane proteins were separated by sodium dodecyl sulfate-polyacrylamide gel electrophoresis (SDS-PAGE) and isoelectric focusing.^{17,18} Samples were homogenized in glass-glass microhomogenizers in Tris buffer, pH 7.2 containing of 1 % SDS, 0.05 % 2-mercaptoethanol, 1 mM EDTA, 1 mM phenylmethylsulfonyl fluoride, 50 mcg mL^{-1} leupeptin, 50 mcg mL^{-1} antipain, and 100 mcg mL^{-1} aprotinin. The homogenates were centrifuged at 13000 g for 30 min at 4 °C and pellets were re-suspended in cold buffer solution. Slab gel was composed of a stacking gel of 4.75 % (W/v) acrylamide, pH 7.2, and running gel of 10 % acrylamide, pH 8.9. After electrophoresis the radioactivity of $^{45}\text{Ca}^{2+}$ was measured from the gel plates using a gas-flow meter Berthold-II (Germany).¹⁹ Specific binding of $^{45}\text{Ca}^{2+}$ to the SR membrane proteins is expressed in counts per minute (cpm) \cdot mg^{-1} protein. Interaction between protein and bound calcium was evaluated by Scatchard plot analysis.^{20, 21}

Protein was determined by the method of Lowry et al, using crystalline bovine serum albumin as standard.²²

Statistical analysis

Data are presented as the mean \pm SEM. All statistical analysis was performed by *t*-Test for independent samples, or a one-way ANOVA followed by Holm-Sidak post hoc test (SigmaStat 3.5 for Windows). The *P*-values of 0.05 or less are considered as statistically significant differences.

RESULTS AND DISCUSSION

According to current concepts heart failure is considered as the result of changes to the heart cellular and molecular components and to mediators that drive homeostatic control.^{1–4} New hypothalamic cytokine, PRP-1 (primary structure, AGAPEPAEPAQPGVY and apparent molecular mass of 1475.26 Da) represented the C-terminal 25–39 fragment of neurophysin-vasopressin-associated glycoprotein, produced in hypothalamus nuclei (n. paraventricularis and n. supraopticus) and might be involved in the regulation of homeostasis via multiple mechanisms.¹¹

PRP-1 impact on the calcium binding by the cardiomyocyte membrane proteins in the dynamics of pancreatic necrosis

The sarcoplasmic reticulum (SR), the intracellular storage site of Ca^{2+} plays a major role in the contraction/relaxation machinery, and cardiac dysfunction is commonly associated with impairment in SR function, sarcolemmal calcium

influx and damage in calcium regulatory proteins.²³ Alterations in proteins involved in intracellular Ca^{2+} handling may affect cardiomyocyte contraction and contribute to heart failure.²⁴ Our previous findings showed that both experimental pancreatic necrosis (PN) and crush syndrome (CS) are accompanied by significant alterations in the qualitative and quantitative properties of the cardiomyocyte SR proteins, and by heart failure up to myocardial infarction.^{6, 7}

The same models were applied to study the effect of PRP-1 on common molecular mechanisms of cardiac dysfunction observed at the mentioned pathological states. The effect of PRP-1 was studied at early, reparative, chronic, and chronic recurrent stages of PN (1, 7, 14 and 21 days after PN initiation respectively). Measurement of cardiac-specific Troponin I and histomorphological analysis suggested the PN-induced damage to the heart muscle.

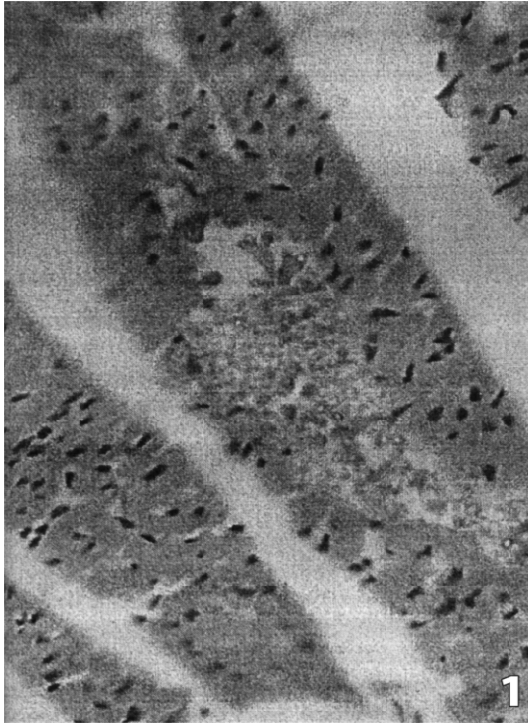


Figure 1. Focal lymphocytic infiltrate (hematoxylin, magnification 400X).

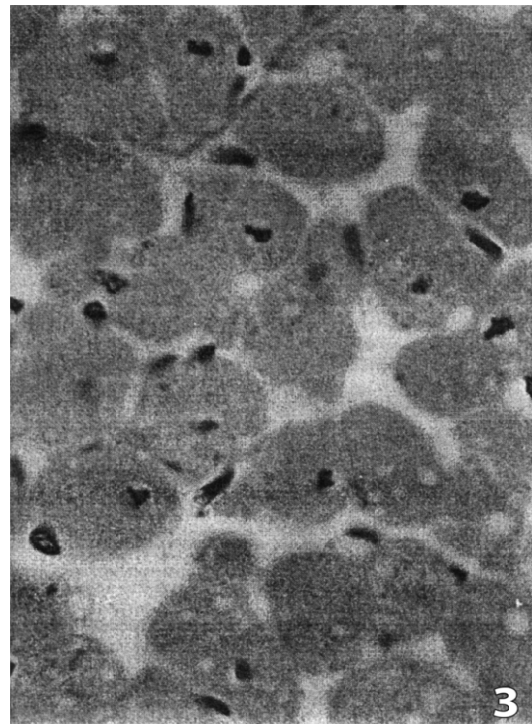


Figure 3. Myocytolysis and fuchsin stained changes in left ventricular wall (magnification 1000X).

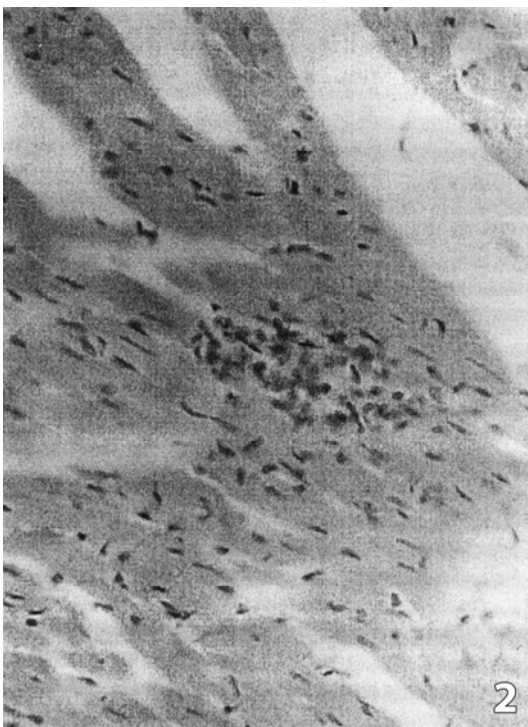


Figure 2. Vacuolation of the cardiomyocyte sarcoplasm (hematoxylin, magnification 1000X).



Figure 4. Hypertrophic cardiomyocytes with elongated nuclei (hematoxylin, magnification 400X).

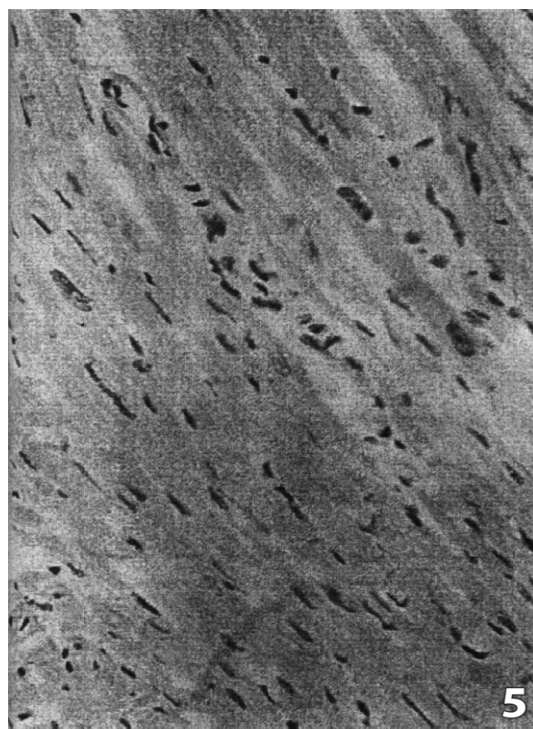


Figure 5. Contracture and degeneration of cardiomyocytes (hematoxylin, magnification 1000X).

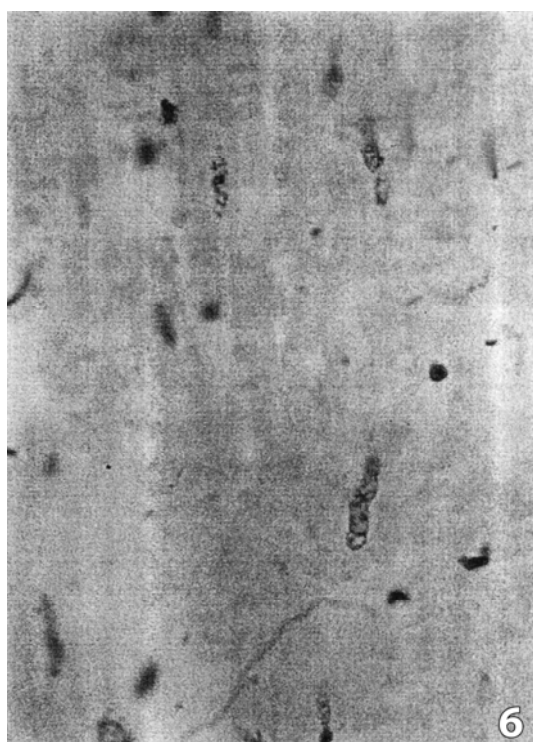


Figure 6. Perinuclear myocytolysis (staining with acid fuchsin by Selye, magnification 1000X).

Results presented in Figures 1-6 show histopathological changes in cardiac muscle corresponding to general morphologic criteria accepted for the diagnosis of degenerative myocardial lesions described for rats.²⁵ It may be noted that degenerating cardiomyocytes typically contained cytoplasmic vacuoles often occupied the sarcoplasm. Myocardial degeneration is associated with

diffuse vacuolation of cardiomyocytes (Figure 2). In figure 5, multifocal mineralization of degenerating cardiomyocytes can be seen in hearts with more severe degeneration.

A cardiomyopathy in rats begins histologically with degeneration and necrosis of individual cardiomyocytes or small focal clusters of myofibers with eventual myofiber loss, and these foci infiltrated by inflammatory cells, and by proliferating interstitial cells.²⁶ Focal lymphocytic infiltrate, vacuolation of cardiomyocytes, their degeneration, and myocytolysis were observed in the heart specimens of rats with PN, as well as of those with CS.

It should be noted that certain areas of the myocardium may be more predisposed to toxic damage. So, toxins produced during PN and/or CS appeared to be contributed to the myocardial lesions found preferentially in the left ventricular wall (Figure 3), and this coincided with findings of other authors on the selective damage of the left ventricular wall by cardiotoxic compounds in Sprague-Dawley rats.²⁷

Treatment with the effective doses of PRP-1 (10^{-6} M, found in the preliminary experiments) could protect from the PN-induced cardiac damage and normalize histopathological changes observed (data not shown).

At the same time, we demonstrated the beneficial effect of PRP-1 on the molecular alterations involved in the cardiomyopathy. As seen in figure 7 a, under physiological circumstances calcium binding ability is detected for five acidic proteins (3 fractions (Mr 60-80 kDa) and 2 fractions (Mr 20-30 kDa), calsequestrin (Mr 55 kDa), and Ca^{2+} -ATPase (Mr 100 kDa) (presented by two subunits after SDS-PAGE) commonly contributed to calcium accumulation in the cardiomyocyte SR. For this prior to initiation of PN 45CaCl_2 was administered and its binding assessed after SDS-PAGE separation of the cardiomyocyte SR membrane proteins. PRP-1 was injected 24 and 48 h after the PN initiation.

24 h after the PN initiation, all the above-mentioned proteins lost their calcium binding ability, with the exception of Ca^{2+} -ATPase, which continued its affinity to calcium, presumably, protect against an instant cardiac arrest (Figure 7 b). Moreover, a concomitant manifestation of calcium binding ability of the 32-kDa cardiomyocyte SR membrane protein was observed and not only during PN, but also in the CS (vide infra), possibly, a transient attempt of heart cells to compensate hypocalcemia and protect against myocardial injury.⁸ Administration of the PRP-1 cardinaly prevents the loss of affinity to calcium of the Ca^{2+} depot proteins, as well as completely suppresses the calcium binding ability of the SR membrane 32-kDa protein induced under PN condition (Figure 7, c, d, e). Our previous findings show that experimental PN is accompanied by a conversion of 32-kDa alkaline protein to acidic one and its isoelectric point changes from 8.3 to 5.9, because of a 2.4-fold increase in the acidic amino-acid content (aspartic and glutamic acids) and associated manifestation of bound calcium.²⁸ To evaluate the PRP-1 impact on the affinity of calcium ions to the cardiomyocyte SR 32-kDa membrane protein at different stages of PN, we examined a binding curve on Scatchard coordinates that makes distinction more

Table 1. PRP-1 impact on the cardiomyocyte 32-kDa protein affinity to calcium in the dynamics of pancreatic necrosis

Calcium-binding properties Groups	B_{max} , nmol calcium·mg ⁻¹ protein		K_d , nmol calcium·mg ⁻¹ protein	
	Center of low affinity	Center of high affinity	Center of low affinity	Center of high affinity
Early stage of PN (24 h)	47.63 ± 1.1	245.43 ± 9.92	4.58 ± 0.37	13.28 ± 0.31
Reparative stage of PN (7 d)	48.17 ± 0.72 [#]	245.16 ± 8.06 [#]	1.81 ± 0.15 ^{***}	9.07 ± 0.49 ^{**}
Chronic stage of PN (14 d)	37.15 ± 0.91 ^{**}	221.54±8.87 [#]	1.54 ± 0.22 [#]	7.51 ± 0.35 ^{**}
Chronic recurrent stage of PN (21 d)	44.35 ± 0.76 [*]	226.68 ± 7.71 ^{**}	1.79 ± 0.3 ^{***}	8.02 ± 0.31 ^{***}
PRP-1 treatment/Early stage of PN (24 h)	6.73 ± 0.5 ^{***}	36.5 ± 2.98 ^{***}	0.3 ± 0.02 ^{***}	2.43 ± 0.02 ^{***}
PRP-1 treatment/ Reparative stage of PN (7 d)	6.25 ± 0.21 ^{***}	34.44 ± 2.24 ^{***}	0.12 ± 0.01 ^{***}	1.24 ± 0.05 ^{***}
PRP-1 treatment/ Chronic stage of PN (14 d)	2.23 ± 0.29 ^{***}	22.35 ± 2.98 ^{***}	0.62 ± 0.02 ^{***}	1.01 ± 0.02 ^{***}
PRP-1 treatment/Chronic recurrent stage of PN (21 d)	5.65 ± 0.74 ^{***}	29.96 ± 2.02 ^{***}	0.73 ± 0.04 ^{***}	1.32 ± 0.03 ^{***}

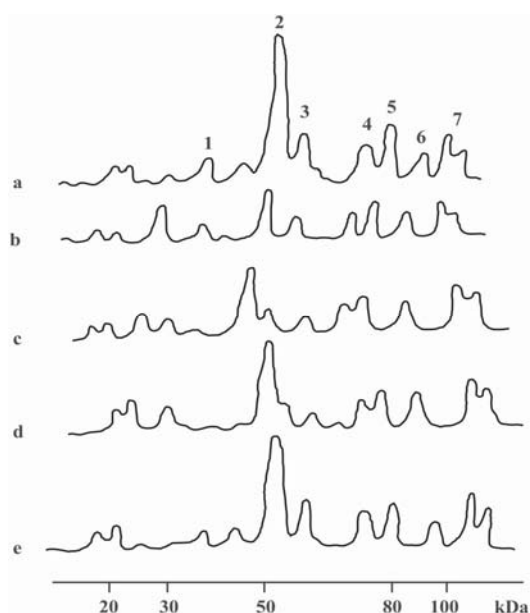


Figure 7. Effect of PRP-1 on the calcium binding to the cardiomyocyte SR membrane proteins in the dynamics of pancreatic necrosis (PN). 1, 3-6 - acidic proteins; 2 - calsequestrin; 7 - two subunits of Ca²⁺-ATPase (a) control; (b) early stage of PN - the 24th h after PN initiation; (c) reparative stage of PN - the 7th day of PN / PRP-1 treatment; (d) chronic stage of PN - the 14th day of PN / PRP-1 treatment; (e) chronic recurrent stage of PN - the 21st day of PN / PRP-1 treatment.

pronounced, and shows more than one population of binding sites.²⁰ Determined parameters are B_{max} - the maximal binding capacity of the protein(s) and K_d - the steady state dissociation constant (K_d is the free concentration of calcium for which the bound concentration is equal to $B_{max}/2$; the inverse of K_d is K_a , the steady-state constant of affinity).²¹

The data obtained clearly show that PRP-1 may prevent PN-induced modification of the 32-kDa protein in cardiomyocytes that is also suggested by B_{max} and K_d values

for centers of low and high affinity to calcium which are drastically decreased (Table 1). Under PN condition the number of proteins isolated from cardiomyocyte inner membrane (cytoplasmic membrane) was decreased from 28 to 5 molecules and a diminution in the energy metabolism was observed.¹¹

The PRP-1 may stimulate the protein synthesis in the cardiac tissues of the rats with PN, especially at chronic recurrent stage. However, negligible changes were observed in the expression of the calcium depot proteins, as well as in that of the 32-kDa protein in the cardiomyocytes (data not shown). Therefore, it could be speculated that PRP-1 impact on the calcium binding properties of the cardiomyocyte SR membrane proteins could be realized not by their synthesis de novo, but indirectly via triggering multiple mechanisms maintaining homeostasis.

PRP-1 impact on the calcium binding by the cardiomyocyte membrane proteins in the dynamics of crush syndrome

Histomorphological changes observed in early stages of decompression (2- 48 hours) were strikingly similar to those seen in PN (data not shown), it also concerns to alterations in the calcium binding of the cardiomyocyte SR membrane proteins in CS (Figure 8, b). Moreover, the same efficient doses of PRP-1 (10⁻⁶ M) administered at the end of compression and an hour later modulate the calcium-binding abilities of the Ca²⁺ depot-proteins (Figure 8, c and d). PRP-1 markedly attenuates the histopathological alterations associated with cardiac injury caused by PN and/or CS. We have previously shown that PRP-1 can prevent detrimental changes in the tissues during CS.^{12, 13} For this series of experiments prior to initiation of muscle crush injury ⁴⁵CaCl₂ was administered, and its binding assessed after SDS-PAGE separation of the cardiomyocyte SR membrane proteins. PRP-1 was injected immediately at the end of compression and an hour later.

Table 2. PRP-1 impact on the the cardiomyocyte 32-kDa protein affinity to calcium in the dynamics of crush syndrome

Calcium-binding properties Groups	B_{max} , nmol calcium·mg ⁻¹ protein		K_d , nmol calcium·mg ⁻¹ protein	
	Center of low affinity	Center of high affinity	Center of low affinity	Center of high affinity
Crush syndrome (immediately at the end of compression)	45.62 ± 0.86	231.58 ± 9.51	1.92 ± 0.28	8.71 ± 0.26
2 h decompression	36.27 ± 0.53***	± 8.17#	3.15 ± 0.38#	11.13 ± 0.28*
4 h decompression	48.81 ± 0.92**	243.49 ± 10.01*	4.71 ± 0.42**	12.82 ± 0.29*
24 h decompression	42.39 ± 0.67**	232.68 ± 7.83#	4.68 ± 0.39**	14.73 ± 0.31**
48 h decompression	44.12 ± 0.71#	258.91 ± 8.82*	5.63 ± 1.01**	17.18 ± 0.38**
PRP-1 pretreatment crush syndrome	4.19 ± 0.08***	61.7 ± 1.34***	1.78 ± 0.26***	3.65 ± 0.13***
PRP-1 pretreatment 2 h decompression	2.53 ± 0.06***	54.22 ± 0.49***	0.92 ± 0.19***	2.45 ± 0.38***
PRP-1 pretreatment 4 h decompression	2.39 ± 0.09***	48.43 ± 0.37***	0.85 ± 0.22***	2.03 ± 0.27***
PRP-1 pretreatment 24 h decompression	1.98 ± 0.07***	31.28 ± 0.45***	0.77 ± 0.19***	1.98 ± 0.21***
PRP-1 pretreatment 48 h decompression	1.55 ± 0.08***	29.25 ± 0.33***	0.65 ± 0.21***	1.87 ± 0.23***

Scatchard plot analysis data represent the mean of 12 separate experiments ± SEM. Differences are considered significant if $P=0.05$.

$P > 0.05$, * $P < 0.05$, ** $P < 0.01$, *** $P < 0.001$ (vs. Crush syndrome).

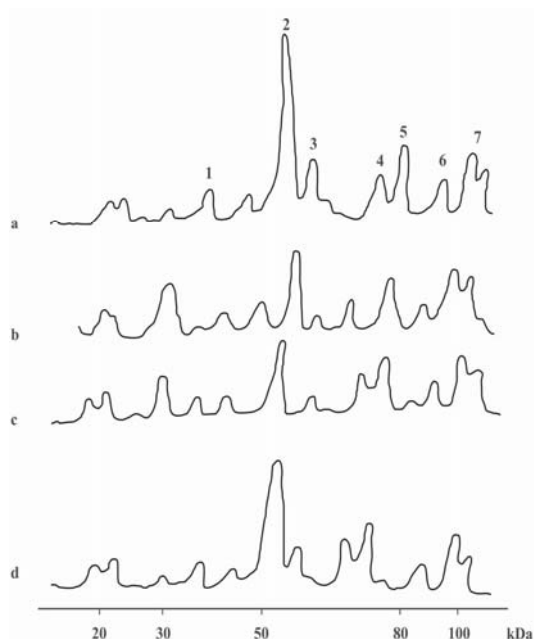


Figure 8. Effect of PRP-1 on the calcium binding to the cardiomyocyte SR membrane proteins in the dynamics of crush syndrome. 1, 3-6 - acidic proteins; 2- calsequestrin; 7 - two subunits of Ca²⁺-ATPase (a) control; (b) 2 h decompression; (c) 4 h decompression / PRP-1 treatment; (d) 48 h decompression / PRP-1 treatment.

Both PN and CS induce similar changes in myocardial 32-kDa protein calcium-binding properties (B_{max}) and its interaction with calcium (K_d), suggesting that there are common mechanisms involved in heart failure, regardless of pathology. As shown in Table 2, PRP-1 significantly diminishes the cardiomyocyte SR 32-kDa membrane protein affinity to calcium ions restoring its native properties which confirmed also by isoelectric focusing of 32-kDa protein (data not shown).

Notably, our previous findings on calcium-binding ability of the cardiomyocyte SR membrane proteins in experimental isoproterenol-induced myocardial injury show similar changes in the qualitative and quantitative spectra of the proteins associated with a loss of their affinity to calcium, and vice versa a simultaneous posttranslational modification of the 32-kDa protein with a compensatory increase of its affinity to calcium.^{10, 28}

A diffuse and granular immunoreactivity of PRP-1 was detected within the network of muscle fibers the synatrial node of the human heart.¹¹ It can be only speculated that PRP-1 deficiency is one of the possible causes of the rat heart injury. It is known that PRP-1 is involved in the regulation of the cytokine expression (TNF- α , IL-1 and IL-6), activity of caspases, as well as lipid peroxidation.¹¹ On the other hand pathophysiological changes in heart failure include oxidative stress which is closely linked to apoptosis and inflammatory cytokines.²³ That is one of the reasons why the replenishment of PRP-1 may prevent histomorphological and molecular alterations implicated in heart injury induced under PN and/or CS conditions.

CONCLUSION

In summary, the results of the present study confirm that new neurosecretory cytokine, hypothalamic proline-rich peptide-1 preserve calcium-binding ability of the cardiomyocyte SR membrane proteins, which serve as the main calcium depot in cardiac muscle and protect against hypocalcemia implicated in common cellular and molecular mechanisms of myocardial damage during experimental acute pancreatitis and/or long-term compression injury, thus emerge from an otherwise pathological outcome. The results highlight new prospects over the functional implications of PRP-1 and its possible therapeutic potential for the treatment of patients at high risk of cardiovascular disease associated with different pathologies.

ACKNOWLEDGMENTS

The authors greatly thank Dr. M.I. Titov from acad. A.A. Galoyan's Moscow laboratory, who kindly provided us with proline-rich peptide-1, Prof. A.S. Kanayan for histomorphological analysis, Ms. Ani Hakobyan for editing the manuscript.

References

- ¹Eisner, D., Bode, E., Venetucci, L., Trafford, A., *J. Mol. Cell. Cardiol.*, **2013**, *58*, 110–117.
- ²Lu, X., Wang, Y., Meng, H., Chen, P., Huang, Y., Wang, Z., Yang, Z., *PLoS ONE*, **2014**, *9*(6), e99895.
- ³Baron, T. H., Morgan, D. E., *N. Engl. J. Med.*, **1999**; *340*:1412–1417.
- ⁴Liu, S., Yu, Y., Luo, B., Liao, X., Tan, Z., *Heart Lung Circ.*, **2013**, *22*(4), 284–290.
- ⁵Kevorkian, G. A., Galoyan, A. A., Kanayan, A. S., Voskanyan, L. H., *J. Appl. Cardiol.* **1995**, *5*(3), 212–219.
- ⁶Guevorkyan, A. G., Barseghyan, V. H., Hairapetyan, H. L., Alchujyan, N. Kh., Movsesyan, N. H., Kevorkian, G. A., *Med. Sci.Arm.*, **2015**, *55*(1), 36–45.
- ⁷Guevorkyan, A. G., *Inter. J. Biochem. Res. & Rev.*, **2014**, *3*(1), 1–10.
- ⁸Galoyan, A. A., Srapionian, R. M., *Neurochem. Res.*, **1983**, *8*(12), 1511–1535.
- ⁹Galoyan, A.A., *Biochemistry of novel cardioactive hormones and immunomodulators of the functional system neurosecretory hypothalamus – endocrine heart*. Nauka Publishers. Moscow, **1997**.
- ¹⁰Galoyan, A. A., Kevorkian, G. A., Voskanyan, L. H., Alexanian, S. S., Muradian, M. S., *Neurochem. Res.*, **1988**, *13*(5), 493–498.
- ¹¹Galoyan, A. A., *Brain Neurosecretory Cytokines: Immune Response and Neuronal Survival*. Kluwer Academic / Plenum Publishers, New York, **2004**.
- ¹²Kevorkian, G. A., Marukhyan, G. L., Arakelyan, L. N., Guevorkian, A. G., Galoyan, A. A., *Neurochem. Res.*, **2001**, *26*(7), 829–832.
- ¹³Kevorkian, G. A., Hayrapetyan, H. L., Guevorkian, A. G., Kanayan, A. S., Chailyan, G. G., Barseghyan K. A., *Cent. Nerv. Syst. Agents Med. Chem.*, **2011**, *11*(3), 184–188.
- ¹⁴Bertinchant, J. P., Larue, C., Pernel I., Beck, L., Bouges, S., *Arch. Mal. Coeur. Vaiss.*, **1996**, *89*(1), 63–68.
- ¹⁵Wientzek, M., Katz, S., *J. Mol. Cell Cardiol.*, **1992**, *23*, 1149–1163.
- ¹⁶Kazaryan, K. V., Hovhannisyan, H. S., Kevorkian, G. A., Martirosov, S. M., *Gen. Physiol. Biophys.*, **1991**, *10*, 163–174.
- ¹⁷Hames, B. D, ed., *Gel Electrophoresis of Proteins: A Practical Approach*. 3rd ed., Oxford University Press, New York, **1998**.
- ¹⁸Righetti, P. G., *Isoelectric focusing: theory, methodology and application*. Elsevier, Amsterdam, **1983**.
- ¹⁹Duncombe, W. G., Johnson, P., *Radiochromatography and Radioelectrophoresis* (chapter 6). In: Coomber, D. I., ed.: *Radiochemical Methods in Analysis*, Plenum Press, New York, **1975**.
- ²⁰Scatchard, G., *Ann. NY. Acad. Sci.*, **1949**, *51*, 660–672.
- ²¹Mikaelyan, H. M., Guevorkyan, A. G., Kevorkian, G. A., *Med. Sci.Arm.*, **2016**, *56*(3), 22–33.
- ²²Lowry, O. H., Rosebrough, N. J, Farr, A. .L, Randall, R. J., *J. Biol. Chem.*, **1951**, *193*, 265–75.
- ²³Azevedo, P. S., Polegato, B. F., Minicucci, M. F., Paiva, S. A. R., Zornoff, L. A. M. *Arq. Bras. Cardiol.* **2016**, *106*(1), 62–69.
- ²⁴Luo, M., Anderson, M.E., *Circ Res.*, **2013**, *113*(6), 690–708.
- ²⁵Ruben, Z., Arceo, R. J., Bishop, S. P., Elwell, M. R., Kerns, W. D., Mesfin, G. M., Sandusky, G. E., Van Vleet, J. F., *Guides for Toxicologic Pathology*, STP/ARP/AFIP, Washington, DC, **2000**.
- ²⁶Jokinen, M. P., Lieuallen, W. G., Boyle, M. C., Johnson, C. L., Malarkey, D. E., Nyska, A., *Toxicol. Pathol.*, **2011**, *39*(5), 850–860.
- ²⁷Kemi, M., Matsumoto, H., Nomura, Y., Takahashi, R., *J. Vet. Med. Sci.*, **1996**, *58*, 699–702.

Received: 07.07.2016.

Accepted: 20.08.2016.